Space-time evolution of nonlinear three-wave interactions. I. Interaction in a homogeneous medium*

D. J. Kaup

Physics Department, Clarkson College of Technology, Potsdam, New York 13676

A. Reiman

Laboratory of Plasma Studies, Cornell University, Ithaca, New York 14853

A. Bers

Department of Electrical Engineering and Computer Sciences, and Plasma Fusion Center, Massachusetts Institute of Technology, Cambridge, Massachussetts 02139

The authors describe the evolution in time and one spatial dimension (steady-state in two spatial dimensions) of coherent three-wave interactions in a lossless homogeneous medium. They obtain their results by a complementary use of inverse scattering methods and numerical integration of the equations. The nonlinear saturation by pump depletion of instabilities which are absolute in the pump reference frame is found to involve only soliton transfer, thus allowing a complete solution in terms of an N-soliton formula. Threshold formulas for explosive instabilities, and conditions for optimal energy transfer in two-pump interactions, are presented. Nonlinear collisions of wave packets are found to give rise to upconverted packets which are sharply spiked. A nonlinear modulation is described in stimulated backscatter.

CONTENTS

*Work carried out at the Research Laboratory of Electronics, Massachusetts Institute of Technology, Cambridge, MA 02139, and supported in part by National Science Foundation Grant No. ENG 77-00340-A01 and by ONR Contract No. N00014 76 C 0867.

I. INTRODUCTION

A. General introduction

Resonant nonlinear three-wave interactions may play an important role in plasmas (Sagdeev and Galeev, 1969; Tsytovich, 1970; Davidson, 1972; Bers, 1975a; Hasegawa, 1975; Kaw *et al.*, 1976) in the saturation of parametric decay instabilities, in the inception of nonlinear "explosive" instabilities of negative-energy waves, and in nonlinear collisions of large-amplitude wave packets, either externally excited or present in strongly turbulent plasma. The three-wave interaction is the lowest-order nonlinear effect (expanding in the wave amplitudes) for a system approximately described by a linear superposition of discrete waves. The interaction is coherent if the spectral widths in $\mathbf{k}$ and ω of the interacting wave packets are small, respectively, compared to the inverse spatial scale length and the inverse of the interaction time (Tsytovich, 1970). A derivation of the equations will be outlined in Sec. I.B. Nonlinear three-wave interactions have also been studied in the context of parametric amplifiers (Cullen, 1960; Louisell, 1960), nonlinear optics (Armstrong *et al.*, 1962), interactions of water waves (Bretherton, 1964; McGoldrick, 1965; Benney and Newell, 1967), and

interactions of bulk acoustic waves (Shiren, 1965) and surface acoustic waves (Svaasand, 1969; Newhouse *et al.*, 1972; Davis and Newhouse, 1975; Vlannes, 1977). Applications will be described in more detail in Sec. I. C.

In this paper we describe the evolution in time and one spatial dimension of the coherent three-wave resonant interaction (3WRI) in a lossless homogeneous medium (Bers *et al.*, 1976). The equations describing the interaction are (Bers, 1975)

$$\left(\frac{\partial}{\partial t}+v_i\frac{\partial}{\partial x}\right)a_i = p_i K a_j a_k, \tag{1.1a}$$

$$\left(\frac{\partial}{\partial t}+v_j\frac{\partial}{\partial x}\right)a_j = -p_j K^* a_i a_k^*, \tag{1.1b}$$

$$\left(\frac{\partial}{\partial t}+v_k\frac{\partial}{\partial x}\right)a_k = -p_k K^* a_i a_j^*. \tag{1.1c}$$

Here the a's are (complex) wave-packet amplitudes, the v's are group velocities, the p's are the signs of the wave energies, and K is the (complex) coupling coefficient. The three interacting waves must satisfy the resonance conditions:

$$\omega_j + \omega_k = \omega_i , \tag{1.2a}$$

and

$$\mathbf{k}_j + \mathbf{k}_k = \mathbf{k}_i . \tag{1.2b}$$

The subscript i denotes the high-frequency wave. We note that the equations for the two-dimensional (x–y) steady-state three-wave interaction can be transformed to the form of Eqs. (1.1) if v_{1y}, v_{2y}, and v_{3y} are all positive in some reference frame (Bers *et al.*, 1976). All the results which we present for the one-dimensional space–time evolution can be reinterpreted in terms of this two-dimensional steady-state interaction. This reinterpretation will be clarified by the form in which we plot our solutions.

Early work on the nonlinear evolution described by the three-wave equations specialized in space-independent interactions in time only, or steady-state interactions in one spatial dimension (Cullen, 1960; Louisell, 1960; Armstrong *et al.*, 1962; Coppi *et al.*, 1969; Liu and Aamodt, 1976), or in effectively one-dimensional traveling-wave solutions (Armstrong *et al.*, 1970; Nozaki and Taniuti, 1973; Ohsawa and Nozaki, 1974). This work is described in Sec. I. D. A numerical study showed that inclusion of both space and time can lead to qualitatively different behavior (Bers and Reiman, 1975). This work also demonstrated that, for interactions in which one wave amplitude is initially much larger than the other two, many features of the nonlinear evolution can be predicted in terms of the properties of the linear initial evolution. An inverse scattering transform (IST) for the homogeneous-medium three-wave equations in time and one spatial dimension has been developed by Zakharov and Manakov (1973, 1976) and Kaup (1976a) and is described in Appendix A. Case and Chu (1977b) have derived a Bäcklund transformation for Eqs. (1.1), with which one can generate general N-soliton solutions. Haberman (1977) has obtained the infinity of conserved quantities, the first two of which are simply action and momentum.

Zakharov and Manakov (1975) have attempted to understand the behavior of the interactions through an investigation of exactly soluble cases. They solve for the time evolution from the very special initial conditions corresponding to N-soliton solutions. They also derive general formulas for action transfer between colliding wave packets. Our approach has been to work with those initial conditions we consider to be physically interesting, solving numerically for the time evolution to determine the major features of the interaction, and using inverse scattering theory to obtain a time-asymptotic description of those major features. We have found that the numerical and analytical techniques complement each other in a very fruitful way. A few of our main results have been presented in a previous publication (Bers *et al.*, 1976). Here we provide a more detailed description of those interactions previously considered and also describe several interactions which we have not previously discussed. Our numerical method for integrating Eqs. (1.1) is discussed in Appendix C. We have also shown how inverse scattering methods can be applied to the interaction in an inhomogeneous medium (Reiman *et al.*, 1977). A more complete description of our work on the inhomogeneous-medium three-wave interaction is presented in the accompanying article by Reiman, Part II.

In recent years some progress has been made in studying the three-wave equations in time and three spatial dimensions. This work is only described in Sec. I. E.

In applications, we are often concerned with three-wave interactions in which one of the three waves is externally excited. This is the case, for example, in laser pellet interactions or in lower-hybrid heating of tokamak plasmas. The other two waves initially have their amplitudes at the noise level. Thus, the externally excited wave, called the "pump," initially has an amplitude much larger than that of the other two waves. To describe the initial development of the interaction, we discard the term of the three-wave Eqs. (1.1) containing the product of the initially small amplitudes. Thus we obtain a pair of linear equations describing the evolution of the initially small waves. In this approximation the amplitude of the pump is time independent. If, during the course of the interaction, the low-frequency waves become comparable in amplitude to the pump, the linear approximation breaks down, and the subsequent evolution must be described by the full set of nonlinear equations (1.1). We will see that there is a close connection between the linear equations describing the initial stage of the interaction and the Zakharov–Shabat (ZS) equations (Appendices B and D) in terms of which we study the subsequent nonlinear evolution. This will put on a firm basis the connections previously noticed in numerical solutions (Bers and Reiman, 1975) between the behavior of the linear initial evolution and the subsequent nonlinear evolution.

In practice, an externally excited wave will interact with a whole spectrum of pairs of plasma waves. As long as the linear approximation remains valid, each such pair evolves independently of the others. We assume that the unstable spectrum is sufficiently narrow for the subsequent nonlinear interaction to be described

by the coherent three-wave equations. Thus, the nonlinear evolution of the pump is determined by its interaction with the first pair of waves to grow to large amplitude.

The three-wave interactions are conveniently classified according to the signs of the wave energies and the ordering of the group velocities. Interactions of different type, as determined by these parameters, display very different patterns of behavior. Changing the signs of all the energies leaves the interaction unchanged (see Appendix E). When $p_j = -p_k$ and, say, $p_j = p_i$, we transform Eqs. (1.1) by defining $\hat{a}_i = a_j^*, \hat{a}_j = a_i^*, \hat{p}_i = p_j, \hat{p}_j = p_i$, etc. The result is an equivalent set of three-wave equations in which $\hat{p}_j = \hat{p}_k$. Thus in investigating the possible three-wave interactions we can set $p_j = p_k$ without loss of generality. We do so in the remainder of this paper.

Because we believe them to be of primary importance for applications, interactions with one wave initially much larger than the others are the main focus of this paper. In this case, if one of the low-frequency waves is initially large, then the solution for the small-amplitude waves is oscillatory. If, however, the high-frequency wave is initially large then the low-frequency waves may grow exponentially until the nonlinear regime is reached. This is the case of interest. The equations describing the linear initial evolution of this interaction are

$$\left(\frac{\partial}{\partial t} + v_j \frac{\partial}{\partial x}\right) a_j = \gamma_0(x) a_k^*, \tag{1.3a}$$

$$\left(\frac{\partial}{\partial t} + v_k \frac{\partial}{\partial x}\right) a_k = \gamma_0(x) a_j^*, \tag{1.3b}$$

where

$$\gamma_0(x) \equiv K a_i(x) \tag{1.3c}$$

is time independent (taking the reference frame where $v_i = 0$). The solutions to these linear equations have been extensively studied (Cassedy and Evans, 1972; Laval *et al.*, 1973; Bers, 1975a). When $v_j v_k < 0$, Eqs. (1.3) may have growing normal mode solutions, i.e., absolute instabilities. When $v_j v_k > 0$, the instability is convective. If the low-frequency modes become comparable in amplitude to the pump, the effect of the nonlinear interaction is either to deplete the pump or to amplify it, depending on whether $p_i = p_j = p_k$ or $-p_i = p_j = p_k$.

In Sec. II we develop the analytical tools which we shall use in this paper. There we include a brief introduction to those elements of inverse scattering theory necessary for our treatment of the three-wave interaction. From this we proceed to describe our method for solving for the evolution of three-wave interactions.

In Secs. III and IV we discuss interactions with $v_j v_k < 0$. Section III deals with those where $-p_i = p_j = p_k$ (e.g., negative-energy pump with positive-energy daughter waves). Thresholds for explosive instability of finite-width wave packets are found. Area and action transfer is determined for nonexplosive interactions. Section IV deals with the interactions where $p_i = p_j = p_k$ (e.g., all waves positive energy). We find that the nonlinear saturation of absolute instabilities involves only soliton transfer, thus allowing a complete solution in terms of an N-soliton formula. In Sec. V we discuss convective instabilities of positive-energy waves, focusing in particular on the nonlinear evolution of stimulated backscatter. A nonlinear modulation of the backscatter is described.

Aside from initial conditions with $|a_i(x, t=0)| \gg |a_j(x, t=0)|, |a_k(x, t=0)|$, we also look at those initial conditions corresponding to binary wave-packet collisions. Nonlinear wave-packet collisions may arise in physical applications where two waves are externally excited or may occur in a strongly turbulent medium. For the interactions of Sec. III we describe such collisions between the high-frequency wave packet and one of the low-frequency wave packets. In Sec. IV we determine conditions for maximal pump depletion in a "two-pump interaction": an interaction where the high-frequency wave and one of the low-frequency waves are initially excited. We also describe collisions between two low-frequency packets. We find that these give rise to upconverted wave packets which are sharply spiked.

In solving initial value problems in Secs. III, IV, and V, we shall always be working with finite-width wave packets. Of course this is not an essential restriction, as we can let the widths be arbitrarily large. Note that we are not treating here the case where the interaction is restricted to a finite spatial region (Manheimer, 1974; Harvey and Schmidt, 1975; Fuchs and Beaudry, 1976). The only boundaries in our problem are those of the wave packets themselves.

Because we are studying interactions of coherent waves, we assume that each wave packet initially has a space-independent phase. For the initial value problems we are considering we can, without loss of generality, take the wave amplitudes as initially real. In Appendix E we prove this, as well as the fact that we may always take the coupling constant K to be real.

B. Nonlinear coupling of three waves

The nonlinear coupling of three waves is typically encountered in the description of any conservative nonlinear medium where: (a) The nonlinear dynamics can be considered as a perturbation of the linear wave solutions. (b) The lowest-order nonlinearity is quadratic in the field amplitudes. (c) The three-wave resonance conditions [Eqs. (1.2)] can be satisfied. Thus, for example, the nonlinearly coupled three-wave equations can be obtained from an appropriate model nonlinear equation (Benney and Newell, 1967). We illustrate the derivation of the basic equations in the context of the *electrodynamics of weakly nonlinear media* in general (Karpman, 1963; Klimontovich, 1967; Bers, 1975a).

The linear electrodynamics of a medium can be represented in general by a linear (space-time integral) dependence of the electric current density $\bar{J}(\bar{r}, t)$ upon the electric field $\bar{E}(\bar{r}, t)$. For a homogeneous medium, using complex Fourier transforms for the fields $\{\exp[i(\bar{k}\cdot\bar{r} - \omega t)]$ dependence$\}$, this relationship can be written as

$$J_i(\bar{k}, \omega) = \sigma_{ij}(\bar{k}, \omega) E_j(\bar{k}, \omega). \tag{1.4}$$

When this is substituted into Maxwell's equations one

finds the homogeneous set of equations

$$D_{ij}(\bar{k},\omega)E_j(\bar{k},\omega)=0 \tag{1.5}$$

where the dispersion tensor (MKS units) is

$$D_{ij}=\left(1-\frac{c^2k^2}{\omega^2}\right)\delta_{ij}+\frac{c^2}{\omega^2}k_ik_j+\frac{i\sigma_{ij}(\bar{k},\omega)}{\omega\epsilon_0}. \tag{1.6}$$

The field solutions are thus constrained by the dispersion relation

$$D(\bar{k},\omega)=\det D_{ij}(\bar{k},\omega)=0\,, \tag{1.7}$$

giving $\omega(\bar{k})\equiv\omega_k$. The linear field solutions can therefore be written in general as

$$\bar{E}(\bar{r},t)=\sum_{\bar{k}}\bar{E}_k\exp[i(\bar{k}\cdot\bar{r}-\omega_k t)]\,. \tag{1.8}$$

For *weakly dissipative media* ($|\sigma^h_{ij}|\ll|\sigma^a_{ij}|$, where the superscript h stands for the Hermitian part and the superscript a stands for the anti-Hermitian part) we take these fields to be the weakly damped (or growing) propagating waves, i.e., for $\bar{k}$ real $|\nu|\equiv|\mathrm{Im}\omega_k|\ll|\mathrm{Re}\omega_k|\equiv|\omega|$ and thus from (1.7) with $|D_i|\equiv|\mathrm{Im}D(\bar{k},\omega)|\ll|\mathrm{Re}D(\bar{k},\omega)|\equiv|D_r|$ one obtains

$$D_r(\bar{k},\omega)=0 \text{ giving } \omega(\bar{k}) \tag{1.9}$$

and

$$\nu(\bar{k})=\left.\frac{-D_i}{(\partial D_r/\partial\omega)}\right|_{D_r=0}. \tag{1.10}$$

Consider now the nonlinear electrodynamics of the medium as a perturbation. The nonlinear electric current density to second order in the electric field will be given by

$$J^{(2)}_i=\sigma^{mn}_{ijk}E^m_jE^n_k\,, \tag{1.11}$$

where for brevity the superscripts m and n stand for the dependence upon $(\bar{k}_m,\omega_m)$ and $(\bar{k}_n,\omega_n)$, respectively, of the field variables and the third-rank tensor. We now assume that this second-order current will produce a slowly varying space-time amplitude variation in the linear field solutions, so that (1.8) now becomes

$$\bar{E}(\bar{r},t)=\sum_{\bar{k}}\bar{E}_ku_k(\bar{r},t)\exp[i(\bar{k}\cdot\bar{r}-\omega t)], \tag{1.12}$$

where the $\bar{r}\equiv x_i$ and t variation in u_k is slow compared to, respectively, k_i^{-1} and ω^{-1}. [Note: In general, the perturbation will produce a slowly varying amplitude and polarization (i.e., orientation) of the electric field vector. It can, however, be shown that to second order the dynamic equations for the amplitude are decoupled from those for the polarization (Karpman, 1963; Bers, (1975a). Here we shall only consider the amplitude equations.] When (1.11) and (1.12) are substituted into Maxwell's equations and the nonlinearity is ordered with the slow variation, we obtain an infinite set of coupled partial differential equations for the slowly varying amplitudes. From the structure of (1.11) it is clear that the simplest coupling will consist of a *resonant triplet* of linear waves satisfying

$$\bar{k}_1=\bar{k}_2+\bar{k}_3 \tag{1.13}$$

and

$$\omega_1=\omega_2+\omega_3\,. \tag{1.14}$$

We shall write down the resulting coupled equations for the slowly varying amplitudes of the three waves which one obtains when the *nonlinearity is conservative*. It is convenient to normalize the slowly varying amplitude $u(\bar{r},t)$ so that its magnitude square is the action density of the wave; let this normalized, slowly varying amplitude be $a_k(\bar{r},t)=a_{k0}u_k(\bar{r},t)$,

$$|a_{k0}|^2=\left|\frac{w_{k0}}{\omega}\right|=\frac{\epsilon_0E^2_{k0}}{4}\left|\frac{\partial D_k}{\partial\omega}\right|_{D_r=0}, \tag{1.15}$$

where we have set $\bar{E}_k=\bar{e}E_{k0}$ and $(\partial D_k/\partial\omega)=e_i^*(\partial D^h_{ij}/\partial\omega)e_j$. Then the three coupled equations are:

$$\left(\frac{\partial}{\partial t}+\bar{v}_1\cdot\nabla+\nu_1\right)a_1=p_1Ka_2a_3\,, \tag{1.16a}$$

$$\left(\frac{\partial}{\partial t}+\bar{v}_2\cdot\nabla+\nu_2\right)a_2=-p_2K^*a_1a_3^*\,, \tag{1.16b}$$

$$\left(\frac{\partial}{\partial t}+\bar{v}_3\cdot\nabla+\nu_3\right)a_3=-p_3K^*a_1a_2^*\,, \tag{1.16c}$$

where, assuming $\omega>0$, $p_k=\mathrm{sgn}(w_{k0})=\pm1$ is the energy parity,

$$\bar{v}_k=\frac{\partial\omega}{\partial\bar{k}} \tag{1.17}$$

is the group velocity, and K is given by

$$|a_{10}a_{20}a_{30}|^{1/2}K=-\frac{\bar{E}_1^*\cdot\bar{J}^{(2)}_{2,3}}{4\omega_1}=\frac{\bar{E}_2\cdot\bar{J}^{(2)*}_{1,-3}}{4\omega_2}=\frac{\bar{E}_3\cdot\bar{J}^{(2)*}_{1,-2}}{4\omega_3}. \tag{1.18}$$

In Eq. (1.18) the subscripts on the second-order current indicate the wave amplitudes on which it depends [viz., superscripts on the right-hand side of Eq. (1.11)]. Equations (1.16a)–(1.16c) with all $\nu=0$ and each $\bar{v}\cdot\nabla=v_x(\partial/\partial x)$ are just Eqs. (1.1a)–(1.1c) for the one-dimensional space and time evolution of the three-wave resonant interaction (3WRI). Also, with all $\nu=0$, all $(\partial/\partial t)=0$, and each $\bar{v}\cdot\nabla=v_x(\partial/\partial x)+v_y(\partial/\partial y)$, Eqs. (1.16a)–(1.16c) describe the two-dimensional steady-state resonant interaction of three waves.

It should be remarked that in nonlinear optics of media where spatial dispersion is usually ignored, the nonlinear susceptibility of the medium is characterized by the form of the potential energy of the atom or molecule (Bloembergen, 1965). In such cases, for an isotropic medium with a center of inversion, the lowest-order nonlinearity in the dynamic equations is cubic and the three-wave interaction as described by (1.1) or (1.16) does not occur. On the other hand, for a medium which lacks a center of symmetry, the lowest-order nonlinearity in the dynamic equations is quadratic, as in (1.11), and the three-wave interaction is then possible.

C. Physical applications

The principles of nonlinear coupling of modes were first recognized almost a century and a half ago for various mechanical systems (Faraday, 1831; Melde, 1859; Lord Rayleigh, 1883, 1887). Similar ideas developed in relation to electrical circuits in the early days of radio-telephone communication before World

War I. (See the historical review in Mumford, 1960.) After World War II, the technological development of materials, semiconductors, and ferrites led to a renewed interest in such nonlinear phenomena and generated novel high-frequency *electronic devices* (Uhlir, 1956; Suhl, 1957a, 1957b). Soon afterwards these ideas were extended to the nonlinear interaction of waves using ferrites (Tien and Suhl, 1958), or semiconductor diodes (Engelbrecht, 1958), or electron beams (Adler, 1958; Louisell and Quate, 1958). The interest was mainly in generating new types of low-noise amplifiers at microwave frequencies (Louisell, 1960). One-dimensional (guided-wave) versions of (1.1) were most commonly studied (Cullen, 1960), and the nonlinear solutions involved only the steady-state evolution in space, i.e., Eqs. (1.1) without the time derivative (Jurkus and Robson, 1960 and 1961; Akhmanov and Dimitriyev, 1963; Kravtsov, 1963).

Several standard *nonlinear optics* texts describe the relevant effects of three-wave interactions (see, for example, Yariv, 1975). Parametric amplifiers and oscillators make use of three-wave interactions in an essential way, using an externally excited high-frequency mode to drive lower-frequency "signal" and "idler" waves. Other important effects of three-wave interactions are second harmonic generation and spontaneous parametric fluorescence. Spontaneous parametric fluorescence is a parametric decay in which the amplitudes of the idler and signal are initially determined by the ground-state energy of the electromagnetic modes.

Effects of pump depletion relevant to nonlinear optics were first considered by Armstrong *et al.* (1962), where a one-dimensional steady-state interaction was treated. Equations (1.1) without the time derivatives were found, and the elliptic function solutions derived. In later work with Eqs. (1.1), Armstrong *et al.* (1970) derived the traveling-wave solutions and showed that self-induced transparency effects could occur. These early papers dealt with interactions between three electromagnetic waves. Recently Steudel (1977) has analyzed the stimulated Raman scattering (SRS) problem in some depth and has pointed out that when there is no inhomogeneous broadening and when the excitation of the Raman level can be neglected, then the SRS equations reduce to the 3WRI equations. Along this line, we should also point out the review by Bullough (1977), which treats, in general, interactions of radiation with matter and discusses how solitons occur in coherent pulse propagation, the sine-Gordon equation, the nonlinear Schrödinger equation, and the 3WRI.

In studies of *water waves* the first wave–wave interactions which were obtained were not the 3WRI, but rather the more complicated four-wave resonant interaction (4WRI). This was first noted by Phillips (1960), where for deep water gravity waves he found that the 3WRI did not occur, but that the 4WRI did. However, when surface tension effects were included, McGoldrick (1965) found that 3WRI did indeed occur for these gravity-capillary waves. Similar results were also found by Kenyon (1966) and Longuet-Higgins and Gill (1966) for Rossby waves in the atmosphere. Bretherton (1964) found solutions of the 3WRI in time only in terms of elliptic functions. More recently, Case and Chu (1977a) have refined and extended McGoldrick's calculations for gravity-capillary waves, and have discussed these interactions and the soliton solutions in terms of the inverse scattering solution of Kaup (1976a).

In *plasma physics*, and especially for high-temperature plasmas in a magnetic field, the linear dynamics of plasmas involves a very rich variety of waves (Stix, 1962; Allis *et al.*, 1963). Nonlinear dynamics of plasmas can involve both wave–particle interactions and wave–wave interactions. The latter, in its simplest form, is described by Eqs. (1.16). A large number of these interactions have been studied since the early 1960's (Oraevskii and Sagdeev, 1963; Silin, 1965; Goldman, 1966; Dubois and Goldman, 1967; K. Nishikawa, 1968). Such interactions are of importance in ionospheric propagation (Fejer, 1977), in the evolution of various plasma instabilities (Coppi *et al.*, 1969; Tsytovich, 1970; Hasegawa, 1975), and more recently in problems of plasma heating with high-power electromagnetic sources, e.g., with lasers for pellet fusion (DuBois, 1974; Drake *et al.*, 1974; Manheimer and Ott, 1974), and with rf to microwave and millimeter sources for magnetically confined fusion plasmas (Bers, 1975b; Ott, 1975; Watson and Bers, 1977; Bers, 1978; Porkolab, 1978). In all cases where the nonlinear interactions were solved for pump depletion, only their evolution in time was considered.

D. One-dimensional and traveling-wave solutions

When the spatial derivatives can be neglected, Eqs. (1.1) become

$$\frac{d}{dt}a_i = p_i K a_j a_k , \tag{1.19a}$$

$$\frac{d}{dt}a_j = -p_j K^* a_i a_k^* , \tag{1.19b}$$

$$\frac{d}{dt}a_k = -p_k K^* a_i a_j^* , \tag{1.19c}$$

These equations can be solved exactly in terms of Jacobi elliptic functions (Armstrong *et al.*, 1962). The solution for positive-energy waves ($p_i = p_j = p_k$) was obtained independently by Armstrong *et al.* (1962) and Bretherton (1964). These solutions are periodic in time. The solution for $p_j = p_k = -p_i$ may be derived in a similar manner (Coppi *et al.*, 1969). These solutions are singular at some finite time, corresponding to explosive behavior.

The complete solutions to Eqs. (1.19) are presented in several plasma physics books (see, for example, Sagdeev and Galeev, 1969; Davidson, 1972; Weiland and Wilhelmson, 1977). We limit ourselves here to describing the solution when initially $a_k = 0$ and $|a_j| \ll |a_i|$. This solution will provide a useful comparison when we later discuss the evolution of the interactions in space and time. Note that for $p_i = p_j = p_k$, if initially $|a_j| \gg |a_i|$, $|a_k|$ or $|a_k| \gg |a_i|$, $|a_j|$, then the large-amplitude mode performs small sinusoidal oscillations about its initial value consistent with the Manley–Rowe constants of the motion ($p_i|a_i|^2 + p_j|a_j|^2$) and ($p_i|a_i|^2 + p_k|a_k|^2$). These conservation laws follow di-

rectly from Eqs. (1.19).

We first consider the solution when $p_i = p_j = p_k$. Initially, a_i is approximately time independent, and Eqs. (1.19) can be approximated by the linear pair of equations

$$\frac{d}{dt}a_j = -p_j K^* a_i a_k^*, \tag{1.20a}$$

$$\frac{d}{dt}a_k = -p_k K^* a_i a_j^*. \tag{1.20b}$$

Thus for $p_j = p_k$, a_j and a_k are initially growing exponentially with a growth rate $|Ka_i(t=0)|$. When a_j and a_k become comparable in amplitude to a_i, depletion of a_i becomes important and the linear equations are no longer a good approximation. Define $a_{\mu 0} \equiv a_\mu(t=0)$. Then the solution to the linear equations (1.20) begins to diverge substantially from the exact nonlinear solution at a time t_D given by

$$t_D = \frac{1}{|Ka_{i0}|}\ln\left(\frac{2|a_{i0}|}{|a_{j0}|}\right). \tag{1.21}$$

At this time the linear solution has overshot the nonlinear solution by about 25% (Kulberg, 1975). The nonlinear solution shows that depletion of a_i now becomes very rapid, with a_i going to zero and a_k going to $a_i(t=0)$ at a time t_0 given by

$$t_0 = \frac{1}{|Ka_{i0}|}\ln\left(\frac{4|a_{i0}|}{|a_{j0}|}\right). \tag{1.22}$$

Then a_j and a_k in turn begin to get depleted. The low-frequency amplitudes a_j and a_k are even functions of $t_0 - t$, while a_i is an odd function of $t_0 - t$. The whole process is periodic, with period $2t_0$.

When $-p_i = p_j = p_k$ the initial behavior is again well approximated by the solution of the linear equations (1.20), with a divergence time given by Eq. (1.21). Now when a_j and a_k become comparable in amplitude to a_i, a_i begins to grow rapidly. This leads to enhanced growth of a_j and a_k, and therefore of a_i. The result is an explosive growth of all three amplitudes, leading to a singularity at a time given approximately by

$$t_{\text{expl}} = \frac{1}{|Ka_{i0}|}\ln\left[\frac{4|a_{i0}|}{|a_{j0}|}\right]. \tag{1.23}$$

The one-dimensional steady state (if one exists) satisfies the equations

$$v_i\frac{d}{dx}a_i = p_i K a_j a_k, \tag{1.24a}$$

$$v_j\frac{d}{dx}a_j = -p_j K^* a_i a_k^*, \tag{1.24b}$$

$$v_k\frac{d}{dx}a_k = -p_k K^* a_i a_j^*. \tag{1.24c}$$

Define $\hat{a}_i = a_i/|v_j v_k|^{1/2}$, $\hat{a}_j = a_j/|v_i v_k|^{1/2}$, $\hat{a}_k = a_k/|v_i v_j|^{1/2}$. These amplitudes with carets satisfy the equations

$$\frac{d}{dx}\hat{a}_i = \text{sgn}(v_i)p_i K \hat{a}_j \hat{a}_k, \tag{1.25a}$$

$$\frac{d}{dx}\hat{a}_j = -\text{sgn}(v_j)p_j K^* \hat{a}_i a_k^*, \tag{1.25b}$$

$$\frac{d}{dx}\hat{a}_k = -\text{sgn}(v_k)p_k K^* \hat{a}_j a_j^*. \tag{1.25c}$$

If all the velocities are of the same sign, then the problem is equivalent to that of the time-only interaction. The exact solutions to (1.25) can be given in terms of Jacobi elliptic functions (Jurkus and Robson, 1960). If the velocities are not all of the same sign, we must solve a two-point boundary value problem, rather than an initial value problem.

The steady-state equations with $v_i, v_j > 0, v_k < 0$ and $p_i = p_j = p_k$ were studied by Manheimer (1974), by Harvey and Schmidt (1975), and by Forslund *et al.* (1973, 1975), in both finite and semi-infinite interaction regions. The solution in the interior of the interaction region is again exactly expressible in terms of Jacobi elliptic functions. However, the solutions are now subject to the boundary conditions of fixed $a_i(x=0)$, $a_j(x=0)$, and $a_k(x=L)$ [or $a_k(x\to\infty)$]. The boundary conditions of primary interest are those where $a_j(x=0)=0$, $a_i(x=0) \gg a_k(x=L)$. In that limit there is a threshold length below which there are no nontrivial solutions of the steady-state equations,

$$L_t \approx \frac{\pi}{2}\frac{|v_j v_k|^{1/2}}{|Ka_{i0}|}. \tag{1.26}$$

For $L > 3L_t$ the solution is not unique. However, there is only one solution which is stable in time (Harvey and Schmidt, 1975). The unstable solutions are all oscillatory functions of x, while the stable solutions are monotonic.

The *traveling-wave solutions* to Eqs. (1.1) may be found by making the ansatz that all three amplitudes are functions only of $\xi \equiv x - Vt$, V being the velocity of the traveling wave. This ansatz reduces Eqs. (1.1) to three ordinary differential equations of the form (1.19), with t replaced by ξ. The Jacobi function solutions for $p_i = p_j = p_k$ have been enumerated by Armstrong *et al.* (1970). These traveling-wave solutions have also been studied by Nozaki and Taniuti (1973) and Ohsawa and Nozaki (1974). Although the Jacobi function solutions are generally periodic, there are particular limits in which the period goes to infinity. One of the amplitudes is then shocklike (a hyperbolic tangent), while the other two are bounded pulses (hyperbolic secants). For those solutions in which a_i is the hyperbolic tangent, either V is greater than all of v_i, v_j, v_k or V is less than all of these velocities. These solutions are therefore somewhat unphysical, depending sensitively on the exponential tails of the low-frequency waves. In the traveling-wave solutions of Eqs. (1.1), at least one wave amplitude is always nonzero as $|x| \to \infty$. In this paper we shall be concerned with time-asymptotic solutions to interactions of bounded wave packets, and therefore will not encounter such traveling-wave solutions.

E. The three-dimensional problem

Although in this paper we shall not discuss the general three-dimensional form of the 3WRI (3D-3WRI), we shall briefly mention the current theoretical state of this more general problem. There are certain important developments in this area of which one should be aware, although a full theoretical treatment of the 3D-3WRI is yet to be presented. The first step in this

direction was made by Zakharov and Shabat (1974), when they were able to obtain the 3D-3WRI as an integrability condition for two operators. Zakharov (1976) has refined this technique to the point where he can now obtain special solutions of the 3D-3WRI. However, the general solution of the initial value problem is still to come. Earlier, Craik (1971) had analyzed the effects of the 3D-3WRI in shear flows in boundary layers, and he had found that explosivelike solutions can occur and also gave some special solutions. More recently, Craik (1978) has found a class of exact solutions for the 3D-3WRI which is identical to a special case of the inverse scattering solution of Zakharov (1976). These solutions tend to develop singularities and to "burst" in a finite time. Craik has also developed a criterion for the bursting to occur and relates the bursting to the initial wave energies.

In the three-dimensional Zakharov–Shabat (1974) scheme, there are several difficulties, some of which have been pointed out by Miles (1977) and Newell and Redekopp (1977). They noted that wherever a breakdown occurred in the inverse scattering soliton solutions, one had an exact resonance between three interacting solitons. Yajima, Oikawa, and Satsuma (1978) have observed the same thing for three-dimensional ion-acoustic solitons, which they analyzed by the Hirota (1976) scheme for constructing soliton solutions, instead of the Zakharov–Shabat (1974) scheme. The exact significance of these results for the general 3D-3WRI is still uncertain, but it does indicate some of the problems involved. So, for the present, we shall leave the 3D-3WRI and from now on shall only consider the special case of time–one-space coordinate, or the steady state two-space coordinates.

Note added in proof. Just recently, Cornille (1978) has found another means for solving the 3D–3WRI, based on the scattering problem of Ablowitz and Haberman (1975). And with his result, Kaup (1979) has solved the initial value problem for the 3D–3WRI when the initial envelopes are nonoverlapping.

II. INVERSE SCATTERING TRANSFORM FOR THE THREE-WAVE EQUATIONS

In this brief introduction to the method of the "inverse scattering transform," IST, we emphasize those features of the method which we have found useful in this study of the three-wave problem. For a more complete discussion of the inverse scattering transform, the reader is referred to the literature (Zakharov and Manakov, 1973; Kaup 1976a; Gardner *et al.*, 1967; Scott *et al.*, 1973; Flaschka and Newell, 1975; Zakharov and Shabat, 1971; Ablowitz *et al.*, 1974; Kaup, 1977; Zakharov and Manakov, 1976).

A. The method

The overall strategy of the method of the IST is the same as that of any transform method: we define a transform of the original problem into a space in which the time dependence is particularly simple. After determining the transformed data at a later time, we invert our transform to obtain the solution. The IST has actually been shown to be a nonlinear extension of the Fourier transform (Ablowitz *et al.*, 1974). To convey an understanding of the method of the IST and an appreciation of its power, we find it helpful to pursue this connection.

To use the IST, we must first construct an appropriate eigenvalue problem from the wave amplitudes [see Eqs. (2.1) and (A5) for two such eigenvalue problems]. This eigenvalue problem can be reformulated an an integral equation which reduces to the Fourier integral in the small-amplitude limit. The "scattering problem" consists of determining the space-asymptotic behavior of the eigenfunctions of our eigenvalue problem. This asymptotic behavior is expressed in terms of the "scattering data." Thus our eigenvalue problem provides a mapping of the wave amplitudes into a set of scattering data (analogous to Fourier components). The nonlinear equations can then themselves be expressed in scattering space, which is analogous to Fourier space. A certain class of physically interesting nonlinear equations of motion can be transformed in this manner, using appropriate eigenvalue problems, to linear equations of motion (analogous to the class of constant coefficient, linear partial differential equations, which are soluble by Fourier transforms). The scattering data at any time t is then easily calculated in terms of the initial scattering data. The wave amplitudes at time t can be reconstructed using the inverse scattering equations (also called "Marchenko" or "Gelfand–Levitan" equations in the literature), which are a nonlinear extension of the inverse Fourier transform. If we let S represent the scattering data, we can summarize the inverse scattering procedure by:

$$a_i(0) \xrightarrow[\text{problem}]{\text{eigenvalue}} S(0) \to S(t) \xrightarrow[\text{equations}]{\text{inverse scattering}} a_i(t) .$$

Just as the Fourier transform decomposes a function into its linear normal modes, so does the inverse scattering transform decompose a function into its analogous nonlinear "normal modes," linearly independent in scattering space. Of these normal modes, there are two distinct types in the nonlinear theory. The first is the "soliton," which has no linear analog, vanishing in the small-amplitude, linear limit. It has been studied in the context of ion-acoustic waves, the phenomenon of laser pulse compression, and other effects as well. The solitons are the manifestation of a discrete bound-state spectrum of the particular eigenvalue problem (to be introduced later) and are localized, permanent (or oscillatory), traveling waveforms. Meanwhile, the continuous part of this eigenvalue spectrum gives the other type of normal mode, which is called "radiation," since when dispersion is present, it propagates away from a disturbance as radiation would. This type of normal mode does have a linear analog. For weak fields when the nonlinearity can be neglected, it becomes simply the linear Fourier transform of the weak field. But even in the nonlinear limit it retains many of the properties of the linear Fourier transform, so that one can get a feel for what it is by simply considering it to be, at least qualitatively, a "nonlinear Fourier transform."

B. Application to the three-wave interaction

Since the three-wave resonant interaction does belong to that special class which can be solved by an inverse scattering transform, we can apply this method for an understanding of how the interaction proceeds. Many of the required mathematical details are given in Appendix A, which is divided into four parts. What we shall do here will be simply to describe each part of Appendix A, and discuss the results, their implications, and utility. The inverse scattering solution for these equations is more complicated than for equations previously solved by this method, in that the particular eigenvalue problem required is, in general, of third order. This third-order eigenvalue problem is briefly discussed in Sec. 1 of Appendix A, and it is presented there only to allow the reader to orient himself to the original problem if he so desires. But, we must firmly emphasize that we shall never need to use this most general solution directly. Rather, by considering only the case in which the three envelopes initially are well separated or have small overlap, we can considerably simplify the original solution. Also note that this is frequently the physical situation, in that the envelopes are often initially separated.

When these envelopes are separated one from another with no overlap, the scattering data of the third-order Zakharov–Manakov (ZM) problem, which contains all information on the profile shapes and positions of the three envelopes, can be factored into three sets of scattering data. Each set of this new scattering data contains all information on the profile shape and position of just one of these three envelopes. Furthermore, one can determine each of these new sets of scattering data directly from the original profile shape and position of each envelope individually, by solving the much simpler second-order Zakharov–Shabat (ZS) eigenvalue problem. Thus when the envelopes are initially separated, one may take each envelope and decompose it into a set of ZS scattering data.

The advantage of the above is that we can now avoid having to solve the third-order ZM eigenvalue problem. We in effect do solve it by solving the ZS eigenvalue problem three times, once for each envelope. However, our fuller understanding of the ZS problem and our ability to readily interpret its scattering data makes this well worth while. The mathematical details involved in this decomposition are discussed in Sec. 2 of Appendix A.

Now, let us consider the typical case where we start with separated envelopes at $t=0$. As each envelope will propagate at its own characteristic velocity, eventually they will collide and start to overlap. However, until they collide, since they will travel with no distortion (because dispersion is absent), each set of ZS scattering date (one for each envelope) will have the very simple time dependence corresponding to translational motion. When they start to overlap, the ZM eigenvalue problem no longer reduces to three ZS eigenvalue problems. Now the nonlinearity has been "turned on." But in general, the envelopes will eventually separate and emerge from the interaction region. Now, no longer are they the same shape as before. How can we determine the final shapes? Well, let us first note that from the three sets of ZS scattering data, for the initial profiles, we can construct the ZM scattering data. Now before, during, and after the interaction, the time dependence of the ZM scattering data is known. So, from the initial three sets of ZS scattering data, we can obtain the ZM scattering data for the time-asymptotic ($t\to\infty$) solution. Let us now assume that the time-asymptotic solution has all envelopes separated. This then means that the time-asymptotic ZM scattering data can also be decomposed into three sets of ZS scattering data, one set for each time-asymptotic envelope. In other words, it is possible to go from the three sets of ZS scattering data of the *initial* envelopes, directly to the three sets of ZS scattering data for the *final* envelopes. The mathematical details for this relation between the initial and final sets of the ZS scattering data are derived in Sec. 3 of Appendix A, with the final result being given by Eq. (A17). Almost all of our theoretical calculations will be based on this result. It is really the only result from the first three parts of Appendix A that is needed to understand the remainder of the paper. From this we shall be able to calculate final-state quantities directly from initial-state quantities. Of course, if one chooses to, one may use the inverse scattering equations for the ZS scattering problem to reconstruct the actual final envelopes. However, we shall see that to obtain the essential information about the interaction, it is not necessary to solve even these inverse scattering equations for the ZS problem.

Before continuing, at this point it is worthwhile to pause briefly and to describe the Zakharov–Shabat eigenvalue problem referred to above, as well as the definition of its scattering data. The ZS equation is

$$v_{1x}+i\lambda v_1=qv_2\,, \tag{2.1a}$$

$$v_{2x}-i\lambda v_2=rv_1\,, \tag{2.1b}$$

where

$$v=\begin{pmatrix}v_1\\ v_2\end{pmatrix}$$

is the eigenvector, λ is the eigenvalue, and q and r are the potentials where $r=\pm q^*$. When we use Eq. (2.1) to decompose the initial profiles into the three sets of ZS scattering data, we simply set q proportional to each profile in turn, with the exact relation being given by Eq. (A14). Then we solve for the scattering data as described below.

To define the ZS scattering data, we first define ϕ to be a solution of (2.1) which satisfies the boundary condition

$$\phi\to\begin{bmatrix}1\\ 0\end{bmatrix}e^{-i\lambda x}\ \text{as}\ x\to-\infty\,. \tag{2.2}$$

Then as $x\to+\infty$

$$\phi\to\begin{bmatrix}a(\lambda)e^{-i\lambda x}\\ b(\lambda)e^{+i\lambda x}\end{bmatrix}\ \text{as}\ x\to+\infty\,, \tag{2.3}$$

thus defining $a(\lambda)$ and $b(\lambda)$. For the continuous part of the eigenvalue spectrum (λ real) it is sufficient to determine

$$\rho(\lambda) \equiv \frac{b(\lambda)}{a(\lambda)}, \tag{2.4}$$

where ρ is called the ZS "reflection coefficient." The function ρ specifies the continuous part of the spectrum and is also frequently called the "radiation." In the linear limit, ρ is essentially the linear Fourier transform of $q(x)$. It is convenient to define also

$$\Gamma(\lambda) \equiv [1 \mp |\rho(\lambda)|^2]^{\mp 1} - 1 \tag{2.5}$$

for $r = \pm q^*$. The function Γ is analogous to a "power spectrum" of the linear theory and shall be referred to as the "density of radiation."

The soliton part of the eigenvalue spectrum is determined by the zeros of $a(\lambda)$ in the upper half λ-plane, which correspond to discrete eigenvalues (bound states). We designate these zeros by $\{\lambda_k\}_{k=1}^{N}$ and assume N to be finite. At an eigenvalue, we have

$$\varphi(\lambda_k, x) \to \begin{bmatrix} 0 \\ b_k e^{i\lambda_k x} \end{bmatrix} \text{ as } x \to +\infty, \tag{2.6}$$

and when $b(\lambda)$ can be analytically continued into the upper half λ-plane,

$$b_k = b(\lambda_k). \tag{2.7}$$

Finally, to complete the specification of the scattering data, we define

$$D_k = -i \frac{b_k}{a_k'}, \tag{2.8a}$$

where

$$a_k' = \left. \frac{\partial a(\lambda)}{\partial \lambda} \right|_{\lambda = \lambda_k}. \tag{2.8b}$$

Each pair of $[\lambda_k, D_k]$ corresponds to one soliton, where the imaginary part of λ_k determines the amplitude and width, the real part of λ_k determines the spatial phase modulation, and D_k determines its initial position and phase. The ZS eigenvalue problem is discussed in more detail in Appendix B. However, the above are the essential features of which the reader should be aware.

The ZS eigenvalue problem also has a remarkable physical interpretation for the three-wave problem. This interpretation is discussed in detail in Appendix D and is remarked on at this point in order to give the reader a better physical understanding of the ZS scattering data before continuing. In order to understand this interpretation and connection, consider any one of these envelopes when it is well separated from the other two. We shall call this envelope the pump. Consider the linear stability problem for this pump, whereby we assume the other two waves now to be infinitesimal. We linearize Eqs. (1.1) in the small amplitudes and Fourier transform in time. Then by linear scaling and taking out appropriate phase factors, we find that Eqs. (1.1) become simply the ZS equation (2.1), where the ZS q is proportional to the envelope of the pump, and the ZS eigenvalue λ is proportional to the frequency ω. In light of this one can see a physical correspondence of these "normal modes" used in the inverse scattering transform. When the equations for the middle envelope have bound states, it is known to be linearly unstable, with each bound state corresponding to one growing normal mode. These bound states can also occur for the fast or slow envelope, but then cannot give rise to any linear instabilities (see Appendix D). But, in the language of inverse scattering, the physical manifestation of a bound state is a soliton, so we then have that the existence of a soliton in the middle envelope corresponds to a linear instability. To interpret the continuous part of the spectrum, scatter an infinitesimal wave of time dependence $e^{-i\omega t}$ off the pump. Part of this wave will be transmitted through the pump, and the remainder will be converted into the other wave. The fraction which is transmitted is then either a or $1/a$, depending on the relative group velocities of the waves. In inverse scattering theory, a is known as the "transmission coefficient." The ratio of the converted wave to the incident wave is either b or the ratio b/a from inverse scattering theory, where b/a is known as the "reflection coefficient."

The "scattering data" consist of the bound-state eigenvalues, the normalization coefficients of the associated bound-state eigenfunctions, and the "reflection coefficient," b/a, for real λ. From this information it is possible to completely reconstruct the pump (potential) (see Appendix B). Clearly, when we do the same thing for all three well separated envelopes, we shall end up with three separate sets of ZS scattering data. According to the above remarks, these sets of scattering data are nothing more than the complete information about the behavior of the three well separated envelopes for linear perturbations. The remarkable thing is that, given only this information about their linear behavior, *we can completely determine how this system evolves, even in the nonlinear regime.*

Unfortunately the formal solution of the inverse scattering problem is expressed in terms of the solution of linear integral equations, which, although mathematically sound, is in general not easily carried out. We note as an exception to this the situation when $\rho(\lambda) = 0$ for λ real. Then the inverse scattering equations have a closed-form solution—the "N-soliton formula" (see Appendix B). We find such solutions emerging in some cases, but more often we are not so fortunate. Anyway, in most cases, *simply knowing certain properties of the final envelopes may be more than adequate.* We find that as we look at some of the most readily accessible information, one can obtain much information by rather simple techniques. We shall now turn to a discussion as to what this information is. Derivations of the statements made here are given in Appendix B.

C. Extracting information directly from the scattering data

The three most readily accessible pieces of information about the final envelopes are the (1) solitons, (2) areas or modal numbers, and (3) actions (energy in an envelope divided by its central frequency). We shall discuss each of these in turn. First, the soliton part of each envelope is always exchanged as indicated in Fig. 1. The details and reasons for this are discussed in Sec. 4 of Appendix A. Simply note that the middle envelope always surrenders any and all of its solitons to the other envelopes. (The time reversal of this is in gen-

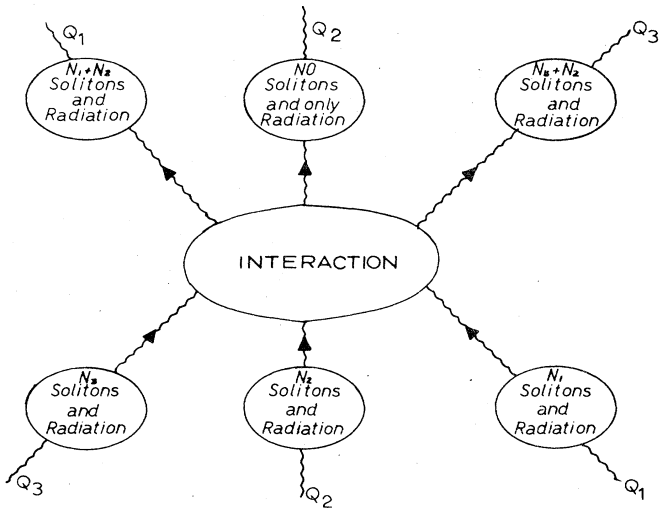

FIG. 1. The manner in which solitons are exchanged in three-wave interactions.

eral unstable.) Thus the existence of any soliton in the middle envelope corresponds to a linear instability (in the nonlinear limit, they are simply "given away"), while the existence of solitons in the fast or slow envelopes does not correspond to any linear instability (thus in the nonlinear limit they are always "retained"), in agreement with the results in Appendix D. Thus, anytime the middle envelope contains solitons, we can expect it to decay, emitting one soliton into the fast and one into the slow envelope, for every soliton which it contained. From the initial scattering data, we can predict the final soliton configuration of the fast and slow envelopes. The mathematical relation between the final eigenvalues in the fast and slow envelopes and initial eigenvalues of the middle envelope is given by (A18). Each of these final eigenvalues is always smaller than the original corresponding eigenvalue from the middle envelope, due to the ordering of the velocities. How we can apply these considerations will be illustrated in each section.

We define "area" as

$$\int_{-\infty}^{\infty} q\,dx\,,$$

where q is the ZS q, and "absolute area," or "modal number," by

$$\int_{-\infty}^{\infty} |q|\,dx\,.$$

This "area" is dimensionless, but since it is simply the total area under the curve $q(x)$, we shall call it nevertheless an area [as is done in nonlinear optics for the 2π pulse of SIT (Kaup, 1977)]. When one can treat the ZS equation by WKB, one then finds a very simple relation existing between the "absolute area" and the number of solitons in a ZS envelope [see Appendix B, Eqs. (B33)–(B35)]. Thus, by simply knowing the number of solitons in a ZS envelope, we can already know something about the absolute area of that envelope. The area of the final envelopes can be calculated precisely if we include some information from the continuous part of the spectrum. Like the area theorem of McCall and Hahn (1967, 1969) in nonlinear optics, all systems which can be solved by the ZS inverse scattering transform do have an "area theorem." This area is simply related to the reflection coefficient of the scattering data at $\lambda = 0$, which is detailed in Appendix B, Eqs. (B27)–(B31). (Recall that the linear Fourier transform at $k = 0$ is equal to the area. The same idea applies here, except the relation is nonlinear.) Then by knowing the relation between the initial and final reflection coefficients of our three envelopes [Eq. (A17)], it is fairly simple to determine the final areas (mod2π) from the initial areas. Applications of these ideas will be illustrated in each section.

For the third piece of information, we look at what is called "action" by plasma physicists. In terms of the ZS q, this action is proportional to

$$\mathfrak{N} \equiv \int_{-\infty}^{\infty} q^* q\,dx$$

(which has units of "inverse length"), which is one of the infinity of conserved quantities associated with the ZS equation (Eq. 2.1) and can be given very simply in terms of the ZS scattering data. In fact, this $\mathfrak{N}$ decomposes linearly into a soliton part, $\mathfrak{N}_s$, and a radiation part, $\mathfrak{N}_r$, as

$$\int_{-\infty}^{\infty} q^* q\,dx = \mathfrak{N} = \mathfrak{N}_r + \mathfrak{N}_s\,, \tag{2.9a}$$

where

$$\mathfrak{N}_s = 2i \sum_{j=1} (\lambda_j^* - \lambda_j)\,, \tag{2.9b}$$

$$\mathfrak{N}_r = \frac{1}{\pi} \int_{-\infty}^{\infty} d\lambda \ln[1 + \Gamma(\lambda)]\,. \tag{2.9c}$$

During an interaction, $\mathfrak{N}$ is exchanged between envelopes, subject to the two well known global conservation laws for the three actions, Eq. (A24). As shown by Eqs. (2.9), the total action can be determined from the bound-state eigenvalues and the radiation density, $\Gamma(\lambda)$. For the time-asymptotic envelopes, since we know how to determine the final eigenvalues (as discussed above), we can readily calculate the final soliton action. Similarly, since we also know how to determine the final scattering data for each envelope from the initial scattering data [Eqs. (A17)], we can also determine the time-asymptotic value of the radiation action for each envelope, and therefore know exactly how much radiation has been exchanged between these envelopes. The mathematical details of these calculations are given in Sec. 4 of Appendix A. The calculation of "soliton action" and "radiation action" for each pulse provides a check on the applicability of the N-soliton formula.

By expressing the quantities (such as areas, action, etc.) describing the behavior of the interaction directly in terms of the scattering data, we circumvent the inverse scattering equations. The only difficult step remaining is that of solving for the scattering data of the initial pulses. Closed-form solutions are easily obtained for square pulses, and the general ZS solution

for a square pulse is given at the end of Appendix B. WKB theory may also be used to calculate approximate scattering data.

D. Symmetric form of the equations

For purposes of the inverse scattering method, it is convenient to transform Eqs. (1.1) to a more symmetric set of equations. To do so, we first rewrite our equations in terms of a_i^* rather than a_i and let $K=|K|e^{i\nu}$, to obtain

$$\left(\frac{\partial}{\partial t}+v_i\frac{\partial}{\partial x}\right)a_i^*=p_i|K|e^{-i\nu}a_j^*a_k^*, \tag{2.10a}$$

$$\left(\frac{\partial}{\partial t}+v_j\frac{\partial}{\partial x}\right)a_j=-p_j|K|e^{-i\nu}(a_i^*)^*a_k^*, \tag{2.10b}$$

$$\left(\frac{\partial}{\partial t}+v_k\frac{\partial}{\partial x}\right)a_k=-p_k|K|e^{-i\nu}(a_i^*)^*a_k^*. \tag{2.10c}$$

Now let

$$Q_i=|K|a_i^*e^{-i\nu/3}, \tag{2.11a}$$

$$Q_j=|K|a_je^{-i\nu/3}, \tag{2.11b}$$

$$Q_k=|K|a_ke^{-i\nu/3}, \tag{2.11c}$$

so that the resulting equations become

$$\left(\frac{\partial}{\partial t}+v_i\frac{\partial}{\partial x}\right)Q_i=p_iQ_j^*Q_k^*, \tag{2.12a}$$

$$\left(\frac{\partial}{\partial t}+v_j\frac{\partial}{\partial x}\right)Q_j=-p_jQ_i^*Q_k^*, \tag{2.12b}$$

$$\left(\frac{\partial}{\partial t}+v_k\frac{\partial}{\partial x}\right)Q_k=-p_kQ_i^*Q_j^*. \tag{2.12c}$$

Finally we let *index 3 correspond to the mode of highest velocity, index 2 to that of next-highest velocity,* and *index 1 to the mode of lowest velocity*; we denote these velocities by c's. We also define $\gamma_i\equiv p_i, \gamma_j\equiv -p_j, \gamma_k\equiv -p_k$, and thus obtain

$$\left(\frac{\partial}{\partial t}+c_1\frac{\partial}{\partial x}\right)Q_1=\gamma_1Q_2^*Q_3^*, \tag{2.13a}$$

$$\left(\frac{\partial}{\partial t}+c_2\frac{\partial}{\partial x}\right)Q_2=\gamma_2Q_1^*Q_3^*, \tag{2.13b}$$

$$\left(\frac{\partial}{\partial t}+c_3\frac{\partial}{\partial x}\right)Q_3=\gamma_3Q_2^*Q_3^*. \tag{2.13c}$$

E. Subscript notations

In the following three sections we treat specific three-wave interactions: the explosive case, the cases with soliton exchange, and the stimulated backscatter. Table I should be useful in relating the different forms of the coupled three-wave equations. The form given by Eqs. (1.1) will be called "plasma notation" while the form given by Eqs. (2.13) will be called "IST notation."

III. THE EXPLOSIVE CASE
$[p_j=p_k=-p_i,\ (v_i-v_j)(v_k-v_i)>0]$

When the energy of the highest-frequency envelope is opposite in sign from that of the other two, the three-wave interaction may develop a singularity in a finite time. Without loss of generality we may take the energy of the high-frequency mode to be negative. We then have

$$(\gamma_1,\gamma_2,\gamma_3)=(-,-,-). \tag{3.1}$$

Explosive behavior appears only if the negative-energy wave has the middle group velocity. Then the ZS q's and r's are given by (A14) as

$$q^{(1)}=\frac{-|K|e^{+i\nu/3}a_j^*}{\sqrt{(c_2-c_1)(c_3-c_1)}},\ r^{(1)}=+q^{(1)*} \tag{3.2a}$$

$$q^{(2)}=\frac{-|K|e^{-i\nu/3}a_i^*}{\sqrt{(c_2-c_1)(c_3-c_2)}},\ r^{(2)}=-q^{(2)*}, \tag{3.2b}$$

$$q^{(3)}=\frac{-|K|e^{+i\nu/3}a_k^*}{\sqrt{(c_3-c_1)(c_3-c_2)}},\ r^{(3)}=+q^{(3)*}, \tag{3.2c}$$

since we have $(i,k,j)=(2,1,3)$.

As is well known, when one ignores the spatial variation in the envelopes, the solution for this case always grows explosively in time (Davidson, 1972). It has also been recognized that when one takes into account the spatial variation this need not occur (Bers, 1975a). A necessary and sufficient condition for stability when $A_1,A_3\ll A_2$ (where A is the area) has been previously derived from an IST analysis (Kaup, 1976a) and deduced from numerical solutions (Reiman *et al.*, 1977). In the WKB limit (slowly varying, real envelopes which never cross zero), this necessary and sufficient condition for stability becomes

$$\bar{A}_2=\int_{-\infty}^{\infty}|q^{(2)}|\,dx<\frac{\pi}{2}, \tag{3.3}$$

TABLE I. Forms of the coupled three-wave equations.[a]

Explosive		Soliton exchange		Stimulated backscatter	
Plasma notation	IST notation	Plasma notation	IST notation	Plasma notation	IST notation
$(i,j,k)=(2,1,3)$		$(i,j,k)=(2,1,3)$		$(i,j,k)=(3,1,2)$	
$p_i=p_j=-p_k;\gamma_1=\gamma_2=\gamma_3$		$p_i=p_j=p_k;\gamma_1=-\gamma_2=\gamma_3$		$p_i=p_j=p_k;\gamma_1=\gamma_2=-\gamma_3$	
$(v_i-v_j)(v_k-v_i)>0;c_1<c_2<c_3$		$(v_i-v_j)(v_k-v_i)>0;c_1<c_2<c_3$		$(v_j-v_i)(v_i-v_k)<0;c_1<c_2<c_3$	
$a_i^*\propto q^{(2)}$		$a_i^*\propto q^{(2)}$		$a_i\propto q^{(3)}$	
$a_j^*\propto q^{(1)}$		$a_j^*\propto q^{(1)}$		$a_j\propto q^{(1)}$	
$a_k^*\propto q^{(3)}$		$a_k^*\propto q^{(3)}$		$a_k\propto q^{(2)}$	

[a] $a_i\equiv$ complex wave amplitudes; $q^{(1)}\equiv$ Zakharov-Shabat potentials.

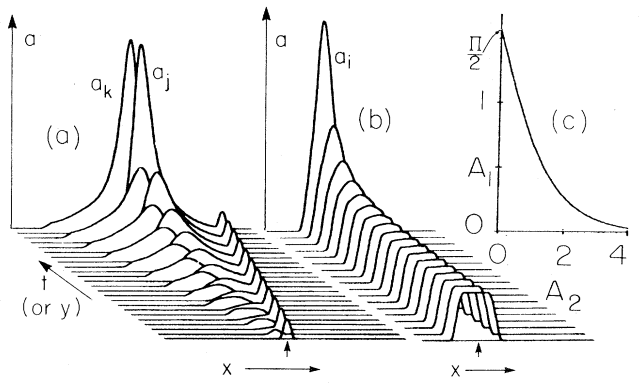

FIG. 2. (a), (b) Explosive interaction with $A_2(t=0)=2.4$, $A_1(t=0)=0.14$, and $A_3(t=0)=0$ in a homogeneous medium. Time step between consecutive plots is $0.3t_c$, with $t_c=1/|Ka_{imax}(t=0)|$; x is in units of $1/|q^{(2)}_{max}(t=0)|$. The evolution of the decay wave packets is shown in (a), and that of the high-frequency wave packet in (b). (c) Explosion threshold in $A_1(t=0)$ and $A_2(t=0)$ for initially nonoverlapping pulses 1 and 2 with $a_k(x,t=0)\equiv 0$. Values above the curve are explosive.

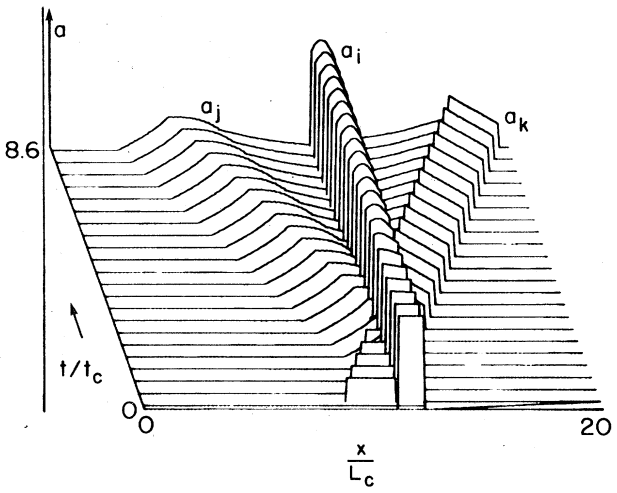

FIG. 3. Collision of initially rectangular pulses in a homogeneous medium: $p_j=p_k=p_i$, $v_i=0$, $v_j=-v_k$, $a_k(x,t=0)=0$, $|a_{jmax}(t=0)|=0.25\,|a_{imax}(t=0)|$, $A_2(t=0)=1.13$, $A_1(t=0)=0.389$. Normalization in terms of $t_c\equiv 1/|Ka_{imax}(t=0)|$ and $L_c\equiv 1/|q^{(2)}_{max}(t=0)|$.

where $\bar{A}$ is the absolute area. If this condition is violated, then singular spikes will develop.

Figure 2 shows a numerical solution for such an explosive interaction for $A_2(t=0)=2.4>\pi/2$. Note the initial buildup of the normal modes in Fig. 2(a). The modification of a_i remains small until a_j and a_k become comparable to it in amplitude. The instability then proceeds very rapidly. This contrasts sharply with Fig. 3, where the interaction is dying away. Here $A_2(t=0)=1.13<\pi/2$.

As discussed in Appendix A, whenever the middle envelope has N_2 solitons ($N_2\geq 1$), then after any interaction with either $q^{(1)}$ or $q^{(3)}$ (even a perturbation), both the fast and the slow envelope must each contain exactly N_2 solitons (see Fig. 1). But due to (3.2), $r=+q^*$ for both the fast and the slow envelope, which if (B1) is to be satisfied, forbids these envelopes from having any solitons! Thus from the IST method, clearly either (B1) must be violated for the final envelopes or the envelopes do not separate. As seen in Fig. 2, numerical solutions show that (B1) is violated by the formation of a singularity in a finite time, and also that the envelopes do not separate. Further analysis of the IST method does suggest a singular solution. To show this, one simply solves Eqs. (B11)–(B14) for the case of $r=+q^*$, retaining only a soliton term (bound state) in (B11). Solving these equations then gives the one-soliton solution for this case as being the same as Eq. (B20a), but with cosh replaced by a sinh. Thus the solution is expected to be singular as $t\to+\infty$.

Thus a necessary condition for stability is that the middle envelope must not initially contain solitons. As discussed in Appendix D, this is equivalent to requiring the stability of the linear equations (1.3). This condition is also sufficient, as we shall see, when $A_1, A_3 \ll A_2$. With the WKB approximation to the solution of the corresponding ZS equations (Appendix B, Sec. 6), this condition reduces to Eq. (3.3). A sufficient (but not necessary) criterion for infinitesimal stability regardless of whether the WKB approximation is valid is (Ablowitz *et al.*, 1974)

$$\bar{A}_2<0.903\,. \tag{3.4}$$

Our computer simulations show formation of only a single spike during the explosion, regardless of the number of initial modes or solitons. The position of that spike can be determined approximately for arbitrarily shaped pumps by solving for the WKB amplitudes $a_j(x)e^{\rho t}$, $a_k(x)e^{\rho t}$, for the fastest-growing mode, and finding where $a_j(x)a_k(x)$ is a maximum.

Requiring the middle envelope to contain no solitons is not sufficient to give stability against finite perturbations of a_j or a_k. Figures 3 and 4 are plots of numerical solutions for $A_2(t=0)<\pi/2$. The interaction of Fig. 4 is nevertheless explosive. By the time the initial a_i pulse has passed through a_k, A_2 has been increased above $\pi/2$. The tails of a_k and a_j then grow up in a normal mode pattern, leading to an explosion.

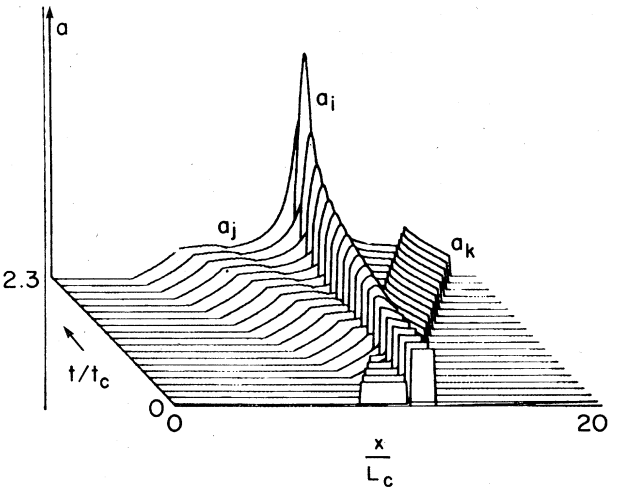

FIG. 4. Same as Fig. 3 except $|a_{jmax}(t=0)|=0.35\,|a_{imax}(t=0)|$, $A_1(t=0)=0.545$.

This contrasts with Fig. 3. There, after the initial a_i pulse has passed through a_k, the tails of a_i and a_k inside the interaction region simply die away.

To calculate the nonlinear threshold for explosive behavior, note that condition (B26e) is satisfied by the $\Gamma_f^{(3)}$ of (A22a) only when

$$\frac{1}{1+\Gamma_0^{(1)}}+\frac{1}{1+\Gamma_0^{(2)}}+\frac{1}{1+\Gamma_0^{(3)}}\geq 2+2\,\mathrm{Re}\Sigma_0 . \tag{3.5}$$

This follows by requiring the denominator of (A22a) to be positive definite. If this is violated, it follows that one of our initial assumptions must be violated; either the wave packets become nonintegrable as $t\to\infty$, or the overlap of wave packets does not go to zero at $t\to\infty$. In fact, we find from our numerical solutions that whenever (3.5) is violated, the interaction is explosive.

Thus we conclude that if an explosive spike is to be avoided in the explosive case, (i) the middle envelope must contain no solitons (or linear instabilities), *and* (ii) condition (3.5) must be satisfied by the initial data. This is a necessary and sufficient condition for *nonlinear* stability. Note that whenever one of the Γ_0's is zero, Σ_0 then vanishes.

If one takes the fast (middle) ZS envelope to be a square pulse of amplitude $Q_3(Q_2)$, of width $L_3(L_2)$, and the slow envelope zero initially, then the corresponding Γ_0's from Eqs. (2.5), (B38), and (B39) are

$$\Gamma_0^{(3)}=Q_3^2\left[\frac{\sin\Delta_3 L_3}{\Delta_3}\right]^2, \tag{3.6a}$$

$$\Gamma_0^{(2)}=\frac{Q_2^2\sin^2\Delta_2 L_2}{(\lambda^{(2)})^2+Q_2^2\cos^2\Delta_2 L_2}, \tag{3.6b}$$

$$\Gamma_0^{(1)}=0, \tag{3.6c}$$

where

$$\Delta_3^2=(\lambda^{(3)})^2-Q_3^2, \tag{3.7a}$$

$$\Delta_2^2=(\lambda^{(2)})^2+Q_2^2, \tag{3.7b}$$

with $\lambda^{(3)}$ and $\lambda^{(2)}$ given by Eq. (A14). If we choose Eq. (3.3) to be satisfied, then for $Q_2L_2=A_2<\pi/2$, and at $\zeta=0=\lambda^{(3)}=\lambda^{(2)}$, Eq. (3.5) requires that

$$\sinh^2 A_3\leq\cot^2 A_2, \tag{3.8}$$

where $A_3=Q_3L_3$. A plot of these critical values is shown in Fig. 2c. Thus, if we choose $A_2=1.133<\pi/2$, then the critical value of A_3 is 0.452. [For $A_2=1.133$ and for $A_3<0.452$, Eq. (3.5) is satisfied for all values of ζ, while if A_3 is just above 0.452, Eq. (3.5) is violated only for a corresponding range of ζ about zero.] The computer runs for Figs. 3 and 4 have $A_2=1.133$ and $A_3=0.389$ and 0.545, respectively.

Finally, we also note that for Fig. 3 we can compare the area theorem and the transfer of action as given by simulation and theory. From Eqs. (A17), (3.2), (B29), and (B31), we have

$$\tanh A_{3f}=\tanh A_{30}/\cos A_{20}, \tag{3.9a}$$

$$\tan A_{2f}=\cosh A_{3f}\tan A_{20}, \tag{3.9b}$$

$$\tanh A_{1f}=-\tan A_{20}\sin A_{30}, \tag{3.9c}$$

for $A_{10}=0$. We find good agreement between the theory and our numerical results.

The action transfer, we simply use Eqs. (3.2), (A22a), and (2.9). Then

$$\int_{-\infty}^{\infty}[|q_f^{(3)}|^2-|q_0^{(3)}|^2]\,dx=\frac{1}{\pi}\int_{-\infty}^{\infty}d\lambda^{(3)}\ln\left(\frac{1}{1-\Gamma_0^{(3)}\Gamma_0^{(2)}}\right). \tag{3.10}$$

This gives the final actions in Fig. 3.

IV. THE SOLITON EXCHANGE INTERACTIONS $[p_i=p_j=p_k\ ,(v_i-v_j)(v_k-v_i)>0]$

For this case, where the highest frequency has the middle group velocity and the energies are all positive, we have

$$(\gamma_1,\gamma_2,\gamma_3)=(-,+,-) \tag{4.1a}$$

or

$$(p_i,p_j,p_k)=(+,+,+), \tag{4.1b}$$

so that by (A14),

$$q^{(1)}=\frac{+|K|e^{i\nu/3}a_j^*}{\sqrt{(c_2-c_1)(c_3-c_1)}},\ r^{(1)}=-q^{(1)*}, \tag{4.2a}$$

$$q^{(2)}=\frac{-|K|e^{-i\nu/3}a_i^*}{\sqrt{(c_2-c_1)(c_3-c_2)}},\ r^{(2)}=-q^{(2)*}, \tag{4.2b}$$

$$q^{(3)}=\frac{+|K|e^{i\nu/3}a_k^*}{\sqrt{(c_3-c_1)(c_3-c_2)}},\ r^{(3)}=-q^{(3)*}, \tag{4.2c}$$

where $(i,j,k)=(2,1,3)$. Since from Eq. (4.2), $r=-q^*$ for all three envelopes, all envelopes may contain solitons. The general soliton exchange results for both decay and collisions can be seen from Fig. 1; the high-frequency mode invariably loses solitons to the other modes. Furthermore, one can easily show that the ZS inverse scattering equations (B12) for this case always have a unique solution, and that the envelopes will always separate asymptotically as $t\to\infty$ (Ablowitz *et al.*, 1974). This follows from the fact that there are no restrictions on the magnitudes of the final b/a's in (A17), and thus (B1) will be satisfied for the final envelopes. Consequently, in this case, we expect no singularities ever to develop as in the explosive case. There are two types of initial conditions of interest here, (i) decay of the middle envelope (pump), and (ii) collision of the fast and slow envelopes.

A. Soliton decay

1. Small perturbations

First we consider the decay of the high-frequency pump when it is perturbed by a small amount of the slow envelope, a_j. The initial development of the system can be described by the set of equations (1.3) obtained by linearizing in the initially small amplitudes a_j, a_k. The behavior of the interaction is determined by the normal mode structure that develops before the nonlinear regime is entered. This means that the general character of the solution to the equations in this case should be determined by the number of initial growing normal modes. The WKB criterion for having exactly N normal modes in the pump when a_i is a pulse with only one internal extremum is

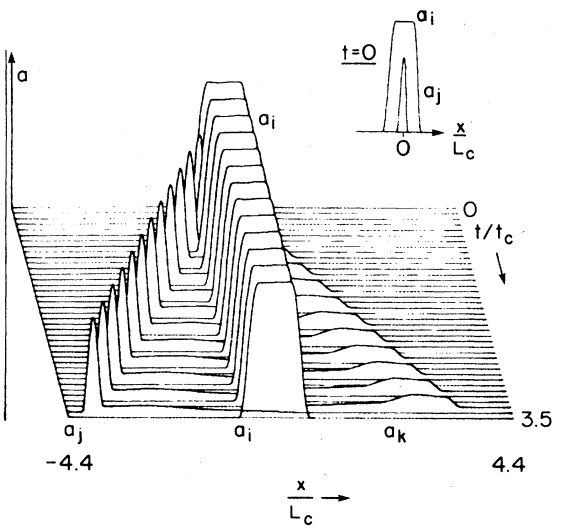

FIG. 5. Interaction in reference frame with $v_i = 0$; $v_j = -v_k$, $\int_{-\infty}^{\infty} dx\,|K\,a_i(x,t=0)| / |(v_j - v_i)(v_i - v_k)|^{1/2} = 1$, $a_k(x,t=0) \equiv 0$. Normalization in terms of $t_c \equiv 1/|Ka_{imax}(t=0)$ and $L_c \equiv 1/|q^{(2)}_{max}(t=0)|$. Reference frame fixed by $v_i = 0$.

$$(N - \tfrac{1}{2})\pi \leq \bar{A}_i \leq (N + \tfrac{1}{2})\pi\,, \tag{4.3}$$

where $\bar{A}_i$, the absolute "area" of the high-frequency pump, is

$$\bar{A}_i = \bar{A}_2 = \int_{-\infty}^{\infty} |q^{(2)}(x, t=0)|\,dx\,. \tag{4.4}$$

This condition is the same as that for the existence of N solitons in the pump, as discussed in Appendix D. The criterion is exact for a square pump.

Our numerical results show that, again, when there are no initial normal modes, little happens (Fig. 5). But the presence of growing normal modes now leads to pump depletion, instead of an explosive singularity (Figs. 6, 7). The nonlinear interaction between the pump

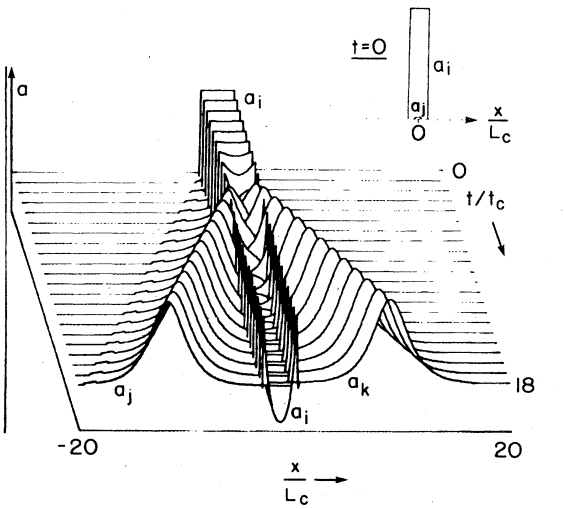

FIG. 6. Interaction of initially rectangular pulses with $v_j - v_i = v_i - v_k$, $p_i = p_j = p_k$, $l_1/l_c = 3.25$, $|a_{j\,max}(t=0)| / |a_{i\,max}(t=0)| = 0.02$. Reference frame chosen with $v_i = 0$. Normalization as in Fig. 5. (a) Amplitudes at $t = 0$. (b) Initial mode buildup. (c) First pair of pulses emerging from flipped pump. (d) Mode buildup in flipped pump.

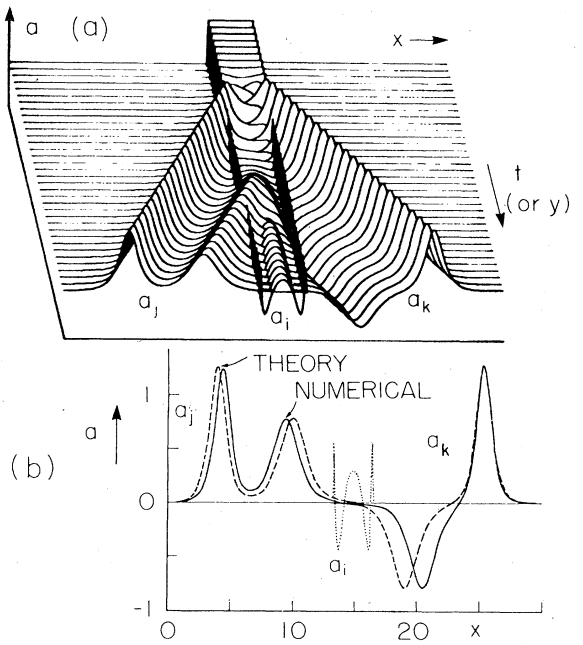

FIG. 7. (a) The interaction differs from that shown in Fig. 6 only in that $l_i/l_c = 6.4$ and $|a_{j\,max}(t=0)| / |a_{i\,max}(t=0)| = 0.002$. Interaction run to $t = 28t_c$. (b) The time-asymptotic profiles obtained numerically for (a) are superimposed on the prediction of the two-soliton formula.

and each growing mode leads, in our computer simulations, to the emission of a pair of pulses (one fast and one slow) from the interaction region. Once a given pair is emitted, they of course simply propagate along their own characteristics without any further amplitude changes. And the number of pairs of pulses emitted is always equal to the number of initial normal modes in the pump. After all of these pulses are emitted, the high-frequency pulse is left with a small nonzero amplitude, not large enough to sustain a normal mode.

The solutions of the spatially independent equations for this case are periodic in time. Some remnant of that periodicity is seen, in that a sufficiently large pump will flip its sign due to the nonlinear interaction with the other two modes.

In Figs. 5–7, we show graphs of the time (spatial) development of the wave amplitudes from three different sets of initial conditions. The initial pulse profiles are shown alongside in Figs. 5 and 6. The initial perturbation for Fig. 7 was too small to be visible in such a plot. In these three runs the pulse profiles are initially rectangular.

For Fig. 5, $A_2(t=0) < \pi/2$. After the initial perturbation leaves wave packet 2, its tail simply decays away.

Figure 6 shows an interaction when there is initially one growing normal mode. Mode buildup leads to depletion of the pump and subsequent emission of a pair of pulses. The interaction has now gone to completion. Decaying tails of the emitted pulses are all of waves 1 and 3 that remain in the interaction region. Wave packet 2 is no longer capable of sustaining growing normal modes of the linearized equations (3). Note that the initial a_j perturbation is visible on the tail of the emitted a_j pulse.

During the course of the interaction shown in Fig. 6, wave packet 2 flips, being pushed into the negative by the interaction with waves 1 and 3. Our computer runs show that as $A_2(t=0)$ is made larger, $A_2(t\to\infty)$ goes more negative, until the flipped a_i has an area of $\pi/2$ and is itself capable of supporting growing normal modes. This transition takes place exactly at the point where a_i can initially support two growing normal modes. An interaction with two initial growing normal modes is shown in Fig. 7. Two pulses are eventually emitted from the interaction region (these are filaments in a 2-D steady-steady interpretation). Because the pump has flipped, the relative sign of the second pair of emitted pulses is opposite that of the first pair of pulses.

Turning now to the inverse scattering solution for this case, we find that these simulation results can be explained also in terms of IST concepts. First, we consider the final envelope shapes of the two low-frequency pulses and show that they are essentially exact N-soliton solutions. This can be seen from Eq. (A17) as follows. Take $b_0^{(1)}=o(\epsilon)$ with ϵ small, $b_0^{(3)}=0$, and we have for real values of the eigenvalue λ, $b_f^{(3)}=o(\epsilon)$ and $b_f^{(1)}=o(\epsilon)$. Thus as the perturbation is made smaller and smaller, $(\epsilon\to 0)$, both $b_f^{(3)}$ and $b_f^{(1)}$ vanish for real values of λ, which is the definition of an N-soliton solution. Only the discrete part of the spectrum then remains in the daughter waves [(B11) with $p=0$].

In fact, with $q_0^{(2)}$ as a square pulse, it is possible to determine exactly the scattering data for the final envelopes in the limit of $q_0^{(1)}\to 0$. This we shall now proceed to do, as well as to show how well this analytical result agrees with numerical solution of the equations. Let $q_0^{(2)}$ be a square pulse of area A_2 and width L, take $c_1=-c_3$, $c_2=0$, and let $q_0^{(1)}$ be a small symmetric blip centered at a distance l from the left edge of $q_0^{(2)}$, as shown in Figs. 5 and 6. First, one determines the number and values of the bound-state eigenvalues for the middle envelope (pump) by using ZS eigenvalue problem of Eqs. (2.1). The eigenvalues are given by the common solution of

$$k^2+\kappa^2=A_2^2, \tag{4.5a}$$

$$\kappa=-k\cot k, \tag{4.5b}$$

where the eigenvalues are

$$\lambda_j^{(2)}=i\kappa/L\ \ (j=1,2,\ldots N), \tag{4.6}$$

and N is the total number of solutions of Eq. (4.5). (See Appendix B.6.) Then by Eq. (A18), the eigenvalues for the bound states contained in the fast and slow final envelopes will be given by

$$\lambda_j^{(1)}=\lambda_j^{(3)}=\tfrac{1}{2}i\kappa_j/L\ \ (j=1,2,\ldots N). \tag{4.7}$$

Lastly, we need the D_j's to construct the N-soliton solution (B19). D_j is $-i$ times the residue of b/a at the jth eigenvalue. From Eqs. (A9) and (A16) it follows that

$$\frac{b_f^{(3)}(\zeta)}{a_f^{(3)}(\zeta)}=-\left(\frac{a_{12}}{a_{11}}\right)^*(\zeta^*). \tag{4.8}$$

The scattering data a_{12}, a_{11} are calculated from (A5) for $q_0^{(1)}$ infinitesimal. Taking into account the time dependence, (A11), we find for $c_1=-c_3$, $c_2=0$ that

$$D_j^{(3)}=-(-)^j\frac{k_j\sin(k_jl/L)}{2L(1+\kappa_j)}\hat{q}^{(1)}\left(\frac{k_j}{L}\right)\times\operatorname{sgn}(q_0^{(2)})\exp\left(\frac{\kappa_j(L_++c_3l)}{L}\right), \tag{4.9}$$

where $k_j=\sqrt{A_2^2-\kappa_j^2}$, L_+ is the right edge of $q_0^{(2)}$, and

$$\hat{q}^{(1)}(\gamma)=\int_{-\infty}^{\infty}q_0^{(1)}(x)e^{-i\gamma x}dx\,. \tag{4.10}$$

With Eqs. (4.5), (4.7), and (4.9) we have all the information required for calculating the N-soliton solution $a_k(x,t\to\infty)$ from Eq. (B19). (See Appendix B.4 for a description of this calculation.) Similar calculations give $a_j(x,t\to\infty)$. The resulting theoretical predictions have been superimposed on our numerical solutions for the wave amplitudes in Fig. 7(b). There is a noticeable error in the predicted separation of solitons. This is due to the fact that we have calculated the D's perturbatively, to first order in q_1. A similar plot for the interaction of Fig. 6 reveals no such discernible discrepancy.

In summary, the IST method can give us the final configurations directly from the initial data for the decay of a high-frequency pump. Of course, Eqs. (4.5), (4.7), and (4.9) are only valid when $q_0^{(1)}$ is infinitesimal, but we should remark that for both $q_0^{(2)}$ and $q_0^{(1)}$ as square pulses it is possible to obtain closed-form analytic solutions of Eq. (A5), which would then give us an expression for $D_j^{(3)}$ valid for finite $q_0^{(1)}$. However, we have not done this, due to the complexity of that result. We also point out that, from the initial scattering data, we can calculate the amount of radiation action which is transferred [Eqs. (2.9) and (A22)], and it is well below the numerical noise level in each case. Corresponding to Figs. 6 and 7, the final actions of the a_k envelope in the numerical solutions are 1.389 and 5.863, respectively. From the IST theory [Eq. (2.9)], the values for these soliton actions are 1.388 and 5.865, giving us agreement to within the accuracy of the numerical solution. Moreover the theory shows that these final actions are independent of the D_j's, so the errors arising from the perturbative calculation of D_j have no effect here.

Finally, we note one property of Eq. (4.8) which has not been brought out by the solutions shown in Figs. 5–7, and that is the dependence of D_j on where the initial a_j perturbation is positioned. If $l=L$, since $(-)^{j+1}\sin k_j>0$, all the $D_j^{(3)}$'s would then have the same sign, which would give an N-soliton state which never crosses zero. But for $0<l<L$, the $D_j^{(3)}$'s can have different signs, giving an N-soliton solution crossing zero. In all these simulations, we have taken $l=L/2$, so, as shown in Fig. 7, we have an N-soliton solution crossing zero. The only things which l will affect are the relative phases and the time delay for the emergence of a soliton. For example, if for some j, $k_jl\simeq L\pi$, then $D_j^{(3)}\simeq 0$, which would cause this soliton to be strongly delayed. [The delay time is proportional to $\ln[1/D_j^{(3)}]$. See Eq. (B18).] At $k_jl=L\pi$, $D_j^{(3)}\simeq 0$, which corresponds to an infinite delay time. But in any simulations this would be reduced to a finite value by truncation and round-off errors (since the pump is still unstable). It is also interesting to note that the decay of the pump tends to occur in "quantum jumps." By WKB, as the initial

area of the pump passes through each value of $(n+\frac{1}{2})\pi$, the final areas of each of the fast and slow envelopes jump by $\pm\pi$, while the final area of the pump also changes by $\pm\pi$.

Although we have only discussed soliton decay in the presence of a definite, finite (although small) slow wave, one can also treat the case of an unstable pump ($A_2 > \pi/2$) in the presence of fast and/or slow wave random noise. This is more the physical situation, in that such a decay is more likely to be started by random noise than by any small definite perturbing wave. Assuming the random noise to be an infinitesimal perturbation on the pump, one can use a perturbation expansion to determine how the addition of noise to the problem affects the scattering data. Similar ideas have been used by Kaup (1976b) and Kaup and Newell (1978) in investigating the effects of various perturbations on soliton solutions. Here, if we start off with an unperturbed pump, nothing happens. It doesn't decay until some perturbation is applied. Usually, in the physical situation, this perturbation will be in the form of noise, and if so, now the pump can decay. To determine how long it will take the pump to decay, we simply look at the averaged (with respect to the noise) scattering data of the final ZS envelopes, by determining how the initial noise levels will affect it. This is done in Appendix F, with the final result being given by Eq. (F32). In the special case where $c_1 = -c_3$, $c_2 = 0$, this result reduces to

$$\tau_N = \frac{1}{2\eta_1 c_3} \ln\left(\frac{\frac{1}{4}\eta_1}{E_1^2 + E_3^2}\right),$$

where τ_N is the lifetime due to noise, η_1 is the initial soliton amplitude of the pump, and E_1 and E_3 are the rms average noise amplitudes for q_1 and q_3. Note the logarithmic dependence of τ_N on E_1 and E_3. This is what one would expect, in that $\tau_N \to \infty$ as E_1 and $E_3 \to 0$, while $\tau_N \to 0$ as E_1 or E_3 becomes large.

2. Large perturbations: Two pumps

As shown above, when the pump is infinitesimally perturbed, only the energy contained in the soliton part of the spectrum can be released, and not the energy in the radiation part of the spectrum. However, if we cause a large wave (either $q^{(1)}$ or $q^{(3)}$) to collide with the pump, a large fraction of the energy contained in the radiation spectrum of the pump can be released. To show this, we consider the collision of $q^{(1)}$ with the pump $q^{(2)}$, when $q^{(1)}$ is large. From Eq. (A20), upon setting $\Gamma_0^{(3)} = 0$, we obtain the final radiation densities for $q_f^{(3)}$ and $q_f^{(2)}$,

$$\Gamma_f^{(3)} = \frac{\Gamma_0^{(1)}}{1+\Gamma_0^{(1)}} \Gamma_0^{(2)}, \tag{4.11a}$$

$$\Gamma_f^{(2)} = \frac{\Gamma_0^{(2)}}{1+\Gamma_0^{(1)}(1+\Gamma_0^{(2)})}. \tag{4.11b}$$

Now in Figs. 5–7, $\Gamma_0^{(1)}$ was very small, so that $\Gamma_f^{(3)}$ was also small and $\Gamma_f^{(2)} \simeq \Gamma_0^{(2)}$. But, if we now take $\Gamma_0^{(1)}$ to be large (at least over the region where $\Gamma_0^{(2)}$ is essentially nonzero), then Eq. (4.11) becomes

$$\Gamma_f^{(3)} \simeq \Gamma_0^{(2)}, \tag{4.12a}$$

$$\Gamma_f^{(2)} \simeq 0, \tag{4.12b}$$

showing that almost all of the radiation energy can be taken out of the pump.

To have $\Gamma_0^{(1)}$ large, since $\Gamma = |b/a|^2$, we take $A_1 = \pi/2$ (or $3\pi/2$, $5\pi/2$, etc.) so that at $\zeta = 0$, $\Gamma_0^{(1)} = \infty$ [see Eq. (B29)]. Then to have $\Gamma_0^{(1)}$ broad, so that it remains large over the region where $\Gamma_0^{(2)}$ is essentially nonzero, we want the pulse width of $q^{(1)}$ to be small. An example of this situation is shown in Fig. 8, where $A_1 = 1.571 \cong \pi/2$ and $q^{(2)}$ is exactly the same profile as in Fig. 6. In Fig. 6, the action (total radiation) left in the pump is 0.474, while in Fig. 8, only 0.145 remains. Of course in this case the pump was already unstable, since $A_2 = 3.25 > \pi/2$. But the same can also be done for a smaller pump; when it collides with a narrow pulse with $A_1 \simeq \pi/2$, most of the radiation energy can also be extracted from the pump.

One interesting feature in Fig. 8 is the profile of $q^{(3)}$, which is almost a square pulse except for the ramp-like edges. This shape can be deduced from Eq. (A17a) upon setting $a_0^{(3)} = 1$ and $b_0^{(3)} = 0$, which gives

$$\frac{b_f^{(3)}}{a_f^{(3)}} = \overline{b}_0^{(1)} \frac{b_0^{(2)}}{a_0^{(2)}} \exp(-2i\lambda^{(3)} c_3 t). \tag{4.13}$$

Now, for $q_0^{(1)}$ as a narrow pulse, when we use Eq. (B39) (since $\overline{b} = b^*$), we have for $\lambda^{(1)}$ not too large and as $L \to 0$,

$$\overline{b}^{(1)}(\lambda^{(1)}) \simeq +(\sin A_1) \exp[+i\lambda^{(1)}(l_+^{(1)} + l_-^{(1)})]. \tag{4.14}$$

Since in this case $\lambda^{(3)} = \lambda^{(1)} = (1/2)\lambda^{(2)}$, if we let $\lambda = \lambda^{(3)}$, then

$$\frac{b_f^{(3)}(\lambda)}{a_f^{(3)}(\lambda)} \cong \sin A_1 \exp[i\lambda(l_+^{(1)} + l_-^{(1)} - 2c_3 t)] \frac{b_0^{(2)}(2\lambda)}{a_0^{(2)}(2\lambda)}. \tag{4.15}$$

We ignore the phase factor which corresponds to a simple translation. If $b(\lambda)/a(\lambda)$ is the "reflection coefficient" for $q(x)$, then $b(2\lambda)/a(2\lambda)$ is the reflection coefficient for $\frac{1}{2}q[(1/2)x]$ [for example, see Eqs. (B38) and (B39)]. Thus if $A_1 = \pi/2$, Eq. (4.15) then shows that

$$q_f^{(3)}(x) = \tfrac{1}{2} q_0^{(2)}(\tfrac{1}{2}x), \tag{4.16}$$

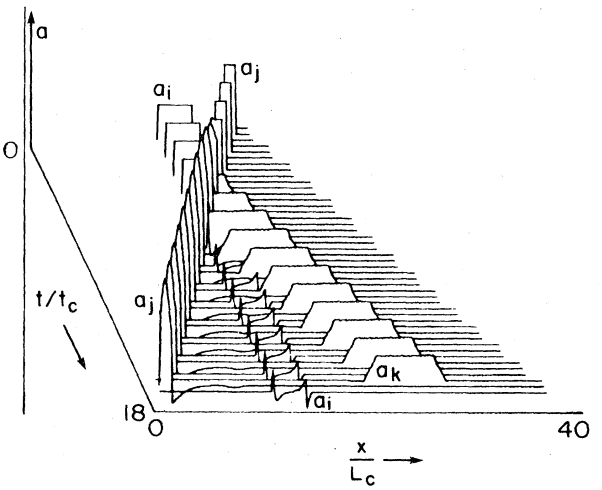

FIG. 8. Binary collision of initially rectangular pulses with $v_i = 0$, $v_j = -v_k$, $A_2(t=0) = 3.25$, $A_1(t=0) = \pi/2$, $|a_{j\max}(t=0)|/|a_{i\max}(t=0)| = 2$.

in the limit of $q^{(1)}$ approaching a delta function of area $\pi/2$. Note that this provides a means of transferring any arbitrary shape of $q_0^{(2)}$ to $q_f^{(3)}$, with the scaling factors being dependent only on the ratios of the relative velocities. The more general relation, for arbitrary velocities, is

$$q_f^{(3)}(x) = \frac{c_2 - c_1}{c_3 - c_1} q_0^{(2)} \left(\frac{c_2 - c_1}{c_3 - c_1} x \right) . \tag{4.17}$$

These results can also be established directly from the three wave equations (1.1). For $|a_{j\max}(t=0)|$ sufficiently large, depletion of a_j by the interaction may be neglected, and the three wave equations (1.1) describing the evolution of a_i and a_k actually become linear. We work in the reference frame in which $v_j = 0$. If $L_i \ll a_i(\partial a_i/\partial x)^{-1}$ then a quasisteady state is established in the interior of a_j and we may in addition neglect $\partial a_i/\partial t$ and $\partial a_k/\partial t$. Suppose that a_j is moving to the left, with $a_i = a_{i0}$ on its left boundary, $x = l_-$. Then the solution in the interior of a_j is

$$a_i(x) = a_{i0} \cos \left(\frac{|K|}{|v_i v_k|^{1/2}} \int_{l-}^{x} |a_j(x)|\, dx \right) \tag{4.18}$$

$$a_k(x) = -\left| \left(\frac{v_i}{v_k} \right) \right|^{1/2} a_{i0} \sin \left(\frac{|K|}{|v_i v_k|^{1/2}} \int_{l-}^{x} |a_j(x)|\, dx \right) . \tag{4.19}$$

If $A_1 \approx \pi/2$, then Eq. (4.18) gives complex action transfer and (4.19) gives just (4.16). However, if a_i and a_k are both nonzero after passing through the initial a_j pulse, they continue to interact. The interaction is then nonlinear and we must resort to our IST analysis.

Note that in Fig. 8 the linear approximation is not valid, a_j being strongly affected by the interaction. Nevertheless, a_i is almost entirely depleted by the interaction and has its initial shape well replicated.

B. Upconversion

We now consider the collision of a fast and a slow envelope. When the initial ZS areas are small, there is little action transfer. Such a weakly nonlinear collision is shown in Fig. 9. Since depletion of the colliding pulses is small, the generated middle envelope is well described by a convolution of the initial fast and slow envelopes. Thus, with the initially rectangular pulses of Fig. 9, a triangular middle pulse is formed.

Before continuing with the other simulations, we show how to calculate the final areas and actions from the initial profiles. Those that we have checked agree well with the simulations. From Eqs. (A17) and (B29), we have for $A_{20} = 0$,

$$\tan A_{1f} = \cos A_{30} \tan A_{10} , \tag{4.20a}$$

$$\tan A_{2f} = \cos A_{3f} \sin A_{10} \tan A_{30} , \tag{4.20b}$$

$$\tan A_{3f} = \cos A_{10} \tan A_{30} . \tag{4.20c}$$

We supplement these equations with the information contained in Eq. (B32), where the signs of the respective cosines are determined by the number of solitons contained in each envelope. This then allows us to calculate the final areas of all pulses in Figs. 9–12. Note that by Eq. (4.2b), the sign of $q^{(2)}$ is opposite to that of a_i (the high-frequency pump) in Figs. 9–11.

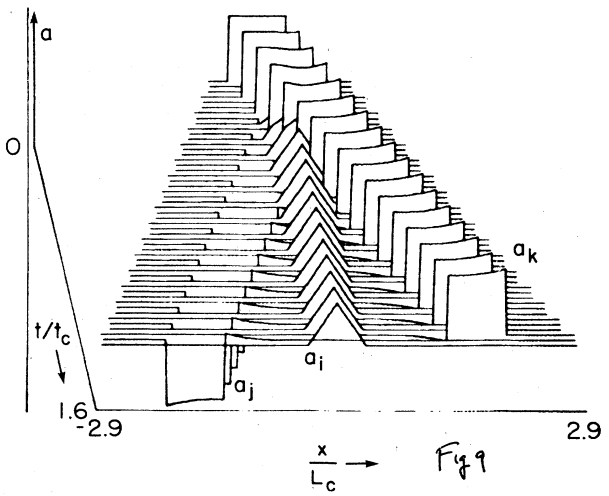

FIG. 9. Binary collision of initially rectangular pulses: $p_i = p_j = p_k$, $v_i = 0$, $v_j = -v_k$, $|a_{j\max}(t=0)| = |a_{k\max}(t=0)|$, $A_1(t=0) = A_3(t=0) = 0.485$. Normalization in terms of $t_c \equiv 1/|Ka_{j\max}(t=0)|$ and $L_c \equiv 1/|q_{\max}^{(1)}(t=0)|$.

For calculating the action transferred, we need to know only the initial bound-state eigenvalues and the initial Γ's as has been discussed in Sec. II. The radiation part of the action is given by Eq. (2.9c) with $\lambda = \lambda^{(2)}$. One can obtain $\Gamma_f^{(2)}(\lambda)$ from Eq. (A20a), since by (A23b) and (B26d) we have

$$1 + \Gamma_f^{(2)} = \frac{1 + \Gamma_0^{(3)}}{1 + \Gamma_f^{(3)}}$$

so

$$\Gamma_f^{(2)}(\lambda) = \frac{\Gamma_0^{(3)}(1/2\,\lambda)\Gamma_0^{(1)}(1/2\,\lambda)}{1 + \Gamma_0^{(3)}(1/2\,\lambda)\Gamma_0^{(1)}(1/2\,\lambda)} , \tag{4.21a}$$

where since $c_2 = 0$, $c_1 = -c_3$, from Eq. (A14), $\lambda^{(1)} = \lambda^{(3)} = 1/2\lambda^{(2)}$. For $\nu = 1$ or 3 and square envelopes, from Eqs. (B37)–(B38) and (B26d),

$$\Gamma_0^{(\nu)}(\lambda) = \frac{A_{\nu 0}^2 \sin^2(k_\nu)}{k_\nu^2 - A_{\nu 0}^2 \sin^2(k_\nu)} , \tag{4.21b}$$

where

$$k_\nu^2 = L_\nu^2 \lambda^2 + A_{\nu 0}^2 , \tag{4.21c}$$

and $A_{\nu 0}$ and L_ν are the initial areas and lengths of the two envelopes. Equation (2.9c) is then evaluated by quadrature. For the soliton part of $\mathfrak{N}$, we simply solve Eqs. (B41)–(B42) for λ and substitute in Eq. (2.9b). The ZS action is then simply the sum of these two contributions, as given by Eq. (2.9a).

Let us now return to the simulations. In Fig. 10, the generated middle pulse is no longer a convolution of the initial envelopes; it is a slightly distorted triangle. Depletion of the colliding pulses is just beginning to be important. Here the initial pulses have ZS areas just below $\pi/2$.

The initial areas in Fig. 11 are well above $\pi/2$. A large spike is now generated by the collision, and subsequently decays as described in Sec. IV A. The initial colliding pulses are almost completely depleted, with most of their energy transferred into the soliton tail.

This spike formation can also be understood in terms

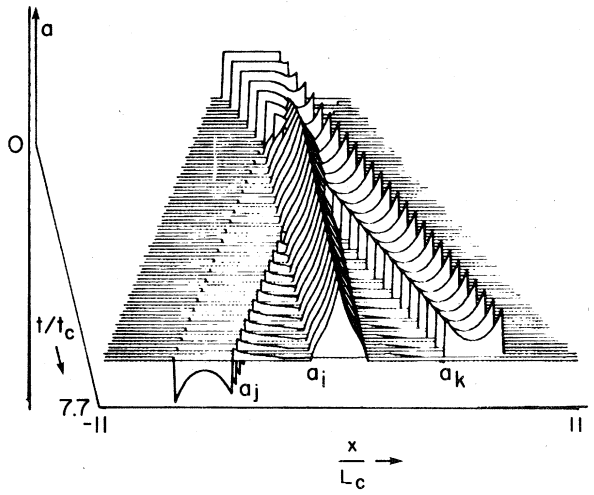

FIG. 10. Same as previous figure except that $A_1(t=0)=A_3(t=0)=1.82$.

of the IST theory. In the collision of Fig. 11, we have the time reversal of the soliton exchange shown in Figs. 6 and 1. Whenever there are solitons in the fast and slow envelopes which are resonantly paired (as is the case in Fig. 11) according to

$$\lambda_j^{(1)}(c_2-c_1)=\lambda_j^{(3)}(c_3-c_2)\,, \tag{4.22}$$

then each of these resonantly paired eigenvalues can be transferred to the middle envelope, giving it an additional soliton of eigenvalue

$$\lambda_j^{(2)}=\frac{c_3-c_1}{c_3-c_2}\lambda_j^{(1)}\,. \tag{4.23}$$

This eigenvalue is larger in magnitude than either $\lambda_j^{(1)}$ or $\lambda_j^{(3)}$, and consequently during the collision, when this exchange takes place, one can expect to see the middle pulse rise dramatically, and to become higher and narrower than the initial envelopes (See Fig. 11). We find that when such a spike forms in our numerical solutions, the overlap between envelopes becomes small for at least a short time. Thus we can analyze this situation in terms of the ZS envelopes. The spatial ordering of the envelopes is the same as in the final configuration. In doing this analysis, we must recognize that the only difference between this intermediate state and the final state is the way in which the solitons are distributed between the envelopes. In particular, after this intermediate state is created, no more significant radiation density is exchanged. Letting i designate this intermediate time, we find that

$$\Gamma_i^{(2)}=\Gamma_f^{(2)}\,, \tag{4.24}$$

with $\Gamma_f^{(2)}$ given by Eq. (4.21b). Taking the number of solitons in the intermediate envelopes to be $N_i^{(2)}=1$ and $N_i^{(1)}=N_i^{(3)}=0$, gives the intermediate areas in Fig. 11, in reasonably good agreement with Eq. (4.20). Thus, what has happened is that upon reaching this intermediate state, the middle envelope has "absorbed" one soliton from each of the fast and slow envelopes and has also absorbed a certain amount of radiation from each envelope. When the interaction goes to completion the absorbed solitons are finally reemitted, but with the middle envelope retaining the absorbed radiation.

This then suggests the following description of the collision process. In a collision of a fast and a slow envelope, the middle envelope absorbs the amount of radiation determined by Eq. (4.21) from these envelopes, as well as any resonantly paired solitons [according to Eq. (4.22)]. The remainder of the radiation then will pass on through, without experiencing any significant delay. Later, the resonantly absorbed solitons are reemitted, tacking N-soliton tails onto the fast and slow envelopes.

To see what happens to nonresonant solitons, we tried a computer run in which the fast envelope had two solitons ($\lambda^{(3)}=1.52$ and 2.56) and the slow envelope had one soliton ($\lambda^{(1)}=2.54$) which was resonantly paired with the largest soliton in the fast envelope, since $c_2=0, c_1=-c_3$. The results are shown in Fig. 12. As before, the resonant solitons and some radiation are initially

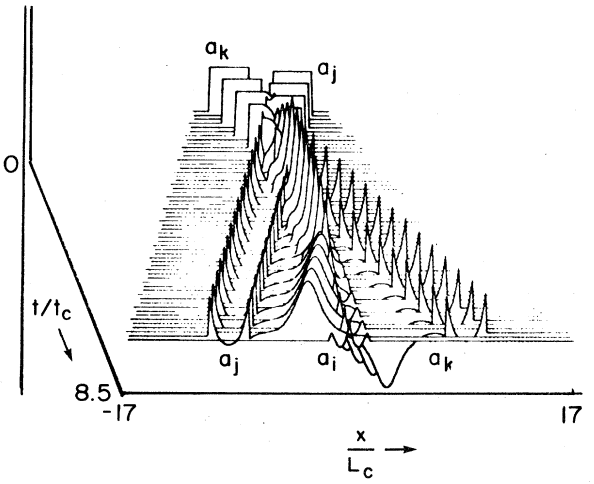

FIG. 11. Same as Fig. 9 except that $A_1(t=0)=A_3(t=0)=2.84$.

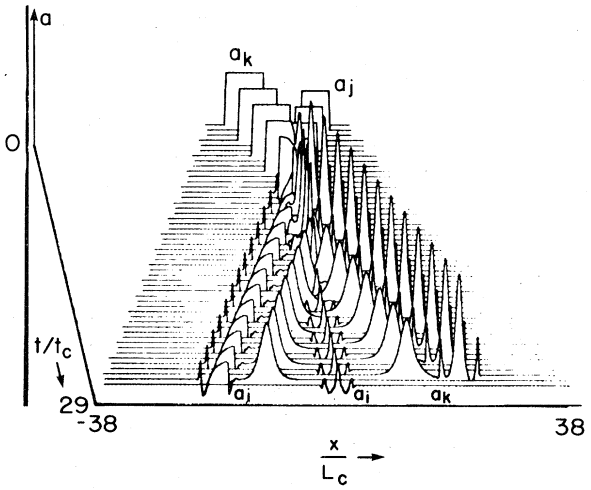

FIG. 12. Binary collision of initially rectangular pulses with $v_i=0$, $v_j=-v_k$, $A_1(t=0)=3.6$, $A_3(t=0)=6.4$, $|a_{k\max}(t=0)|/|a_{j\max}(t=0)|=1.3$.

deposited in the middle envelope, which takes the form of a narrow spike. The spike, again, subsequently loses its soliton, tacking a one-soliton tail onto each of the wave packets 1 and 3. The nonresonant soliton is unaffected by the collision, except that its characteristic profile emerges clearly as the resonant soliton and some of the radiation of the initially square pulse are stripped away.

Of course, in practice, one can never have exact resonance, so one needs to determine just how close to resonance is sufficient. As we have already seen, the resonant solitons are unaffected by the radiation and other solitons (after the initial collision); we can then justify considering only these two resonant solitons. In this case, the solution is given in Kaup, 1976a, Sec. VII. Upon redesigning some of the constants, and using the notation that $\lambda^{(1)}=\xi_1+i\eta_1$ and $\lambda^{(3)}=\xi_3+i\eta_3$ are the eigenvalues for the $q^{(1)}$ and $q^{(3)}$ solitons, respectively, we have

$$q^{(1)}=\frac{4\eta_1}{D}\exp[i(\phi_1-2\xi_1 z_1)]\times\left[\exp(2\eta_3 z_3)+\frac{\zeta_1-\zeta_3}{\zeta_1-\zeta_3^*}\exp(-2\eta_3 z)\right], \tag{4.25a}$$

$$q^{(2)}=\frac{-16i\eta_1\eta_3(c_3-c_1)}{D(\zeta_1-\zeta_3^*)(c_2-c_1)(c_3-c_2)}\times\exp[i(\phi_1+\varphi_3-2\xi_1 z_1-2\xi_3 z_3)], \tag{4.25b}$$

$$q^{(3)}=\frac{4\eta_3}{D}\exp[i(\phi_3-2\xi_3 z_3)]\times\left[\exp(-2\eta_1 z_1)+\frac{\zeta_1^*-\zeta_3^*}{\zeta_1-\zeta_3^*}\exp(2\eta_1 z_1)\right], \tag{4.25c}$$

where

$$z_1\equiv x-c_1 t-x_{10}, \tag{4.26a}$$

$$z_3\equiv x-c_3 t-x_{30}, \tag{4.26b}$$

$$\zeta_1\equiv\frac{2\lambda^{(1)}}{c_3-c_2}, \tag{4.27a}$$

$$\zeta_3\equiv\frac{2\lambda^{(3)}}{c_2-c_1}, \tag{4.27b}$$

and

$$D\equiv\exp[2(z_1\eta_1+z_3\eta_3)]+\exp[2(z_3\eta_3-z_1\eta_1)]+\left|\frac{\zeta_1-\zeta_3}{\zeta_1^*-\zeta_3}\right|^2\exp[2(z_1\eta_1-z_3\eta_3)]+\exp[-2(z_1\eta_1+z_3\eta_3)]. \tag{4.28}$$

From the above we have, as $t\to-\infty$,

$$q^{(1)}\simeq\frac{2\eta_1}{\cosh(2\eta_1 z_1)}\exp[i(\phi_1-2\xi_1 z_1)], \tag{4.29a}$$

$$q^{(2)}\simeq 0, \tag{4.29b}$$

$$q^{(3)}\simeq\frac{2\eta_3}{\cosh(2\eta_3 z_3)}\exp[i(\phi_3-2\xi_3 z_3)], \tag{4.29c}$$

which corresponds to a $q^{(1)}$ and $q^{(3)}$ soliton approaching each other.

First, assume $\zeta_3\neq\zeta_1$ so that the solitons are not resonant. Then when $t\simeq(x_{10}-x_{30})/(c_3-c_1)$, these solitons collide, are converted into $q^{(2)}$, and as $t\to+\infty$, $q^{(2)}$ decays, giving back the $q^{(1)}$ and $q^{(3)}$ solitons but shifted so that

$$q^{(1)}\simeq\frac{2\eta_1\exp[i(\phi_1+\theta-2\xi_1 z_1)]}{\cosh(2\eta_1 z_1-\delta)}, \tag{4.30a}$$

$$q^{(2)}\simeq 0, \tag{4.30b}$$

$$q^{(3)}\simeq\frac{2\eta_3\exp[i(\phi_3-\theta-2\xi_3 z_3)]}{\cosh(2\eta_3 z_3+\delta)}, \tag{4.30c}$$

where θ and δ are defined by

$$\frac{\zeta_1-\zeta_3}{\zeta_1^*-\zeta_3}=e^{-\delta}e^{i\theta}. \tag{4.31}$$

The time delay τ that these two solitons have experienced is therefore

$$\tau=\frac{(\eta_1+\eta_3)\delta}{\eta_1\eta_3(c_3-c_1)}. \tag{4.32}$$

One-half of this time delay is therefore the time required for the pump $q^{(2)}$ to reach its maximum amplitude and energy, and similarly is also the decay time.

When $\zeta_1\simeq\zeta_3$ and the solitons are almost in resonance, then τ is very large or infinity since $\delta\to\infty$. In this case, due to natural noise in any system, $q^{(2)}$ will probably start to decay before it can reach its maximum amplitude. The critical time would be the time required for A_2 to reach $\pi/2$, since that is the limit of stability. For $\eta_1\simeq\eta_3$, $c_1=-c_3$, $c_2=0$, one can determine from Eq. (4.25b) that

$$A_2=2\frac{w\ln w^2}{w^2-1}, \tag{4.33}$$

where

$$w=\tfrac{1}{2}(Z+e^{-2\delta}/Z)+\tfrac{1}{2}\sqrt{(Z+e^{-2\delta}/Z)^2-4}, \tag{4.34}$$

with

$$Z=\exp\{-2\eta_1[(c_3-c_1)t+x_{30}-x_{10})]\}. \tag{4.35}$$

Thus for $A_2=\pi/2$, $w\cong 3.44$ and the first value of t at which $A_2=\pi/2$ when δ is large is approximately

$$t\cong\frac{x_{10}-x_{30}}{c_3-c_1}-\frac{1}{2\eta_1(c_3-c_1)}\left(1.32-\frac{e^{-2\delta}}{13.8}\right). \tag{4.36}$$

Now, since the two solitons appear to collide at $t=(x_{10}-x_{30})/(c_3-c_1)$, then for δ large, $q^{(2)}$ has reached an area of $\pi/2$ before the apparent collision, and this time is essentially independent of δ. If the natural noise would induce a decay time less than that given by Eq. (4.32), then these decays would dominate, since $q^{(2)}$ would reach the critical area of $\pi/2$ at or just before the apparent collision of the two solitons. The calculation of the decay time due to noise is given in Appendix F.

V. STIMULATED BACKSCATTER (SBS) $[p_i=p_j=p_k,\ (v_j-v_i)(v_i-v_k)<0]$

Without loss of generality, we may take the high-frequency envelope to be the fastest in this case. Then $(i,j,k)=(3,1,2)$ and

$$(\gamma_1,\gamma_2,\gamma_3)=(-,-,+). \tag{5.1}$$

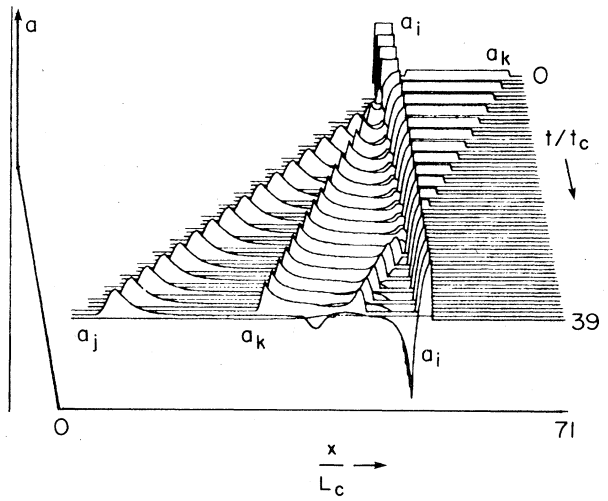

FIG. 13. Backscatter interaction of initially rectangular pulses: $v_j - v_i = v_i - v_k$, $a_j(x, t=0) \equiv 0$, $|a_{i\max}(t=0)| = 10\,|a_{k\max}(t=0)|$, $A_3(t=0) = 2.59$, $A_2(t=0) = 2.03$. Normalization in terms of $t_c \equiv 1/|Ka_{i\max}(t=0)|$, $L_c \equiv 1/|q^{(3)}_{\max}(t=0)|$.

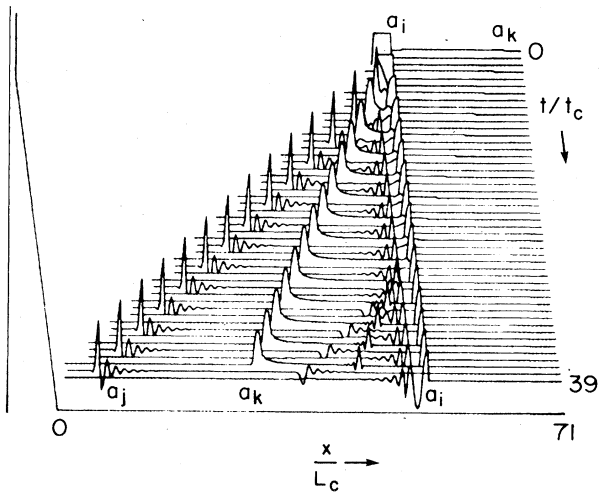

FIG. 15. Same as Fig. 13 except $|a_{i\max}(t=0)|/|a_{k\max}(t=0)| = 30$, $A_3(t=0) = 7.78$.

So from Eq. (A14) we have (we have assumed $c_1 < c_2 < c_3$)

$$q^{(1)} = \frac{+|K|e^{i\nu/3}a_j^*}{\sqrt{(c_2-c_1)(c_3-c_1)}},\quad r^{(1)} = -q^{(1)*}, \tag{5.2a}$$

$$q^{(2)} = \frac{-|K|e^{-i\nu/3}a_k}{\sqrt{(c_2-c_1)(c_3-c_2)}},\quad r^{(2)} = +q^{(2)*}, \tag{5.2b}$$

$$q^{(3)} = \frac{-|K|e^{-i\nu/3}a_i}{\sqrt{(c_2-c_3)(c_1-c_3)}},\quad r^{(3)} = +q^{(3)*}, \tag{5.2c}$$

as the transformation from the a's to the ZS q's. Note that by Eq. (5.2), only the slow (BS) envelope may contain solitons. Thus in this case no soliton exchange effects can occur, since the middle and the fast envelopes can never contain solitons.

Without any possible soliton exchange in this case, there are no nonlinear instabilities, and the interesting process is the collision of various envelopes. In Figs. 13–15, we show numerical solutions where the fast envelope collides with the middle envelope, with progressively larger values of a_i. Both envelopes are initially rectangular. As one can see, the most obvious feature in this case is the strongly oscillatory nature of the final state, as well as the slow approach to the final state. Although it is clear from Fig. 15 that the final configuration for the backscattered pulse (the slow envelope) is essentially achieved for the last time shown, one can see that there is still considerable interaction going on in the intermediate region. However, due to the strong peak on the left of the middle envelope, the part of the backscattered pulse in the interaction region is being prevented from emerging and is being converted back into the incident pulse. In the case of SBBS, the fast envelope corresponds to the incident laser pulse, the middle envelope to the acoustic wave, and the slow envelope to the backscattered laser pulse.

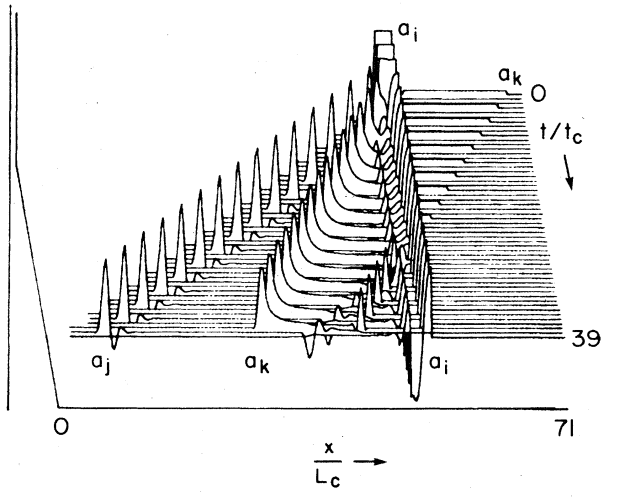

FIG. 14. Same as previous figure except $|a_{i\max}(t=0)|/|a_{k\max}(t=0)| = 20$, $A_3(t=0) = 5.19$.

When the initial envelopes are all well separated and each one satisfies the condition in Eq. (B1), then it follows that unique solutions will exist for the final envelopes. This can be shown because by Eq. (A21), we have $\Gamma_f^{(3)}$ (and $\Gamma_f^{(1)}$ and $\Gamma_f^{(2)}$ as well) satisfying Eq. (B26e), and thus well defined reflection coefficients will exist where $|\rho_f^{(2)}|$ and $|\rho_f^{(3)}| < 1$. In passing and for further completeness, we should point out that the above argument depends both on the initial envelopes being integrable *and* also being well separated, whereas in the decay case no such further conditions were necessary. This is because in the decay case, $r = -q^*$ for all envelopes, and thus none of the final reflection coefficients had to be bounded by unity, as in this case. For example, we cannot guarantee that initial overlapping, but integrable, envelopes will have a unique solution. For a unique solution to exist by the IST one must insure that $|\rho_f^{(2)}|$ and $|\rho_f^{(3)}| < 1$. However we note that when the initial envelopes are *square integrable* (and even if they are initially overlapping) then from Eqs. (5.1), (A7), and (A24), we have that the final envelopes must also be square integrable. As a consequence of the above we cannot presently *a priori* rule out the possi-

bility of certain initial overlapping configurations (with square integrable envelopes) giving rise to final envelopes with long tails which drop off like $x^{-\beta}$ with $1/2 < \beta \leq 1$. If such occurred, the final envelopes of course would still be square integrable, but not integrable, in which case the final scattering data would not be well defined. However, also note that since square integrability is preserved by this interaction, square integrable initial profiles (overlapping or not) can never give rise to singular solutions, as occurred in the explosive case.

From the IST theory, we can again discuss how areas and actions are exchanged between colliding envelopes for this case; however, due to the strong oscillatory nature of the final envelopes, the area will not be as useful a concept as it was in the previous two cases. This is clear from the typical oscillatory structure as seen in Fig. 15. Since the final states are not slowly varying, all of the previous conclusions which were based on the WKB approximation are not valid. For example, since the backscattered pulse (for which $r = -q^*$) cannot contain any solitons, if the WKB approximation were valid we would expect the absolute area to be bounded by $\pi/2$. This bound on the absolute area of the BS pulse would then suggest a bound on the BS energy, and thus one could expect the ratio for the BS energy to the incident energy (which is the reflection coefficient R) to decrease at sufficiently high incident energies. This is clearly not the case, and thus WKB is not valid. Due to the strong oscillations, it is possible for the BS pulse to contain no solitons and at the same time to have its absolute area and energy unbounded. Although the area concept is no longer as useful as before, the area theorem is still valid and can again be used to predict the final wave-packet areas. From Eqs. (A17), (B29), and (B31), when $q_0^{(1)} = 0$, we have

$$\tanh A_{3f} = \tanh A_{30} / \cosh A_{20}, \tag{5.3a}$$

$$\tanh A_{2f} = \tanh A_{20} \cosh A_{3f}, \tag{5.3b}$$

$$\tan A_{1f} = \sinh A_{30} \tanh A_{20}, \tag{5.3c}$$

where $\mathrm{sgn}(\cos A_{1f}) = +1$, since no solitons are present.

For the action transfer, we have from Eqs. (A26) and (5.1)

$$\ln(1+\Gamma^{(3)}) + \ln(1+\Gamma^{(2)}) = \text{const}, \tag{5.4a}$$

$$\ln(1+\Gamma^{(3)}) + \ln(1+\Gamma^{(1)}) = \text{const}, \tag{5.4b}$$

so that if the fast envelope gains (loses) radiation density, then the middle and slow envelopes both must simultaneously lose (gain) a corresponding amount of radiation density.

From Eqs. (2.9) and (A21) we can calculate the amount of radiation in the final backscattered envelope, and when this envelope is initially zero we have

$$\mathfrak{N}_f^{(1)} = \frac{1}{\pi} \int_{-\infty}^{\infty} d\lambda \ln[1+\Gamma_f^{(1)}], \tag{5.5}$$

where $\lambda = \lambda^{(1)}$ and

$$\Gamma_f^{(1)} = \frac{\Gamma_0^{(2)} \Gamma_0^{(3)}}{1+\Gamma_0^{(2)}}. \tag{5.6}$$

From Eqs. (5.5) and (5.6) we can calculate the reflection coefficient R for SBS,

$$R \equiv \frac{\mathfrak{N}_f^{(1)}}{\mathfrak{N}_0^{(3)}} = \frac{c_2 - c_3}{c_2 - c_1} \frac{\int_{-\infty}^{\infty} |a_{1f}|^2 dx}{\int_{-\infty}^{\infty} |a_{30}|^2 dx} = \left(\frac{c_2 - c_3}{c_2 - c_1} \right) \left| \frac{\omega_3}{\omega_1} \right| \frac{\int_{-\infty}^{\infty} \langle w_{1f} \rangle dx}{\int_{-\infty}^{\infty} \langle w_{30} \rangle dx}, \tag{5.7}$$

where w is the energy density.

When the initial pulses are square pulses, as in Figs. 13–15, we have closed-form solutions for $\Gamma_0^{(2)}$ and $\Gamma_0^{(3)}$. From Eqs. (A14) and (B37)–(B40), we have for $c_1 = -c_3$ and $c_2 = 0$,

$$\Gamma_0^{(3)}(\lambda) = A_3^2 G(L^2\lambda^2 - A_3^2), \tag{5.8a}$$

$$\Gamma_0^{(2)}(\lambda) = A_2^2 G(4l^2\lambda^2 - A_2^2), \tag{5.8b}$$

where $\lambda = \lambda^{(1)}$, $L(l)$ is the length of the laser (acoustic) pulse, $A_3(A_2)$ is the area of the laser (acoustic) pulse, and

$$G(x) \equiv \begin{cases} \dfrac{\sinh^2(-x)^{1/2}}{(-x)} \; if \; x \leq 0 \\ \dfrac{\sin^2 x^{1/2}}{x} \; if \; x \geq 0 \end{cases}. \tag{5.9}$$

Thus the reflection coefficient R for this model of SBS will be, from Eqs. (5.5)–(5.7) and (A14)

$$R = \frac{1}{\pi L Q_3^2} \int_{-\infty}^{\infty} d\lambda \ln(1+\Gamma_f^{(1)}), \tag{5.10}$$

where Q_3 is the initial amplitude of the laser pulse. With Eqs. (5.5)–(5.7) it is possible to evaluate R by quadrature, and some of the results are shown in Figs. 16–18.

From the analytic expressions given in Eqs. (5.8)–(5.10), one can directly deduce many of the properties seen in the simulations and Figs. 16–18. First, if we let $Q_2 \ll Q_3$, keep Q_3, Q_2, and l fixed, and let $L \to \infty$, we can then approximate the integral in Eq. (5.10), and find that as we expect

$$R \to 1 \text{ as } L \to \infty. \tag{5.11}$$

(Note that even if we are limited to working only with bounded envelopes, the inverse scattering method will still apply to unbounded envelopes, if the proper limits are taken.)

Second, the basic structure of the BS pulse can also be deduced from $\Gamma_f^{(1)}$, which is the square of the magnitude of $(b_f^{(1)}/a_f^{(1)})$. This will follow since (b/a) is like the Fourier transform (although nonlinear) of the potential q (Ablowitz *et al.*, 1974). When the areas of the laser and acoustic pulses are small, then $\Gamma_f^{(1)} \simeq \Gamma_0^{(2)} \Gamma_0^{(3)}$ and the magnitude of (b/a) will have a $(\sin x/x)^2$ behavior when the initial pulses are square pulses. This would be consistent with a triangular-shaped pulse as seen in Fig. 13. Large-area acoustic pulses will not have any dramatic effects on $\Gamma_f^{(1)}$ due to the denominator in Eq. (5.6), but large-area laser pulses will. From Eqs. (5.8) and (5.9), if A_3 increases, say from 1 to 10, then at $\lambda = 0$, $\Gamma_0^{(3)}$ will rise dramatically from an order of unity to an order of e^{20}, with larger values of A_3 giving even more dramatic increases. Now, for $\lambda > A_3/L$, $\Gamma_0^{(3)}$ is bounded by A_3^2, while for $0 < \lambda < A_3/L$, $\Gamma_0^{(3)}$ becomes of the order of e^{2A_3}. Thus for $A_3 \gg 1$, $\Gamma_0^{(3)}$ and thus $\Gamma_f^{(1)}$ take on a localized structure, almost a square

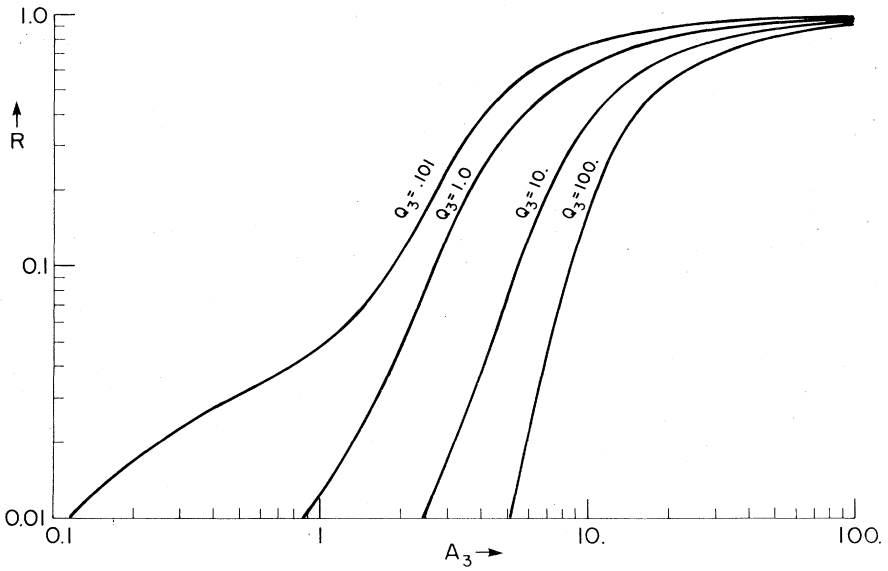

FIG. 16. Reflection coefficient for stimulated backscatter as a function of incident pulse width, for several incident pulse heights. $A_2(t=0)$ is fixed at 0.2, and $|q^{(2)}(t=0)|$ fixed at 0.1. Note, on figure $Q_3 \equiv |q^{(3)}(t=0)|$.

shape. To obtain a qualitative estimate of what $q^{(1)}$ should be, we simply ask what is the Fourier transform of a square pulse. Of course, it is a $\sin x/x$ behavior. Now, the phase variation of b/a (which is not shown) must chop off the front half of this behavior, due to causality, so we are left with a shape consisting of an initial rapid rise followed by rapidly decaying oscillations. Of course, in the fully nonlinear region, we don't and shouldn't expect quantitative agreement, but we do note that we do have qualitative agreement, as can be seen from the simulations. Furthermore, since $b_f^{(1)}/a_f^{(1)}$ is continuously differentiable, we should round off the corners of our square pulse, in which case the Fourier transform should vanish faster than any power of x as $|x| \to \infty$. We note this feature in the simulations giving good qualitative agreement again.

Third, from the above argument, we can also deduce what features of the initial pulses will affect the wavelength of the nonlinearly induced oscillations in the BS pulse. We can expect these wavelengths to be inversely proportional to the width of $\Gamma_f^{(1)}$, which by the above is approximately $A_3/L = Q_3$. In Figs. 13–15 we show a series of simulations where only Q_3 is changed. As can be clearly seen, as Q_3 increases, the wavelength of these oscillations decreases.

Collisions between large laser pulses and large acoustic pulses, or between large laser pulses and large backscatter pulses give similar results. In both cases, very little of the laser pulse is transmitted. In all cases, it is either the buildup or the presence of the large acoustic pulse which limits the transmission. When it is sufficiently large, the acoustic pulse en-

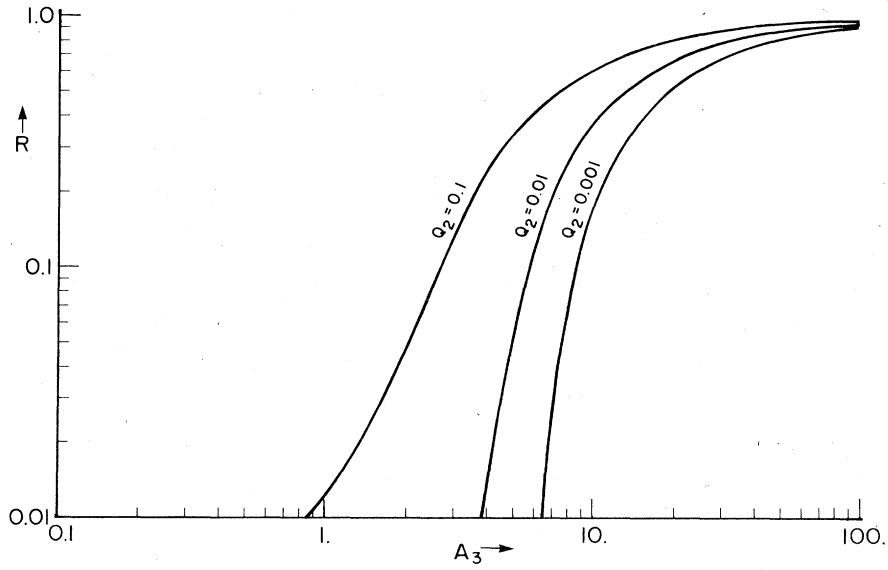

FIG. 17. Reflection coefficient as a function of the area of the incident pulse, for several values of $Q_2 \equiv |q^{(2)}(t=0)|$. $|q^{(3)}(t=0)|=1$, $L_2=2$.

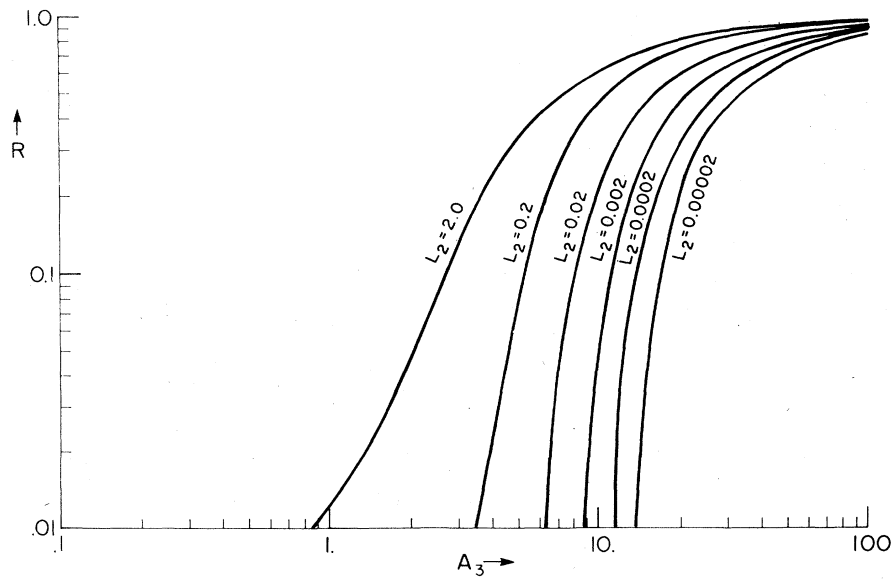

FIG. 18. Reflection coefficient as a function of A_3 for several values of L_2.
$|q^{(3)}(t=0)|=1$.
$|q^{(2)}(t=0)|=0.1$.

hances decay of the laser beam into backscattered and acoustic waves. The larger amplitude of the acoustic pulse then causes further decay of the laser beam to occur still faster, while at best the backscattered wave simply leaves the interaction region. As it leaves, it may interact with the laser beam to transfer energy to the acoustic wave at an earlier point, which causes the laser beam to decay even earlier.

Returning to Figs. 16–18, for the reflection coefficient R we note some interesting general features. First, from Fig. 16, we see that at constant A_3, as the height of the laser pulse Q_3 goes up, R goes down. Thus compression of the pulse (which occurs in the presence of anomalous dispersion) will reduce the backscattering. This reduction becomes almost inversely proportional to the compression when $R \lesssim 1$. On the other hand, from Figs. 17 and 18, we see that as the area of the acoustic pulse A_2 is increased, R increases. This increase is very dramatic for $A_2 \ll 1$, as is seen in Fig. 18, and has the appearance of a threshold in A_3. We can solve for this threshold for $A_2 \to 0$ and $Q_2 \ll Q_3$. From Eqs. (5.6), (5.8), and (5.9) we have in this limit

$$\Gamma_f^{(1)} \simeq A_2^2 \Gamma_0^{(3)}, \tag{5.12}$$

provided that l is not too large. The region of λ where

$$A_2^2 \Gamma_0^{(3)}(\lambda) < 1 \tag{5.13}$$

will contribute a part to R which is proportional to A_2^2, and vanishes as $A_2 \to 0$. But when A_3 is sufficiently large so that there is a region of λ (around zero) which violates Eq. (5.13), that region can give a dramatically large contribution to R. To estimate this contribution, we determine the value of λ at which Eq. (5.13) is just satisfied, then estimate the integral by assuming $\Gamma_f^{(1)}(\lambda) \gg 1$ inside of this region. This region is defined by $\lambda^2 < \Lambda^2$, where

$$\Lambda^2 = (A_3^2 - B^2)/L^2, \tag{5.14}$$

and where B is the solution of

$$\frac{\sinh B}{B} = \frac{1}{A_3 A_2}. \tag{5.15}$$

This region exists only if $A_3 > B$, so $A_3 = B$ is then the threshold value of A_3 for R to become nonzero. Thus the threshold occurs at

$$A_{3t} = \sinh^{-1}(1/A_2). \tag{5.16}$$

When $A_3 > A_{3t}$, one finds that

$$R \simeq 1 - \frac{2}{\pi}\sin^{-1}\left(\frac{B}{A_3}\right) - \frac{2}{\pi}\frac{B-2}{A_3}\left(1 - \frac{B^2}{A_3^3}\right)^{1/2} - \frac{2}{\pi A_3}\ln\left|\frac{1+(1-B^2/A_3^2)^{1/2}}{1-(1-B^2/A_3^2)^{1/2}}\right| - \cdots, \tag{5.17}$$

where, for our estimates to be reasonable, we must require

$$\sinh A_3 \gg 1, \tag{5.18a}$$

$$A_2 A_3 \ll 1. \tag{5.18b}$$

When one compares Eq. (5.14) with the results in Fig. 18 one finds that Eq. (5.17) approximates these curves very well, with an absolute error in R of no more than 0.02 when R is less than 0.1; the approximation is even better when $R > 0.1$. Also, we note that Eq. (5.17) does not give $R \to 1$ exponentially, in distinction to the case treated by Mannheimer (1974) and Fuchs and Beaudry (1976). This arises due to the differences in the boundary conditions, where they are considering a static slab geometry and we are considering traveling pulses inside of a plasma.

We note that Eq. (5.12) is valid only if l remains bounded so that $\Gamma_0^{(2)}$ remains essentially constant for $\lambda^2 < \Lambda^2$. For this to be so, we must also demand

$$l^2 \ll \frac{L^2\pi^2}{4(A_3^2 - B^2)}. \tag{5.18c}$$

If Eq. (5.18c) is violated, then (5.12) must be replaced by

$$\Gamma_f^{(1)} \simeq A_2^2 \left[\frac{\sin 2l\lambda}{2l\lambda}\right]^2 \Gamma_0^{(3)}, \tag{5.19}$$

in which case Eq. (5.17) becomes an upper bound for R instead.

We may derive the reflection threshold in an alternative fashion if we ask for the conditions under which the linear undepleted pump solution of Eqs. (1.3) becomes invalid. The linear solution is $a_j(t)=a_j(0)e^{\gamma t}$, $a_k(t)=a_k(0)e^{\gamma t}$ with $\gamma=|Ka_i(t=0)|$ at the point of maximum growth. The condition that depletion be important across the width of a_k is $L_3(\partial a_i/\partial x)=a_i$. Substituting in Eq. (1.1a) and assuming an interaction time of $L_1/(v_1-v_2)$, we find that the threshold amplitudes obey $A_{3t}\exp(A_2)=2^{-1/2}$. This is approximately the same as Eq. (5.16).

APPENDIX A: ZAKHAROV-MANAKOV EIGENVALUE PROBLEM FOR THE THREE-WAVE INTERACTION

1. Introduction

In this Appendix we outline the IST method for solving the three-wave resonant interaction (Zakharov and Manakov, 1973; Zakharov and Manakov, 1975; Kaup, 1976a) and discuss those features which we have found useful. For the IST, it is convenient to work with the three-wave equations in the form (see Secs. II D and II E)

$$Q_{1t}+c_1Q_{1x}=\gamma_1Q_2^*Q_3^*, \tag{A1a}$$

$$Q_{2t}+c_2Q_{2x}=\gamma_2Q_1^*Q_3^*, \tag{A1b}$$

$$Q_{3t}+c_3Q_{3x}=\gamma_3Q_2^*Q_3^*, \tag{A1c}$$

where $Q_i(x,t)$ are the slowly varying envelopes, c_i are the corresponding group velocities, which satisfy

$$c_1<c_2<c_3, \tag{A2}$$

and

$$\gamma_i=\mathrm{sgn}(E_i\times\omega_i), \tag{A3}$$

where E_i is the energy of the ith wave, and ω_i are the resonant frequencies, whose relative signs are determined from

$$\omega_1+\omega_2+\omega_3=0. \tag{A4}$$

Note that Eqs. (A1) differ from those by Kaup (1976a) by a factor of i.

To solve Eqs. (A1), one first considers the Zakharov–Manakov (ZM) eigenvalue problem defined by

$$-iv_{1x}+V_{12}v_2+V_{13}v_3=-c_1\zeta v_1, \tag{A5a}$$

$$-iv_{2x}+V_{21}v_1+V_{23}v_3=-c_2\zeta v_2, \tag{A5b}$$

$$-iv_{3x}+V_{31}v_1+V_{32}v_2=-c_3\zeta v_3, \tag{A5c}$$

where $v=[v_1,v_2,v_3]^T$ is the eigenvector, ζ is the eigenvalue, the c_i are again the group velocities, and V_{ij} are the "potentials," given by

$$V_{23}=\frac{-iQ_1}{\sqrt{(c_2-c_1)(c_3-c_1)}},\quad V_{32}=-\gamma_3\gamma_2V_{23}^*, \tag{A6a}$$

$$V_{31}=\frac{-iQ_2}{\sqrt{(c_2-c_1)(c_3-c_2)}},\quad V_{13}=\gamma_1\gamma_3V_{31}^*, \tag{A6b}$$

$$V_{12}=\frac{-iQ_3}{\sqrt{(c_3-c_1)(c_3-c_2)}},\quad V_{21}=-\gamma_1\gamma_2V_{12}^*. \tag{A6c}$$

Define $\Phi^{(n)}(n=1,2,3)$ to be the linearly independent solutions of Eqs. (A5) which satisfy the boundary conditions

$$\Phi_j^{(n)}\to\delta_j^n\exp(-ic_j\zeta x)\ \text{as}\ x\to-\infty. \tag{A7}$$

Then as $x\to+\infty$, these solutions will approach

$$\Phi_j^{(n)}\to a_{nj}(\zeta)\exp(-ic_j\zeta x)\ \text{as}\ x\to+\infty \tag{A8}$$

which defines the "scattering matrix,"

$$S(\zeta)=[a_{nm}(\zeta)]. \tag{A9}$$

In going from Eq. (A5) to Eq. (A9) the potentials Q_1,Q_2,Q_3 have been mapped into the scattering data S. For infinitesimal potentials [the linear limit of Eq. (A1)], the diagonal elements of S become unity and the off-diagonal elements become simply the linear Fourier transforms of these potentials (the Born approximation). When the potentials are no longer infinitesimal, then S is no longer so simply related to the potentials. But, the relation is nonetheless of such a form that the time dependence of S [which follows from Eqs. (A1) and (A5)–(A9)] is simply

$$a_{nm}(\zeta,t)=a_{nm}(\zeta,0)\exp\left[i\zeta tc_1c_2c_3\left(\frac{1}{c_m}-\frac{1}{c_n}\right)\right]. \tag{A10}$$

This time dependence for S is exactly the same as that for the linear limit. The nonlinear equations of motion, (A1), have been transformed into linear equations of motion in scattering space. Furthermore, knowing $S(\zeta,t)$, it is possible to reconstruct the potentials at any later or earlier time, by using the "inverse scattering equations" (Kaup, 1976a). However, since we shall never explicitly need these equations, they shall not be given here.

2. Reduction to the second-order ZS problem

Although it does give us the formal solution of Eq. (A1), the ZM problem is unwieldly. Fortunately, we can simplify things. Anytime the three envelopes are well separated (such as happens in general when $t\to\pm\infty$), the scattering data for Eq. (A5) can be given in terms of the scattering data of the simpler ZS eigenvalue problem. To see how this comes about, consider Eq. (A5) in a region of space where Q_1 and Q_2 are zero, but Q_3 is nonzero. Then by Eq. (A6), the only nonzero potentials (in this region) are V_{12} and V_{21}. We see that Eq. (A5c) is now trivial to solve, with v_3 uncoupled from v_1 and v_2. Also, Eqs. (A5a) and (A5b) then constitute only a second-order system, which upon taking out appropriate phase factors, scaling v_1 and v_2, and scaling the eigenvalue gives us the ZS eigenvalue problem, Eq. (2.1),

$$u_{1x}+i\lambda u_1=qu_2, \tag{A11a}$$

$$u_{2x}-i\lambda u_2=ru_1. \tag{A11b}$$

Similarly, one can also consider the region where only Q_2 is nonzero as well as the region where only Q_3 is nonzero. In these cases, we again find that Eq. (A5) reduces to Eq. (A11). Thus when the envelopes are all initially well separated, it is not necessary to solve Eq. (A5), but only to solve (A11) in each of these three regions. Now, to solve Eq. (A1), it is still necessary to find S as given by Eqs. (A7)–(A9). But this S can also be given in terms of the scattering data

of the three ZS eigenvalue problems. One finds that if at some time the envelopes have negligible overlap, with the ith envelope to the right of the jth envelope and the jth envelope to the right of the kth envelope, then S may be factored as

$$S = S^{(i)} S^{(j)} S^{(k)} (i, j, k = 1, 2, \text{ or } 3), \tag{A12}$$

where

$$S^{(1)} = \begin{bmatrix} 1 & 0 & 0 \\ 0 & \overline{a}^{(1)} & -\overline{b}^{(1)} \\ 0 & b^{(1)} & a^{(1)} \end{bmatrix}, \tag{A13a}$$

$$S^{(2)} = \begin{bmatrix} \overline{a}^{(2)} & 0 & -\overline{b}^{(2)} \\ 0 & 1 & 0 \\ b^{(2)} & 0 & a^{(2)} \end{bmatrix}, \tag{A13b}$$

$$S^{(3)} = \begin{bmatrix} \overline{a}^{(3)} & -\overline{b}^{(3)} & 0 \\ b^{(3)} & a^{(3)} & 0 \\ 0 & 0 & 1 \end{bmatrix}, \tag{A13c}$$

and $\overline{a}^{(n)}, a^{(n)}, \overline{b}^{(n)}, b^{(n)}$ are the ZS scattering data (see Appendix B) for the nth envelope, where for each envelope, q, r, and λ are given by

$$q^{(1)} = \frac{-\gamma_2\gamma_3 Q_1^*}{[(c_2 - c_1)(c_3 - c_1)]^{1/2}}, \; r^{(1)} = \gamma_2\gamma_3 q^{(1)*},$$

$$\lambda^{(1)} = \zeta(c_3 - c_2)/2, \tag{A14a}$$

$$q^{(2)} = \frac{-Q_2}{[(c_2 - c_1)(c_3 - c_2)]^{1/2}}, \; r^{(2)} = -\gamma_1\gamma_3 q^{(2)*},$$

$$\lambda^{(2)} = \zeta(c_3 - c_1) \tag{A14b}$$

$$q^{(3)} = \frac{-\gamma_1\gamma_2 Q_3^*}{[(c_3 - c_1)(c_3 - c_2)]^{1/2}}, \; r^{(3)} = \gamma_1\gamma_2 q^{(3)*},$$

$$\lambda^{(3)} = \zeta(c_2 - c_1) \tag{A14c}$$

Thus, when we can ignore the overlap between the envelopes, we need only to solve the ZS eigenvalue problem for each envelope, using Eq. (A14) for the potentials and eigenvalue, and then to construct $S^{(j)}$ using Eq. (A13), which then gives S by Eq. (A12).

3. Relations between initial and final ZS scattering data

If one is not interested in the intermediate state of the system and only desires to know what the final envelopes will be, one never needs to use the ZM eigenvalue problem if the initial envelopes have no overlap. In such a case we express the final ZS scattering data directly in terms of the initial ZS scattering data.

If at $t = 0$ the envelopes are ordered (3, 2, 1) from left to right (if any envelope is zero, it does not matter where it is placed), then

$$S = S_0^{(3)} S_0^{(2)} S_0^{(1)}, \tag{A15}$$

where the subscript "0" indicates the initial value of the ZS scattering data for the initial envelopes. This determines S at all subsequent times by Eq. (A10). If the envelopes separate (sufficient conditions will be discussed later) as $t \to \infty$, we have

$$S = S_f^{(1)} S_f^{(2)} S_f^{(3)}. \tag{A16}$$

Setting these two expressions for S equal, we find

$$\frac{b_f^{(3)}}{a_f^{(3)}} = \frac{a_0^{(1)} b_0^{(3)} + a_0^{(3)} b_0^{(2)} \overline{b}_0^{(1)}}{a_0^{(2)} a_0^{(3)}} \exp(-2i\lambda^{(3)} c_3 t_f), \tag{A17a}$$

$$\frac{b_f^{(2)}}{a_f^{(2)}} = \frac{a_f^{(3)}}{a_0^{(2)} a_0^{(3)}} [a_0^{(3)} b_0^{(2)} \overline{a}_0^{(1)} - b_0^{(1)} b_0^{(3)}] \exp(-2i\lambda^{(2)} c_2 t_f), \tag{A17b}$$

$$\frac{b_f^{(1)}}{a_f^{(1)}} = \frac{a_f^{(2)}}{a_0^{(1)} a_0^{(2)}} [\overline{a}_f^{(3)} a_0^{(2)} b_0^{(1)} + \overline{b}_f^{(3)} b_0^{(2)}] \exp(-2i\lambda^{(1)} c_1 t_f), \tag{A17c}$$

where t_f is the final time, and the arguments of the ZS a's and b's are understood to be the corresponding λ's, given by Eq. (A14). All of our results concerning the exchange of solitons, the exchange of radiation density (or action), and the exchange of areas will follow from Eqs. (A17).

4. Soliton, action, and area exchange

The bound-state eigenvalues are given by the poles of $b(\lambda)/a(\lambda)$ [zeros of $a(\lambda)$] for λ in the upper half plane. From Eq. (A17a) we see that the zeros of $a_0^{(2)}$ and $a_0^{(3)}$ become zeros of $a_f^{(3)}$. It then follows from Eq. (A17b) that $a_f^{(2)}$ has no zeros. From Eq. (A17c) we find that zeros of $a_0^{(1)}$ and $a_0^{(2)}$ become zeros of $a_f^{(1)}$. Thus solitons in the slow or fast envelope are never lost from their respective envelopes. The middle envelope always loses its solitons, giving solitons to both the slow and fast envelopes. This process is pictorially described in Fig. 1.

In the SBS case, the middle envelope can never contain any solitons, so this exchange will never occur. This is due to the sign of the γ's given by Eq. (A3), which by Eq. (A14b) gives $r^{(2)} = +q^{(2)*}$. [The ZS case where $r = +q^*$ can have no eigenvalues (see Appendix B2).] But, in the explosive and soliton decay cases, Eq. (A14b) gives $r^{(2)} = -q^{(2)*}$, which does allow solitons to exist in the middle envelope. When these solitons are present they correspond to a linear instability (see Appendix D). Furthermore, this can be the case only when the middle envelope has the highest frequency, which is a well known result. Also, we note from the relations between the λ's given by Eq. (A14) and from Eq. (A17) that the eigenvalues of the solitons in the final fast and slow envelopes, which have been received from the middle envelope, are related to the eigenvalue of the soliton in the initial middle envelope by

$$\lambda_k^{(1)} = \frac{c_3 - c_2}{c_3 - c_1} \lambda_k^{(2)}, \tag{A18a}$$

$$\lambda_k^{(3)} = \frac{c_2 - c_1}{c_3 - c_1} \lambda_k^{(2)}. \tag{A18b}$$

It follows from Eq. (A2) that these final eigenvalues will be smaller than the initial eigenvalue $\lambda_k^{(2)}$.

Let us now turn to the problem of determining how action is exchanged between the envelopes. From Eq. (B26) we know that the action for a separated ZS envelope is composed of a radiation part $\mathfrak{N}_r$ and a soliton part $\mathfrak{N}_s$. To calculate the soliton part, by Eq. (B21b)

we only need to know the bound-state eigenvalues, and once we know how the solitons are exchanged (which was discussed above), we then know how this part of the action is exchanged. Before discussing this any further and seeing how it is related to the global conservation laws, let us look at the radiation part. For this part, by Eq. (2.9), we only need to know $\Gamma(\lambda)$, which is defined in Eq. (2.5). Now, Eq. (A17) gives us the final scattering data in terms of the initial scattering data, so by Eq. (2.9) we can relate the final Γ's to the initial Γ's and a "cross term" Σ, which we define to be

$$\Sigma \equiv \frac{b^{(1)}}{\bar{a}^{(1)}}\bar{b}^{(2)}\frac{b^{(3)}}{a^{(3)}}. \tag{A19}$$

If we now look at our three distinct cases, we have for the soliton decay case, in which $(\gamma_i)=(-,+,-)$,

$$\Gamma_f^{(3)} = \frac{1+\Gamma_0^{(2)}}{1+\Gamma_0^{(1)}}\left[\Gamma_0^{(3)} + \frac{\Gamma_0^{(1)}\Gamma_0^{(2)}}{1+\Gamma_0^{(2)}} + 2\,\mathrm{Re}\Sigma_0\right], \tag{A20a}$$

$$\Sigma_0^*\Sigma_0 = \frac{\Gamma_0^{(1)}\Gamma_0^{(2)}\Gamma_0^{(3)}}{1+\Gamma_0^{(2)}}; \tag{A20b}$$

for the SBS case, in which $(\gamma_i)=(-,-,+)$,

$$\Gamma_f^{(3)} = \frac{\Gamma_0^{(3)} + (1+\Gamma_0^{(3)})(\Gamma_0^{(1)}\Gamma_0^{(2)} - 2\,\mathrm{Re}\Sigma_0)}{1+(1+\Gamma_0^{(3)})(\Gamma_0^{(1)}+\Gamma_0^{(2)} - 2\,\mathrm{Re}\Sigma_0)}, \tag{A21a}$$

$$\Sigma_0^*\Sigma_0 = \frac{\Gamma_0^{(1)}\Gamma_0^{(2)}\Gamma_0^{(3)}}{1+\Gamma_0^{(3)}}; \tag{A21b}$$

and for the explosive case, in which $(\gamma_i)=(-,-,-)$,

$$\Gamma_f^{(3)} = \frac{\dfrac{\Gamma_0^{(1)}\Gamma_0^{(2)}}{(1+\Gamma_0^{(1)})(1+\Gamma_0^{(2)})} + \dfrac{\Gamma_0^{(3)}}{1+\Gamma_0^{(3)}} - 2\,\mathrm{Re}\Sigma_0}{\dfrac{1-\Gamma_0^{(1)}\Gamma_0^{(2)}}{(1+\Gamma_0^{(1)})(1+\Gamma_0^{(2)})} - \dfrac{\Gamma_0^{(3)}}{1+\Gamma_0^{(3)}} - 2\,\mathrm{Re}\Sigma_0}, \tag{A22a}$$

$$\Sigma_0^*\Sigma_0 = \frac{\Gamma_0^{(1)}\Gamma_0^{(2)}\Gamma_0^{(3)}}{(1+\Gamma_0^{(1)})(1+\Gamma_0^{(2)})(1+\Gamma_0^{(3)})}. \tag{A22b}$$

The other two Γ_f's can always be obtained from the above, from Eq. (2.5), and from the relations

$$a_f^{(1)}a_f^{(2)} = a_0^{(1)}a_0^{(2)}, \tag{A23a}$$

$$a_f^{(2)}a_f^{(3)} = a_0^{(2)}a_0^{(3)}, \tag{A23b}$$

which follow from the 11 and 33 components of (A15) and (A16). Examples of how these equations are applied for calculating the amount of action exchanged are given in each appropriate section.

At this point, we can discuss the conditions necessary for the envelopes to separate, and therefore for Eq. (A16) to be valid. Whenever Eq. (B1) is satisfied, it follows that Eq. (B26e) is valid, and when (B26e) is valid (as well as no bound states when $r=+q^*$), then unique solutions exist to the inverse scattering equations (B11)–(B14). Thus whenever Eq. (B26e) is not valid, Eq. (B1) must certainly be violated, and the solution of Eqs. (B11)–(B14) need not be unique and nonsingular. Consequently, in order to maintain Eq. (B1) for the final envelopes, it is necessary for the $\Gamma_f^{(3)}$'s in Eqs. (A20)–(A22) to satisfy Eq. (B26e). For the soliton decay case and the SBS case, (B26e) is always satisfied, but for the explosive case it is possible for the denominator in Eq. (A22b) to become negative. When this happens, Eq. (B1) must be violated for the final envelopes and/or we cannot expect separation to occur. This point is discussed more fully in Sec. III.

As is well known, there are three globally conserved quantities (in fact there are an infinite number) which follow from Eq. (A.1). These are

$$\gamma_1\int_{-\infty}^{\infty} Q_1^*Q_1dx - \gamma_2\int_{-\infty}^{\infty} Q_2^*Q_2dx = \text{const}, \tag{A24a}$$

$$\gamma_1\int_{-\infty}^{\infty} Q_1^*Q_1dx - \gamma_3\int_{-\infty}^{\infty} Q_3^*Q_3dx = \text{const}, \tag{A24b}$$

$$\gamma_2\int_{-\infty}^{\infty} Q_2^*Q_2dx - \gamma_3\int_{-\infty}^{\infty} Q_3^*Q_3dx = \text{const}, \tag{A24c}$$

of which only two are linearly independent. We shall now proceed to show that, in scattering space, Eq. (A24) is not only globally conserved, but also pointwise conserved, and that the pointwise conservation of the radiation part is directly related to Eq. (A23). (A linear example is the free-space Schrödinger equation, where the probability density in x space is only conserved globally, while in k space it is conserved pointwise and globally.) We go through the proof only for Eq. (A24a). The proof for Eqs. (A24b) and (A24c) is completely analogous. Using Eq. (A14) to convert (A24a) to the ZS q's and Eq. (2.9) to convert into the scattering data, we have

$$2i\left[\gamma_1(c_3-c_1)\sum_{j=1}^{N^{(1)}}(\lambda_j^{(1)*}-\lambda_j^{(1)}) - \gamma_2(c_3-c_2)\sum_{j=1}^{N^{(2)}}(\lambda_j^{(2)*}-\lambda_j^{(2)})\right]$$

$$+\gamma_1(c_3-c_1)\frac{1}{\pi}\int_{-\infty}^{\infty}d\lambda^{(1)}\ln[1+\Gamma^{(1)}]$$

$$-\gamma_2(c_3-c_2)\frac{1}{\pi}\int_{-\infty}^{\infty}d\lambda^{(2)}\ln[1+\Gamma^{(2)}] = \text{const}. \tag{A25}$$

For the soliton part, we need only to consider the decay interaction. (No soliton exchange can occur in the SBS interaction, and if such an exchange occurs in the explosive case the envelopes never separate.) For that interaction $\gamma_1=\gamma_2$. Then due to the manner of soliton exchange (Fig. 1), and the relation between the final and initial eigenvalues, Eq. (A18), the soliton part of Eq. (A25) is conserved independently for each soliton exchanged. For the radiation part, we use Eq. (A14) to replace the integration over the λ's by one over ζ which gives

$$\int_{-\infty}^{\infty}d\zeta[\gamma_1\ln(1+\Gamma^{(1)}) - \gamma_2\ln(1+\Gamma^{(2)})] = \text{const}.$$

Then from Eqs. (B7a), (B26d), and (A14), we find that the integrand in the above equation becomes simply $2\gamma_1\gamma_2\gamma_3\ln|a^{(1)}a^{(2)}|$, which by Eqs. (A13), (A15), and (A16) can be shown to equal $2\gamma_1\gamma_2\gamma_3\ln|a_{33}|$, where a_{33} is defined by Eq. (A9). By Eq. (A10), $\ln|a_{33}|$ is a constant of the motion, not only globally, but also pointwise. Thus we have

$$\gamma_1\ln[1+\Gamma^{(1)}] - \gamma_2\ln[1+\Gamma^{(2)}] = \text{const}. \tag{A26a}$$

It follows in a similar fashion that

$$\gamma_1 \ln[1+\Gamma^{(1)}] - \gamma_3 \ln[1+\Gamma^{(3)}] = \text{const}, \tag{A26b}$$

$$\gamma_2 \ln[1+\Gamma^{(2)}] - \gamma_3 \ln[1+\Gamma^{(3)}] = \text{const}, \tag{A26c}$$

are conserved for each and all real values of the eigenvalue, ζ. Of course, Eq. (A26) is only true when the envelopes are separated. But if the final envelopes do separate, then (A26) will still have the same value for the final envelopes as it had for the initial envelopes. This follows from the time independence of a_{33} (as well as a_{11} and a_{22}), or from the relations (A23) upon taking the natural logarithm and using Eq. (B26d).

Since Eq. (A26) is a pointwise relation, it shows that in scattering space the exchange of radiation density at one value of the eigenvalue ζ is independent of what is exchanged at any other values of ζ. This is a consequence of the fact that this inverse scattering transform separates the original nonlinear system into its "normal modes," consisting of solitons and radiation. Of course, Eq. (A26) only gives us the relative amount of radiation density which is exchanged. To determine the absolute amount we only need to know $\Gamma_f^{(3)}$, which is given by Eqs. (A20)–(A22).

Finally, the last item which we shall discuss here is the manner in which areas are exchanged when q is real. If we consider Eq. (A17) at $\zeta = 0$, then by Eqs. (B27)–(B32) we obtain equations for either the tangent or the hyperbolic tangent of the final area of each envelope in terms of the initial area of each envelope. This gives us another powerful relation describing the behavior of the interaction.

APPENDIX B: THE ZAKHAROV-SHABAT EIGENVALUE PROBLEM

1. The scattering problem

The general properties of the ZS problem have been discussed in Ablowitz *et al.* (1974). Here we simply describe the major features which we shall need. The potentials of the ZS equations (2.1) are assumed to satisfy the condition

$$\int_{-\infty}^{\infty} [|q| + |r|]\, dx < \infty . \tag{B1}$$

This condition guarantees the existence of $a(\lambda), b(\lambda)$ as defined in Eq. (2.7). The other two components of the ZS scattering matrix $\bar{a}(\lambda)$ and $\bar{b}(\lambda)$ are defined from

$$\bar{\phi} \to \begin{bmatrix} 0 \\ -1 \end{bmatrix} e^{+i\lambda x} \text{ as } x \to -\infty , \tag{B2}$$

$$\bar{\phi} \to \begin{bmatrix} \bar{b}(\lambda)\, e^{-i\lambda x} \\ -\bar{a}(\lambda)\, e^{+i\lambda x} \end{bmatrix} \text{as } x \to +\infty . \tag{B3}$$

Wronskian relations of the solutions of Eqs. (2.1) give

$$\bar{a}a + \bar{b}b = 1 . \tag{B4}$$

In analogy to ρ we define

$$\bar{\rho}(\lambda) = \frac{\bar{b}(\lambda)}{\bar{a}(\lambda)} . \tag{B5}$$

2. Specialization to $r = \pm q^*$ and to constant phase

For the three-wave problem we need only the two cases where

$$r = \pm q^* . \tag{B6}$$

When Eq. (B6) is satisfied, we have from the symmetry of Eq. (2.1), if a and b can be extended off the real axis,

$$\bar{a}(\lambda) = [a(\lambda^*)]^* , \tag{B7a}$$

$$\bar{b}(\lambda) = \mp [b(\lambda^*)]^* , \tag{B7b}$$

so these components are not independent of a and b. This also implies

$$\bar{\rho}(\lambda) = \mp [\rho(\lambda^*)]^* .$$

It follows from Eqs. (B4) and (B7) that, if λ is real, then for $r = -q^*$

$$0 \le |\rho(\lambda)| \le \infty , \tag{B8a}$$

and for $r = q^*$

$$0 \le |\rho(\lambda)| < 1 . \tag{B8b}$$

When $r = +q^*$ and Eq. (B1) is satisfied, Eq. (2.1) is self-adjoint. Thus λ must be real, and no bound states can occur. But when $r = -q^*$ and Eq. (B1) is satisfied, bound states can occur.

When $\arg(a_i)$ is independent of x for each envelope, the envelopes may all be taken to be real, because only the phase difference

$$\arg(a_i) - \arg(a_j) - \arg(a_k) - \arg(K)$$

is important (see Appendix E). This implies that the q's and r's can all be taken to be real [Eq. (A14)].

Whenever q is real, the eigenvalue spectrum is further restricted. Equations (2.1) and (2.3) then imply

$$a(-\lambda^*) = a^*(\lambda) , \tag{B9a}$$

$$b(-\lambda^*) = b^*(\lambda) . \tag{B9b}$$

Thus for the bound-state eigenvalues, the zeros of a must either be pure imaginary or occur as conjugate pairs. In the latter case, if λ_k is an eigenvalue with a nonzero real part, then there must exist another eigenvalue, call it λ_j, such that

$$\lambda_j^* = -\lambda_k . \tag{B10a}$$

Examples of this type of two-soliton solution are the "breather" of the sine-Gordon equation (Ablowitz *et al.*, 1974) and the $0-\pi$ pulse in SIT (Lamb, 1971). Furthermore, we also have

$$D_j^* = D_k \tag{B10b}$$

for these conjugate pairs.

3. The inverse scattering equations

The direct scattering problem for the ZS eigenvalue problem is used to decompose each separated envelope in the three-wave interaction into ZS scattering data. In the inverse scattering problem, we are given the ZS scattering data, from which we must reconstruct the ZS potential q, which is an envelope in the three-wave interaction. We shall use only the inverse scattering equations for calculating N-solitons. The gen-

eral formal solution of the inverse scattering problem is as follows. First one constructs $F(x)$

$$F(x)=\sum_{k=1}^{N} D_k \exp(i\lambda_k x)+\frac{1}{2\pi}\int_{-\infty}^{\infty}\rho(\lambda)\exp(i\lambda x)\,d\lambda\,, \tag{B11}$$

and then solves the linear integral equations

$$\overline{K}(x,y)+\int_x^{\infty} K(x,s)F(s+y)\,ds=0\,, \tag{B12a}$$

$$K(x,y)-\overline{F}(x+y)-\int_x^{\infty}\overline{K}(x,s)\overline{F}(s+y)\,ds=0\,, \tag{B12b}$$

where, if Eq. (B6) is true,

$$\overline{F}(x)=\mp F^*(x)\,. \tag{B13}$$

Then one recovers q from

$$q(x)=-2K(x,x)\,. \tag{B14}$$

Note that when $\rho(\lambda)=0$ for λ real, the kernels in Eq. (B12), $F(s+y)$ and $\overline{F}(s+y)$, become separable, allowing a closed-form solution. This is the N-soliton solution. A solution to Eq. (B12) always exists and is unique whenever (i) $r=-q^*$, or (ii) $r=+q^*$, no bound states occur, and $|\rho(\lambda)|<1$ for λ real. In case (ii), those conditions are always satisfied whenever Eq. (B1) is satisfied. Thus if $r=+q^*$, it follows that whenever bound states occur or $|\rho(\lambda)|>1$, then Eq. (B1) must be violated.

Although Eqs. (B11)–(B14) do give the formal solution for determining the envelopes from the ZS scattering data, the information contained therein is not readily accessible. However, as we shall see, there is still much information which can be obtained without the use of these inverse scattering equations, which we shall illustrate. We discuss the N-soliton solution in Sec. B.4. In B.5 we show how one can determine the action and area of an envelope directly from the scattering data, thereby bypassing the need for solving Eqs. (B11)–(B14) in obtaining this information.

4. The N-soliton formula and its numerical evaluation

When $\rho(\lambda)=0$ for all real λ, the inverse scattering equations (B11), (B12) are soluble in closed form. The resulting solutions are called "N-soliton formulas," where N is the number of bound states. Of course, the bound-state part of the spectrum of Eq. (2.1) is only present in Eq. (B11) when $r=-q^*$ [providing that Eq. (B1) is satisfied]. This part of the spectrum is called the "soliton" part.

For the cases we consider the eigenvalues are all pure imaginary. If we let

$$\lambda_i=i\eta_i \tag{B15}$$

(B11) becomes

$$F(x)=\sum_{k=1}^{n} D_k\exp(-\eta_k x)\,. \tag{B16}$$

With Eq. (B13), Eqs. (B12) now give

$$K(x,y)=\sum_k D_k\exp(-\eta_k y)\Big\{\exp(-\eta_k x)+\sum_l D_l\int_x^{\infty}ds\int_s^{\infty}ds'K(x,s')\times\exp[-\eta_l(s+s')-\eta_k s]\Big\}\,, \tag{B17}$$

The solution may be obtained by noting that K is of the form

$$K(x,y)=\sum_{k=1}^{n} J_k(x)D_k\exp(-\eta_k y)\,. \tag{B18}$$

Substituting this into Eq. (B17), solving for J_k, and using Eq. (B14), we find

$$q(x)=\sum_{j,k=1}^{n} D_j\exp[-(\eta_j+\eta_k)x](1+N^2)^{-1}_{jk}\,, \tag{B19a}$$

where the matrix N is

$$N_{ij}=\frac{D_j\exp[-(\eta_j+\eta_k)x]}{\eta_i+\eta_j}\,. \tag{B19b}$$

In particular, the one-soliton solution is

$$q(x)=-2\eta_1\,\mathrm{sgn}(-D_1)\,\mathrm{sech}[2\eta_1(x-x_0)]\,, \tag{B20a}$$

where the phase x_0 is defined by

$$|D_1|=2\eta_1\exp(2\eta_1 x_0)\,. \tag{B20b}$$

When the phases of the solitons are well separated, the N-soliton solution is approximately the linear superposition of the N corresponding one-soliton solutions.

If, rather than using Eq. (B18), we make the alternative substitution

$$K(x,y)=\sum_{k=1}^{n} D_k\exp(-\eta_k y)[\exp(-\eta_k x)+J_k(x)]\,, \tag{B21}$$

we obtain a different form of the formula for q. This form is less convenient for numerical evaluation than is Eq. (B19) because it involves near cancellation of large numbers.

Some care is necessary in numerically inverting the matrix $1+N^2$. Because of their exponential dependence on $\eta_k x$, the elements of this matrix can be of very different magnitude. We handles this problem by a rescaling transformation of the form

$$M(x)=S(x)[1+N^2(x)]T(x)\,. \tag{B22a}$$

After inversion of M, we recover the solution by

$$(1+N^2)^{-1}=TM^{-1}S\,. \tag{B22b}$$

One such transformation that we have found convenient is

$$S_{ij}=\exp(2\eta_i x)\delta_{ij},\quad T_{kl}=\frac{\exp(2\eta_k x)}{D_k}\delta_{kl}\,. \tag{B23}$$

5. Information contained directly in the scattering data

Rewriting the ZS equations in integral form and evaluating the integrals asymptotically in ξ, we find (Zakharov and Shabat, 1971; Ablowitz *et al.*, 1974)

$$a(\zeta) \sim 1 - \frac{1}{2i\zeta}\int_{-\infty}^{\infty} q(x)r(x)\,dx + O\left(\frac{1}{\zeta^2}\right). \tag{B24}$$

Alternatively, we can use the analytic properties of $a(\zeta)$ to get an integral representation

$$a(\zeta) = \prod_{k=1}^{N}\frac{\zeta-\zeta_k}{\zeta-\zeta_k^*}\exp\left\{\frac{i}{2\pi}\int_{-\infty}^{\infty}\frac{d\xi}{\xi-\zeta}\ln[1+\bar{\rho}\rho]\right\}. \tag{B25}$$

Expanding Eq. (B25) asymptotically in ζ and setting the coefficient of $1/\zeta$ equal to that in Eq. (B24), we can express the action directly in terms of the scattering data

$$\mathfrak{N} = \int_{-\infty}^{\infty} q^* q\,dx = \mathfrak{N}_s + \mathfrak{N}_r, \tag{B26a}$$

where

$$\mathfrak{N}_s = 2i\sum_{j=1}^{N}(\lambda_j^* - \lambda_j), \tag{B26b}$$

$$\mathfrak{N}_r = \frac{1}{\pi}\int_{-\infty}^{\infty} d\lambda \ln[1+\Gamma(\lambda)], \tag{B26c}$$

and when $r = \pm q^*$, $\Gamma(\lambda)$ is defined by

$$\begin{aligned} 1+\Gamma(\lambda) &= [1+\bar{\rho}\rho(\lambda)]^{\mp 1}, \\ &= [1 \mp |\rho(\lambda)|^2]^{\mp 1}, \\ &= [\bar{a}a(\lambda)]^{\pm 1}. \end{aligned} \tag{B26d}$$

By Eqs. (B4) and (B7)

$$0 \le \Gamma(\lambda) \le \infty \text{ if } \lambda = \text{real}. \tag{B26e}$$

Note how Eq. (B26a) has naturally decomposed into a soliton part, (B26b), and a radiation part, (B26c). Thus given $\{\lambda_j\}_{j=1}^{N}$ and $|\rho(\lambda)|$ for λ real, one can determine $\mathfrak{N}$ without recourse to the inverse scattering equations (B11)–(B14).

In addition to $\mathfrak{N}$, when the ZS potential is real (or has a constant phase), one can also obtain the area under an envelope directly from the scattering data. Recalling that the Fourier transform of a function at zero argument is just the area under the function, and since the reflection coefficient $\rho(\lambda)$ is like a "nonlinear Fourier transform," it is not surprising that $\rho(0)$ is related (nonlinearly) to the area. To show this, we let

$$\mathfrak{U}(x) \equiv \int_{-\infty}^{x} q\,dx. \tag{B27}$$

Then the solution ϕ of Eq. (2.1) at $\lambda = 0$ for $r = -q^*$ is

$$\phi\Big|_{\lambda=0} = \begin{bmatrix} \cos\mathfrak{U}(x) \\ -\sin\mathfrak{U}(x) \end{bmatrix}. \tag{B28}$$

Thus from Eq. (2.3) we have the *exact* result of

$$a(0) = \cos A, \tag{B29a}$$

$$b(0) = -\sin A, \tag{B29b}$$

where

$$A = \mathfrak{U}(\infty) = \int_{-\infty}^{\infty} q\,dx \tag{B30}$$

is the area under the envelope q. This result is closely associated with the area theorem of McCall and Hahn (1967, 1969) (Kaup, 1977). Similarly, for $r = +q^*$, one finds

$$a(0) = \cosh A, \tag{B31a}$$

$$b(0) = \sinh A, \tag{B31b}$$

with A still given by Eq. (B30).

From the integral representation of $a(\lambda)$, in Eq. (B25), we see that for real q,

$$a(0) = \frac{(-)^N}{\sqrt{1+\bar{\rho}\rho(0)}}, \tag{B32}$$

where N is the total number of the zeros of $a(\lambda)$ in the upper half-plane (and is also the total number of solitons). Comparing Eq. (B32) with (B29a), we see that when the number of solitons is odd (even), $\cos A$ must be negative (positive), which then specifies A to within $2\pi m$. Knowing the N-soliton solution allows us to calculate the areas exactly. The addition of radiation to an N-soliton solution can change the area by at most $\pm\pi$.

6. The direct scattering problem: WKB and an exact solution

First we sketch the WKB solution for bound states which we use in the main text. When q is real, slowly varying, has only one extremum, and does not cross zero, then approximate eigenvalues can be obtained from (Kaup, 1977)

$$\int_{x_1}^{x_2}(q^2-\eta^2)^{1/2}dx = \pi\left(n+\frac{1}{2}\right), \tag{B33}$$

where we have set $\lambda = i\eta$, x_1, and x_2 are the classical turning points, and n is an integer. Letting $\eta \to 0$ in Eq. (B33) allows us to determine the total number of solitons, N, contained in the envelope, and this is

$$N < \frac{1}{\pi}\bar{A} + \frac{1}{2}, \tag{B34}$$

where

$$\bar{A} \equiv \int_{-\infty}^{\infty}|q|\,dx \tag{B35}$$

is the total absolute area under the envelope. Of course, when q does not cross zero, $\cos A = \cos\bar{A}$, and we have complete agreement between Eq. (B34) and the sign of (B29a) as given by (B32).

When q does cross zero, the WKB condition for bound states becomes more complicated. For example, if q crosses zero once, we can have a complex eigenvalue. In this case we never have any real turning points, but still, one can show (Ablowitz *et al.*, 1974) that if

$$\bar{A} < 0.903, \tag{B36}$$

then no bound states can ever occur.

Lastly, we give the solution for a and b when the potential q is a square pulse, as well as the bound-state eigenvalues when $r = -q^*$. We take q to be nonzero only when $l_- < x < l_+$, and then to have the fixed real value of Q inside of this interval. Then if we define

$$\Delta = [\lambda^2 \mp Q^2]^{1/2}, \tag{B37}$$

for $r = \pm q^*$, we find from Eqs. (2.1) and (2.3) that

$$\begin{aligned} a(\lambda) = \frac{1}{2}\exp(i\lambda L)\Big[&\left(1-\frac{\lambda}{\Delta}\right)\exp(i\Delta L) \\ &+ \left(1+\frac{\lambda}{\Delta}\right)\exp(-i\Delta L)\Big], \end{aligned} \tag{B38}$$

$$b(\lambda) = \mp \frac{Q}{2i\Delta}[\exp(i\Delta L) - \exp(-i\Delta L)]\exp[-i\lambda(l_+ + l_-)], \tag{B39}$$

where

$$L = l_+ - l_-, \tag{B40}$$

is the length of the pulse. Note that a and b are even functions of Δ, and thus are analytic functions of λ, even though Eq. (B37) has branch cuts.

When $r = -q^*$, the bound states are given by the zeros of $a(\lambda)$ for λ in the upper half λ-plane. To find these, we define

$$k = \Delta L, \tag{B41a}$$

$$\kappa = -i\lambda L. \tag{B41b}$$

Then Eq. (B37) becomes

$$\kappa^2 + k^2 = A^2, \tag{B42a}$$

where $A = QL$ is the area of the pulse. Requiring $a(\lambda)$ to be zero gives

$$\kappa = -k\cot k. \tag{B42b}$$

One will recognize Eq. (B42) as being the same equation as that which determines the eigenvalues of a Schrödinger particle in a three-dimensional spherical well (Schiff, 1955). To find the eigenvalues by graphic means, one plots Eq. (B42b), draws a circle of radius A, the intercepts to which (for k and κ positive) give the eigenvalues, by Eq. (B41b). Note that in this case of a square pulse, since Eq. (B42) also occurs for the Schrödinger equation (whose eigenvalue, λ^2, must be real), we know that λ cannot be complex in general, and must be either real or imaginary. Thus no breathers can occur. In general, breathers will only occur when the potential is real if it has more than one extremum.

APPENDIX C: NUMERICAL INTEGRATION OF THE PARTIAL DIFFERENTIAL EQUATIONS

The numerical integration of Eqs. (1.1) has been carried out using a stable (Reiman and Bers, 1975) finite difference method.

We first transform Eqs. (1.1) to a set of equations along the characteristics by substituting

$$b_i(x,t) \equiv a_i(x + v_i t, t). \tag{C1}$$

The resulting equations,

$$\frac{d}{dt}b_1(x,t) = p_1 K b_2(x + (v_1 - v_2)t, t)\, b_3(x + (v_1 - v_3)t, t), \tag{C2a}$$

$$\frac{d}{dt}b_2(x,t) = -p_2 K^* b_1(x + (v_2 - v_1)t, t)\, b_3^*(x + (v_2 - v_3)t, t), \tag{C2b}$$

$$\frac{d}{dt}b_3(x,t) = -p_3 K^* b_1(x + (v_3 - v_1)t, t)\, b_2^*(x + (v_3 - v_2)t, t), \tag{C2c}$$

no longer have partial derivatives with respect to x. By writing our finite difference approximation in terms of these transformed equations, we eliminate the restriction on $\Delta x/\Delta t$ imposed by the Courant–Friedrichs–Lewy condition (Richtmyer and Morton, 1969). We pay for this simplification by complicating the arguments of the amplitudes on the right-hand side of the equations.

The solutions to Eqs. (1.1) are known exactly for initial conditions independent of x. Preliminary experimentation using these initial conditions indicated that a relatively high-order difference scheme was expedient for obtaining reasonable numerical accuracy over several periods of oscillation of the amplitudes. We use a fourth-order Runge–Rutta scheme to integrate from one time step to the next. The arguments of the amplitudes on the right-hand side of (C2) generally do not fall on the points of a grid. We use a five-point polynomial interpolation formula to calculate amplitudes on grid points.

The existence of two conserved quantities,

$$c_1 \equiv \int_{-\infty}^{\infty} (p_1|a_1(x)|^2 + p_2|a_2(x)|^2)\,dx \tag{C3a}$$

and

$$c_1 \equiv \int_{-\infty}^{\infty} (p_1|a_1(x)|^2 + p_3|a_3(x)|^2)\,dx, \tag{C3b}$$

provides a running check on the accuracy of our computations. Conservation of both quantities was generally better than 0.01%. In addition, we used the exact solution of the space-independent equations (Armstrong *et al.*, 1962), the solution of the linearized equations for a large amplitude pump, Eqs. (1.3), and the exact Ohsawa–Nozaki soliton solution (Ohsawa and Nozaki, 1974) to initially debug and test the program.

The existence of explosive instabilities in solutions of the equations made the use of a variable time step necessary. The time step

$$\Delta t = c/\sqrt{\|a_1\|_\infty^2 + \|a_2\|_\infty^2 + \|a_3\|_\infty^2},$$

where $\|\ \|_\infty$ denotes a maximum over x and c is a constant determined by the initial step size, was found to work well even in the neighborhood of a singularity. The choice of initial step size was constrained by the existence of two time scales: $\tau_1 = 1/|KA|$, where A is the largest amplitude present, and $\tau_2 = \min(L_i/v_i)$, where L_i is the width of the ith pulse.

The program was run interactively under the time-sharing option (TSO) on MIT's IBM 370/165. The interaction allowed for specification of the number of time steps between pauses in the computation and for specification of the data to be sent to the terminal and to disk files during those pauses. It was sometimes also found convenient to modify the time step size interactively.

APPENDIX D: PHYSICAL INTERPRETATION OF ZS SCATTERING DATA

To find a physical interpretation for the ZS scattering data of each well separated envelope, we consider the effects of linear perturbations on the resonant equations (A1). Replacing the 1, 2, and 3 in (A1) by κ, μ, and ν, due to the symmetric form of (A1) we can analyze all possible cases with one derivation upon permuting

κ, μ, ν. We consider first the κth envelope. In the region where it is nonzero, the μth and νth envelopes are zero, since they are well separated. We go to the Galilean frame, where c_κ is zero, and analyze the linear stability properties of this envelope, as well as its converting characteristics. Allowing infinitesimal amounts of the μth and νth waves to be present, (A1) gives

$$\delta Q_{\mu,t} + c_\mu \delta Q_{\mu,x} = \gamma_\mu Q_\kappa^* \delta Q_\nu^* , \tag{D1a}$$

$$\delta Q_{\nu,t} + c_\nu \delta Q_{\nu,x} = \gamma_\nu Q_\kappa^* \delta Q_\mu^* , \tag{D1b}$$

where δQ_μ and δQ_ν are infinitesimal. To analyze the linear properties of this system, since Q_κ is now time independent (due to $c_\kappa = 0$ and no overlap), we may let δQ_μ and δQ_ν^* vary as $e^{-i\omega t}$. If we define v_1 and v_2 by

$$\delta Q_\mu = \frac{v_1}{\sqrt{|c_\mu|}} \exp(i\Delta x) \exp(-i\omega t) , \tag{D2a}$$

$$\delta Q_\nu^* = \frac{v_2}{\sqrt{|c_\nu|}} \exp(i\Delta x) \exp(-i\omega t) , \tag{D2b}$$

where

$$\Delta = \omega \frac{c_\mu + c_\nu}{2 c_\mu c_\nu} , \tag{D3}$$

then Eq. (D1) becomes

$$v_{1,x} + i\lambda v_1 = q v_2 , \tag{D4a}$$

$$v_{2,x} - i\lambda v_2 = r v_1 , \tag{D4b}$$

which is exactly the ZS equation (2.1), provided we identify

$$\lambda = \omega \frac{c_\mu - c_\nu}{2 c_\mu c_\nu} , \tag{D5}$$

$$q = \gamma_\mu \alpha_\mu \frac{Q_\kappa^*}{\sqrt{|c_\mu c_\nu|}} , \tag{D6a}$$

$$r = \gamma_\mu \gamma_\nu \alpha_\mu \alpha_\nu q^* \text{ (i.e., } r = \pm q^*) , \tag{D6b}$$

where

$$\alpha_\mu \equiv \operatorname{sgn}(c_\mu) , \tag{D7a}$$

$$\alpha_\nu \equiv \operatorname{sgn}(c_\nu) . \tag{D7b}$$

For well separated envelopes, it is exactly Eq. (D4) which is used in the inverse scattering theory to decompose the envelopes into the ZS scattering data, or normal modes. We now see that this scattering data must also be related to the properties of the linear system, (D1), in the presence of the pump Q_κ.

First, we consider the bound-state spectrum of Eq. (D4). This can only occur when $r = -q^*$ in Eq. (D6b) (the $r = +q^*$ form is self-adjoint) and happens for all envelopes in the decay mode, the middle envelope of the explosive mode, and the "backscattered" envelope in the SBS mode. If we have a bound state at $\lambda = \lambda_k$, with λ_k in the upper half λ-plane, then by Eqs. (D2), (D3), and (D5), the eigenmodes of Eq. (D1) have the asymptotic forms of

$$\begin{bmatrix} \delta Q_\mu \\ \delta Q_\nu^* \end{bmatrix} \to \begin{bmatrix} |c_\mu|^{-1/2} \\ 0 \end{bmatrix} \exp\left[\frac{2i\lambda_k c_\nu}{c_\mu - c_\nu} (x - c_\mu t) \right] \text{ as } x \to -\infty \tag{D8a}$$

and

$$\begin{bmatrix} \delta Q_\mu \\ \delta Q_\nu^* \end{bmatrix} \to \begin{bmatrix} 0 \\ b_k |c_\nu|^{-1/2} \end{bmatrix} \exp\left[\frac{2i\lambda_k c_\mu}{c_\mu - c_\nu} (x - c_\nu t) \right] \text{ as } x \to +\infty . \tag{D8b}$$

Of course, for every eigenmode of Eq. (D1) with λ_k in the upper half λ-plane, there is also a conjugate eigenmode for $\lambda = \bar{\lambda}_k$ in the lower half λ-plane, where

$$\bar{\lambda}_k = \lambda_k^* . \tag{D9}$$

This mode is given by Eq. (B6)–(B8) and has the asymptotic forms of

$$\begin{bmatrix} \delta Q_\mu \\ \delta Q_\nu^* \end{bmatrix} \to \begin{bmatrix} 0 \\ -|c_\nu|^{-1/2} \end{bmatrix} \exp\left[\frac{2i\lambda_k^* c_\mu}{c_\mu - c_\nu} (x - c_\nu t) \right] \text{ as } x \to -\infty , \tag{D10a}$$

$$\begin{bmatrix} \delta Q_\mu \\ \delta Q_\nu^* \end{bmatrix} \to \begin{bmatrix} b_k^* |c_\mu|^{-1/2} \\ 0 \end{bmatrix} \exp\left[\frac{2i\lambda_k^* c_\nu}{c_\mu - c_\nu} (x - c_\mu t) \right] \text{ as } x \to +\infty . \tag{D10b}$$

Note that if Eq. (D8) has an exponential growth (decay) in time, then Eq. (D10) has an exponential decay (growth).

Consider Eqs. (D8) and (D10) when the middle envelope is the pump, and take

$$c_\mu > c_\kappa = 0 > c_\nu . \tag{D11}$$

Then Eq. (D8) is exponentially decaying in time and (D10) is exponentially growing in time. Note also that the spatial dependence as $x \to \pm\infty$ is always exponential decay in x. Thus for the middle envelope, the existence of a bound state in the ZS scattering data always corresponds to a linear unstable growth (and decay) mode.

Now, consider Eqs. (D8) and (D10) when the pump is the slow envelope, and take

$$c_\mu > c_\nu > c_\kappa = 0 . \tag{D12}$$

In this case, Eq. (D8) is the growth mode (in time) and (D10) is a decay mode. But note the spatial dependence as $x \to \pm\infty$. Now, Eq. (D8) has exponential growth in x as $x \to -\infty$, and (D10) has exponential growth in x as $x \to +\infty$. [This growth is solely due to the phase factor of Δx in Eq. (D2). The eigenstates of Eq. (D4) have no growth, only decay.] Thus, for the fast envelope, and similarly for the slow envelope, the existence of bound states do not correspond to any linear instabilities (they have none). Rather, they correspond to a growth rate only when the perturbation is exponentially growing in x.

Let us now turn our attention to a physical interpretation of the continuous spectrum of the ZS scattering data. To do this, we shall simply scatter infinitesimal waves off of the pump. From Eqs. (2.1), (2.2) and (D2), (D3), (D5), we want to consider the physical situation where

$$\begin{bmatrix} \delta Q_\mu \\ \delta Q_\nu^* \end{bmatrix} \to \begin{bmatrix} |c_\mu|^{-1/2} \\ 0 \end{bmatrix} \exp[-i\omega(t - x/c_\mu)] \text{ as } x \to -\infty \tag{D13}$$

and then we will have on the right

$$\begin{bmatrix}\delta Q_\mu \\ \delta Q_\nu^*\end{bmatrix} \to \begin{bmatrix}a(\lambda)|c_\mu|^{-1/2}\exp[-i\omega(t-x/c_\mu)] \\ b(\lambda)|c_\nu|^{-1/2}\exp[-i\omega(t-x/c_\nu)]\end{bmatrix} \quad \text{as } x\to+\infty\,, \tag{D14}$$

where λ is given by Eq. (D5). First, consider the case where the pump is the middle envelope, and let

$$c_\nu > 0 > c_\mu\,, \tag{D15}$$

so that λ and ω will have the same sign. By our convention (A2), $\mu=1$, $\kappa=2$, and $\nu=3$, and we can interpret Eqs. (D13) and (D14) as follows. In (D14), δQ_1 is a wave incident on the pump from the right, of amplitude $|a(\lambda)|\,|c_1|^{-1/2}$, while δQ_3^* represents the amount of the fast wave which has been produced by the interaction of δQ_1 with the pump. Meanwhile, Eq. (D13) simply represents that part of the incident wave which is transmitted through the pump. Therefore, $1/a(\lambda)$ is the physical transmission coefficient for this system and $[b(\lambda)/a(\lambda)]|c_1/c_3|^{1/2}$ is the physical "conversion coefficient," $\delta Q_3^*/(\delta Q_1)_{\rm inc}$. Of course, if the pump has any linear instabilities, we can only consider the above as a gedanken experiment and not as an actual physical experiment.

For the fast or slow envelope as the pump, no linear instabilities are present. Considering the slow envelope and taking

$$c_\mu > c_\nu > 0\,, \tag{D16}$$

we have $\mu=3$, $\nu=2$, and $\kappa=1$. In this case, Eq. (D13) gives the incident wave as being δQ_3, then $a(\lambda)$ is the physical transmission coefficient and $b(\lambda)|c_3/c_2|^{1/2}$ is the physical conversion coefficient.

APPENDIX E: THE PHASES IN HOMOGENEOUS INTERACTIONS

Express

$$a_\mu = |a_\mu|\exp(i\varphi_\mu) \tag{E1}$$

and

$$K = |K|e^{i\nu} \tag{E2}$$

with ϕ_μ and ν real. Taking the real and imaginary parts of Eq. (1) we get

$$\left(\frac{\partial}{\partial t}+v_i\frac{\partial}{\partial x}\right)|a_i| = p_i|Ka_ja_k|\cos\theta\,, \tag{E3a}$$

$$\left(\frac{\partial}{\partial t}+v_j\frac{\partial}{\partial x}\right)|a_j| = -p_j|Ka_ia_k|\cos(-\theta)\,, \tag{E3b}$$

$$\left(\frac{\partial}{\partial t}+v_k\frac{\partial}{\partial x}\right)|a_k| = -p_k|Ka_ia_j|\cos(-\theta)\,, \tag{E3c}$$

$$\left(\frac{\partial}{\partial t}+v_i\frac{\partial}{\partial x}\right)\varphi_i = p_i\left|\frac{Ka_ja_k}{a_i}\right|\sin\theta\,, \tag{E4a}$$

$$\left(\frac{\partial}{\partial t}+v_j\frac{\partial}{\partial x}\right)\varphi_j = -p_j\left|\frac{Ka_ia_k}{a_j}\right|\sin(-\theta)\,, \tag{E4b}$$

$$\left(\frac{\partial}{\partial t}+v_k\frac{\partial}{\partial x}\right)\varphi_k = -p_k\left|\frac{Ka_ia_j}{a_k}\right|\sin(-\theta)\,, \tag{E4c}$$

where

$$\theta = \nu+\phi_j+\phi_k-\phi_i\,. \tag{E5}$$

The initial phases enter the equations only through θ. We can alter the initial phases in any manner that does not change θ, without changing the interaction.

When one of the amplitudes is initially zero, the phase of that amplitude is undefined at $t=0$. We must examine Eqs. (1.1) in the neighborhood of $t=0$ to determine the initial θ. There are two cases.

(1) $a_i(x,t=0)\equiv 0$. Then

$$a_i(x,\Delta t)\approx p_iKa_j(x,t=0)a_k(x,t=0)\Delta t \tag{E6a}$$

and

$$\varphi_i(t=\Delta t) = \arg(p_i)+\nu+\varphi_j(t=0)+\varphi_k(t=0)\,. \tag{E6b}$$

If $p_i=1$ then $\theta=0$. If $p_i=-1$ then $\theta=\pi$.

(2) One of the low-frequency amplitudes is initially zero. Without loss of generality we take $a_k(x,t=0)\equiv 0$. Then

$$a_k(x,\Delta t)\approx -p_kK^*a_i(x,t=0)a_j^*(x,t=0)\Delta t\,, \tag{E7a}$$

$$\varphi_k(t=\Delta t) = \pi+\arg(p_k)-\nu+\phi_i(t=0)-\varphi_j(t=0)\,. \tag{E7b}$$

If $p_k=1$ then $\theta=\pi$. If $p_k=-1$ then $\theta=0$.

Thus the phases have disappeared as an initial parameter of our interactions. We can choose the initial phases to be anything we want without affecting the interaction.

From Eqs. (E4) we see that if $\theta=0$ or $\theta=\pi$ initially, then the phases remain unchanged except when one of the a_j's become zero. In that case the argument of the preceding paragraph can be applied again, and the corresponding amplitude changes sign. When one of the wave amplitudes is initially zero, we can choose K and all the a_j's to be real at $t=0$. They will remain real for all time.

We have seen that for $|a_j(x,t=0)|$, $|a_k(x,t=0)| \ll |a_i(x,t=0)|$ the interaction is initially linear. The solution to the initial value problem for t small can therefore be expressed as the superposition of two solutions, the initial conditions for each of which have one amplitude initially zero. For one of these solutions we set $a_j(x,t=0)$ to zero and assume the given $a_k(x,t=0)$. For the other solution we set $a_k(x,t=0)$ to zero. The phases again initially adjust themselves so that either $\theta=0$ or $\theta=\pi$. The argument now proceeds as before. We can again choose the initial amplitudes to be real.

APPENDIX F: NOISE-INDUCED SOLITON DECAY

Here, we shall briefly derive how arbitrary noise levels in all three waves will induce the pump in the soliton decay case to decay. We also calculate the decay time as well as the spread in the eigenvalue of the pump. For simplicity, we shall assume the pump to be a single soliton, although we shall not make this assumption until after the general equations have been derived. The general approach will follow that of Kaup (1976b) and Kaup and Newell (1978).

First, we shall determine how a small change in the potentials δV_{ij} affects the scattering data. As in Kaup (1976a), define $\Psi^{(j)}(j=1,2,3)$ to be solutions of Eq. (A5) which satisfy the boundary conditions:

$$\Psi_n^{(j)} \to \delta_n^j\exp(-ic_j\zeta x) \quad \text{as } x\to+\infty\,, \tag{F1}$$

and $\Phi^{(j)}$ to satisfy the boundary conditions in Eq. (A7). We define the corresponding adjoint states by

$$\epsilon^{ijk}\Phi_n^{(k)A} = -c_n \sum_{m,p=1}^{3} \epsilon_{nmp}\Phi_m^{(i)}\Phi_p^{(j)} \exp[i\zeta x(c_1+c_2+c_3)], \tag{F2}$$

and correspondingly for $\Psi_n^{(k)A}$, where in (F2), ϵ_{ijk} is the totally antisymmetric tensor of rank three. Then due to Eqs. (A5) and (F1)

$$\tilde{\Phi}^{(j)A} C^{-1}\Phi^{(k)} = -\delta_k^j, \tag{F3}$$

where $\tilde{}$ denotes the matrix transpose and

$$C \equiv \mathrm{diag}[c_1, c_2, c_3]. \tag{F4}$$

As $V=[V_{ij}]$ is varied in Eq. (A5), $\Phi^{(j)}$ will also vary, and its variation can be expanded in terms of the independent $\Phi^{(k)}$'s as

$$\delta\Phi^{(j)} = \sum_{k=1}^{3} \alpha_{jk}\Phi^{(k)}. \tag{F5}$$

Inserting Eq. (F5) into the variation of Eq. (A5) then gives

$$\sum_{j=1}^{3} (\partial_x \alpha_{kj})\Phi^{(j)} = -i(\delta V)\Phi^{(k)} \tag{F6}$$

which with Eq. (F3) gives

$$\alpha_{jk} = i\int_{-\infty}^{x} dx \tilde{\Phi}^{(k)A} C^{-1}(\delta V)\Phi^{(j)}. \tag{F7}$$

Then from Eqs. (A8) and (F5), since

$$\Psi^{(k)A} = \sum_{l=1}^{3} \Phi^{(l)A} a_{lk}, \tag{F8}$$

we have

$$\delta a_{jk} = I[\Psi^{(k)}, \Phi^{(j)}], \tag{F9}$$

where

$$I[U, W] \equiv i\int_{-\infty}^{\infty} \tilde{U}^A C^{-1}(\delta V) W dx. \tag{F10}$$

Defining b_{ij} to be the inverse of a_{ij}, then

$$\delta b_{ij} = -I[\Phi^{(j)}, \Psi^{(i)}]. \tag{F11}$$

This allows us to calculate the change in the scattering data due to variations in the potentials.

For the decay of the pump, since it must proportionally distribute its energy and modes between the two other waves, we need to consider only $q^{(3)}$ to see what is happening. As $t \to +\infty$, we have

$$\rho^{(3)} = \frac{b^{(3)}}{a^{(3)}} = \frac{b_{21}}{b_{11}}, \tag{F12}$$

and thus

$$\delta\rho^{(3)} = I[\Phi^{(1)}, \chi], \tag{F13}$$

where

$$\chi \equiv b_{21}\Psi^{(1)} - b_{11}\Psi^{(2)}. \tag{F14}$$

Equation (F12) gives the effect of variations in δV on the radiation part of $q^{(3)}$. In the decay case, we are more interested in the solitons emitted into $q^{(3)}$. To find out how the noise level affects these, we must look at the zeros of b_{11} in the upper half ζ-plane, as well as the residue of $\rho^{(3)}$ at these zeros. At a zero of b_{11},

$$db_{11} = \delta b_{11} + b'_{11}\delta\zeta = 0, \tag{F15}$$

where $b'_{11} = \partial b_{11}/\partial\zeta$. If we designate these zeros by ζ_k, then from Eqs. (F11) and (F15),

$$\delta\zeta_k = \frac{1}{(b'_{11})_k} I[\Phi^{(1)}, \Psi^{(i)}; \zeta_k], \tag{F16}$$

where the subscript k on b'_{11} and the third variable in I indicates that these quantities are to be evaluated at $\zeta=\zeta_k$. To calculate the variation in the residue of $\rho^{(3)}$, we must also take into account the change in $\delta\zeta_k$. Thus

$$\delta\left(\frac{b_{21}}{b'_{11}}\bigg|_{\zeta=\zeta_k}\right) = \left[\delta\left(\frac{b_{21}}{b'_{11}}\right) + \delta\zeta_k\partial_\zeta\left(\frac{b_{21}}{b'_{11}}\right)\right]\bigg|_{\zeta=\zeta_k}. \tag{F17}$$

Then since D_k is $-i(b/a')_k$, we have

$$\delta D_k^{(3)} = (b'_{11})_k^{-2}\left\{-D_k^{(3)} I[\Phi^{(1)}, \Psi^{(1)}; \zeta_k] - i\frac{c_2-c_1}{2} J[\Phi^{(1)}, \chi; \zeta_k]\right\}, \tag{F18}$$

where

$$J[U, W; \zeta_k] \equiv i\int_{-\infty}^{\infty} dx \frac{\partial}{\partial\zeta}[\tilde{U}^A C^{-1}(\delta V) W]\bigg|_{\zeta=\zeta_k}. \tag{F19}$$

To evaluate the decay time of the pump due to noise, we assume that the noise is turned on at $t=0$, that only the initial noise causes the decay, and that initially $q^{(1)}=q^{(3)}=0$, and $q^{(2)}$ is a one-soliton solution. Now to lowest order, we may evaluate the integrals in Eq. (F18) by using the unperturbed states. Thus we can reconstruct the solution of the ZS equation, from which we may construct the solution of Eq. (A5). Then we have

$$b_{jk} = \begin{bmatrix} a^{(2)} & 0 & \bar{b}^{(2)} \\ 0 & 1 & 0 \\ -b^{(2)} & 0 & \bar{a}^{(2)} \end{bmatrix}, \tag{F20a}$$

$$a^{(2)}(\lambda) = \frac{\lambda-\lambda_1^{(2)}}{\lambda-\lambda_1^{(2)*}}, \tag{F20b}$$

$$\Psi^{(1)} = \begin{pmatrix} \psi_2 \\ 0 \\ \psi_1 \end{pmatrix} \exp\left(-i\zeta x\frac{c_1+c_3}{2}\right), \tag{F20c}$$

$$\chi = -a^{(2)}\begin{pmatrix} 0 \\ 1 \\ 0 \end{pmatrix} \exp(-i\zeta c_2 x), \tag{F20d}$$

$$\Phi^{(1)A} = \begin{pmatrix} -c_1\phi_1 \\ 0 \\ c_3\phi_2 \end{pmatrix} \exp\left(i\zeta x\frac{c_1+c_3}{2}\right), \tag{F20e}$$

where

$$\begin{pmatrix} \psi_1 \\ \psi_2 \end{pmatrix} = \exp(i\lambda^{(2)}x)\left[\frac{(1-a^{(2)})Z^*}{1+Z^*Z}\begin{pmatrix} 1 \\ 0 \end{pmatrix} + \frac{1+a^{(2)}Z^*Z}{1+Z^*Z}\begin{pmatrix} 0 \\ 1 \end{pmatrix}\right], \tag{F21a}$$

$$\begin{pmatrix}\varphi_1\\ \varphi_2\end{pmatrix} = \exp(-i\lambda^{(2)}x)\left[\frac{(1-a^{(2)})Z}{1+Z^*Z}\begin{pmatrix}0\\1\end{pmatrix} + \frac{a^{(2)}+Z^*Z}{1+Z^*Z}\begin{pmatrix}1\\0\end{pmatrix}\right], \tag{F21b}$$

with

$$Z \equiv \frac{D_1^{(2)}}{2\eta_1}\exp(2ix\lambda_1^{(2)}), \tag{F21c}$$

$$\lambda_1^{(2)} \equiv \xi_1 + i\eta_1 . \tag{F21d}$$

Then

$$I[\Phi^{(1)}, \Psi^{(1)}; \zeta_1] = -\int_{-\infty}^{\infty}\frac{dx}{(1+Z^*Z)^2}[\delta q^{(2)}Z + \delta q^{(2)*}Z^*(Z^*Z)], \tag{F22a}$$

$$J[\Phi^{(1)}, \chi; \zeta_1] = \frac{c_3-c_1}{4i\eta_1}\int_{-\infty}^{\infty}\frac{dx}{1+Z^*Z}\exp\left(2ix\lambda_1^{(2)}\frac{c_1-c_2}{c_3-c_1}\right) \times[Z\delta q^{(1)} + Z^*Z\delta q^{(3)*}]. \tag{F22b}$$

We let the δq's be white noise where

$$\delta q^{(n)}(x) = \int_{-\infty}^{\infty}\epsilon_n(k)\,e^{ikx}dk \tag{F23}$$

and

$$\langle\epsilon_n(k)\epsilon_m(k')\rangle = 0 , \tag{F24a}$$

$$\langle\epsilon_n^*(k)\epsilon_m(k')\rangle = \delta_n^m\delta(k-k')E_n^2 . \tag{F24b}$$

Then upon defining Δ and β by

$$D_1^{(2)} = 2\eta_1\,e^{\Delta}\,e^{i\beta}, \tag{F25}$$

we have

$$\delta\zeta_1 = \frac{i\pi}{4\eta_1(c_3-c_1)}\int_{-\infty}^{\infty}\frac{(k+2\lambda_1^{(2)*})\,dk}{\sinh\left[\pi\dfrac{k+2\lambda_1^{(2)*}}{4\eta_1}\right]} \times\left[\epsilon_2\,e^{i\beta}\exp\left(i\Delta\frac{k+2\xi_1}{4\eta_1}\right) + \text{c.c.}\right], \tag{F26}$$

and since $D_k^{(3)} = 0$ initially,

$$\delta D_1^{(3)} = \frac{i\pi(c_2-c_1)}{2(c_3-c_1)}\int_{-\infty}^{\infty}dk\left\{\frac{\epsilon_1\,e^{\Delta}\,e^{i\beta}\exp\left(i\Delta\dfrac{k+2\lambda_1^{(1)}}{2\eta_1}\right)}{\sinh\left[\pi\dfrac{k+2\lambda_1^{(1)}}{4\eta_1}\right]} + \frac{\epsilon_3^*\exp\left(-i\Delta\dfrac{k+2\lambda_1^{(3)}}{2\eta_1}\right)}{\sinh\left[\pi\dfrac{k+2\lambda_1^{(3)}}{4\eta}\right]}\right\}. \tag{F27}$$

From Eq. (F26), we can determine how much spread the noise level causes in the eigenvalue. Since $\lambda_1^{(2)} = \frac{1}{2}\xi_1(c_3-c_1)$, we have from Eqs. (F21d) and (F26)

$$\langle\delta\eta_1^2\rangle = \pi\eta_1E_2^2, \tag{F28a}$$

$$\langle\delta\xi_1^2\rangle = \tfrac{1}{3}\pi\eta_1E_2^2 . \tag{F28b}$$

From Eq. (F27) we also have

$$\langle|\delta D_1^{(3)}|^2\rangle = 8\eta_1\exp\left(2\Delta\frac{c_2-c_1}{c_3-c_1}\right) \times\left[\frac{\left(\dfrac{c_2-c_1}{c_3-c_1}\right)E_1^2}{\sin\left[\pi\dfrac{c_3-c_2}{c_3-c_1}\right]} + \frac{\left(\dfrac{c_3-c_2}{c_3-c_1}\right)E_3^2}{\sin\left[\pi\dfrac{c_2-c_1}{c_3-c_1}\right]}\right]. \tag{F29}$$

Since $\lambda^{(3)} = [(c_2-c_1)/(c_3-c_1)]\lambda^{(2)}$, from Eq. (B20b) the average position, $X_0^{(3)}$, of the $q^{(3)}$ soliton emitted by the decay is given by

$$X_0^{(3)} = c_3t + \frac{c_3-c_1}{4\eta_1(c_2-c_1)}\ln\left[\frac{(c_3-c_1)^2\langle|\delta D_1^{(3)}|^2\rangle}{4\eta_1^2(c_2-c_1)^2}\right], \tag{F30}$$

whereas the average position, $X_0^{(2)}$, of the original $q^{(2)}$ soliton was given by

$$X_0^{(2)} = c_2t + \frac{1}{2}\frac{\Delta}{\eta_1}. \tag{F31}$$

Thus the lifetime of $q^{(2)}$ due to noise is

$$\tau_N = \frac{-(c_3-c_1)}{4\eta_1(c_3-c_2)(c_2-c_1)} \times\ln\left\{\frac{2(c_3-c_1)}{\eta_1(c_2-c_1)}\left[\frac{E_1^2}{\sin\left(\pi\dfrac{c_3-c_2}{c_3-c_1}\right)} + \frac{\dfrac{c_3-c_2}{c_2-c_1}E_3^2}{\sin\left(\pi\dfrac{c_2-c_1}{c_3-c_1}\right)}\right]\right\}, \tag{F32}$$

which follows upon determining where the lines given by Eqs. (F30) and (F31) intersect.

REFERENCES

Ablowitz, M. J., D. J. Kaup, A. C. Newell, and H. Segur, 1974, Stud. Appl. Math. **53**, 249.

Ablowitz, M. J. and R. Haberman, 1975, J. Math. Phys. **16**, 2301.

Adler, R., 1958, Proc. IRE **46**, 1300.

Akhmanov, S. A., and V. G. Dimitriyev, 1963, Radio Eng. Electron. Phys. (USSR) **8**, 1378.

Allis, W. P., S. J. Buchsbaum, and A. Bers, 1963, *Waves in Anisotropic Plasmas* (MIT, Cambridge, Mass.).

Armstrong, J. A., N. Bloembergen, J. Ducuing, and P. S. Pershan, 1962, Phys. Rev. **127**, 1918.

Armstrong, J. A., S. J. Sudhanshu, and N. S. Shiren, 1970, IEEE J. Quantum Electron. **QE-6**, 123.

Benney, D. J., and A. C. Newell, 1967, J. Math. Phys. **46**, 133.

Bers, A., 1975a, in *Plasma Physics-Les Houches 1972*, edited by C. De Witt and J. Peyraud (Gordon and Breach, New York).

Bers, A., 1975b, in *Proceedings of the U.S.-Australian Workshop on Plasma Waves*, edited by R. C. Cross (University of Sidney, Sidney, Australia), p. 51.

Bers, A., 1978, in *Proceedings of the Third Topical Conference on RF Plasma Heating*, California Institute of Technology,

Pasadena, Calif., Jan. 1978, p. A1-1.
Bers, A., and A. Reiman, 1975, in *Proceedings of the Seventh Conference on Numerical Simulation of Plasmas*, Courant Institute, N.Y.U., June 1975, p. 192.
Bers, A., D. J. Kaup, and A. Reiman, 1976, Phys. Rev. Lett. **37**, 182.
Bloembergen, N., 1965, *Nonlinear Optics* (Benjamin, New York).
Bretherton, F. P., 1964, J. Fluid Mech. **20**, 457.
Bullough, R. K., 1977, in *Interaction of Radiation with Condensed Matter* (IAEA, Vienna), Vol. 1, p. 381, IAEA-SMR-20/51.
Case, K. M., and S. C. Chiu, 1977a, Phys. Fluids **20**, 742.
Case, K. M., and S. C. Chiu, 1977b, Phys. Fluids **20**, 746.
Cassedy, E. S., and C. R. Evans, 1972, J. Appl. Phys. **43**, 4452.
Coppi, B., M. N. Rosenbluth, and R. N. Sudan, 1969, Ann. Phys. (N.Y.) **55**, 207.
Cornille, H., 1978 "Solutions of the Nonlinear Three-Wave Equations in Three Dimensions" (preprint).
Craik, A. D. D., 1971, J. Fluid Mech. **50**, 393.
Craik, A. D. D., 1978, "Evolution in Space and Time of Resonant Wave Triads. Part II: a Class of Exact Solutions," Preprint.
Cullen, A. L., 1960, Proc. IEF **107B**, 101.
Davidson, R. C., 1972, *Methods in Nonlinear Plasma Theory* (Academic, New York).
Davis, K. L., and V. L. Newhouse, 1975, IEEE Trans. Sonics Ultrason. **SU-22**, 33.
Drake, J. F., P. K. Kaw, Y. C. Lee, G. Schmidt, C. S. Liu, and M. N. Rosenbluth, 1974, Phys. Fluids **17**, 778.
DuBois, D. R., 1974, in *Laser Interaction and Related Plasma Phenomena* (Plenum, New York), Vol. 3A, p. 267.
DuBois, D. F., and M. V. Goldman, 1965, Phys. Rev. Lett. **14**, 544.
DuBois, D. F., and M. V. Goldman, 1967, Phys. Rev. **164**, 207.
Engelbrecht, 1958, Proc. IRE **46**, 1655.
Faraday, M., 1831, Phil. Trans. R. Soc. Lond. **121**, 299.
Fejer, J. A., 1977, J. Phys. (Paris) **38**, Suppl. 12, C6-55.
Flaschka, H., and A. Newell, 1975, in *Dynamical Systems, Theory and Applications. Lecture Notes in Physics*, edited by J. Moser (Springer, Berlin), Vol. 38, p. 355.
Forslund, D. W., J. M. Kindel, and E. L. Lindman, 1973, Phys. Rev. Lett. **30**, 739.
Forslund, D. W., J. M. Kindel, and E. L. Lindman, 1975, Phys. Fluids **18**, 1002.
Fuchs, V., and G. Beaudry, 1976, J. Math. Phys. **17**, 208.
Gardner, C. S., J. M. Greene, M. D. Kruskal, and R. M. Miura, 1967, Phys. Rev. Lett. **19**, 1095.
Goldman, M. V., 1966, Ann. Phys. (N.Y.) **38**, 95, 117.
Haberman, R., 1977, J. Math. Phys. **18**, 1137.
Harvey, R., and G. Schmidt, 1975, Phys. Fluids **18**, 1395.
Hasegawa, A., 1975, *Plasma Instabilities and Nonlinear Effects* (Springer, Berlin).
Hirota, R., 1976, in *Backlung Transformations, the Inverse Scattering Method, Solitons, and Their Applications*, edited by R. M. Miura (Springer, New York).
Jurkus, A., and P. N. Robson, 1960, Proc. IEE **107b**, 119.
Jurkus, A., and P. N. Robson, 1961, Proc. IRE **49**, 1433.
Karpman, V. I., 1963, Zh. Eksp. Teor. Fiz. **44**, 1307 [Sov. Phys. JETP **17**, 882].
Kaup, D. J., 1976a, Stud. Appl. Math. **55**, 9.
Kaup, D. J., 1976b, SIAM J. Appl. Math. **31**, 121.
Kaup, D. J., 1977, Phys. Rev. A **16**, 704.
Kaup, D. J., and A. C. Newell, 1978, Proc. R. Soc. London A **361**, 413.
Kaup, D. J., 1979, "A Method for Solving the Separable Initial Value Problem of the Full Three Dimensional Three-Wave Interaction" (Submitted to Stud. Appl. Math.).
Kaw, P. K., W. L. Kruer, C. S. Liu, and K. Nishikawa, 1976, in *Advances in Plasma Physics*, edited by A. Simon and W. B. Thompson (Wiley, New York), Vol. 6, Part I.
Kenyon, K., 1966, Proc. R. Soc. Lond. **A299**, 141.
Kerst, R. A., and M. Raether, 1976, J. Plasma Phys. **16**, 335.
Klimontovich, Yu. L., 1967, *The Statistical Theory of Non-Equilibrium Processes in a Plasma* (MIT, Cambridge, Mass., and Pergamon, London).
Kravtsov, Yu. A., 1963, Radio Eng. Electron. Phys. **8**, 1479.
Lamb, G. L., Jr., 1971, Rev. Mod. Phys. **43**, 99.
Laval, G., R. Pellat, and D. Pesme, 1973, Phys. Rev. Lett. **A46**, 281.
Liu, C. S., and R. E. Aamodt, 1976, Phys. Rev. Lett. **36**, 95.
Longuet-Higgins, M. S., and A. E. Gill, 1966, Proc. R. Soc. Lond. **A299**, 120.
Louisell, W. H., 1960, *Coupled Mode and Parametric Electronics* (Wiley, New York).
Louisell, W. H., and C. F. Quate, 1958, Proc. IRE **46**, 707.
Mannheimer, W., 1974, Phys. Fluids **17**, 1634.
Manheimer, W. M., and E. Ott, 1974, Phys. Fluids **17**, 1413.
McCall, S. L., and E. L. Hahn, 1967, Phys. Rev. Lett. **18**, 908.
McCall, S. L., and E. L. Hahn, 1969, Phys. Rev. **183**, 457.
McGoldrick, L., 1965, J. Fluid Mech. **21**, 305.
Melde, F., 1859, Ann. Physik Chemie **109**, 193.
Miles, J. W., 1977, J. Fluid Mech. **79**, 157, 171.
Mumford, W. W., 1960, Proc. IRE **48**, 848.
Newell, A. C., and L. G. Redekopp, 1977, Phys. Rev. Lett. **38**, 377.
Newhouse, V. L., C. L. Chen, and K. L. Davis, 1972, J. Appl. Phys. **43**, 2603.
Nishikawa, K., 1968, J. Phys. Soc. Jpn. **24**, 916, 1152.
Nozaki, K., and T. Taniuti, 1973, J. Phys. Soc. Jpn. **34**, 796.
Ohsawa, Y., and K. Nozaki, 1974, J. Phys. Soc. Jpn. **6**, 591.
Oraevskii, V. N., and R. Z. Sagdeev, 1963, Sov. Phys.-Tech. Phys. **7**, 955.
Ott, E., 1975, Phys. Fluids **18**, 566.
Phillips, O. M., 1960, J. Fluid Mech. **9**, 193.
Porkolab, M., 1978, Nucl. Fusion **18**, 367.
Rayleigh, J. W. S. Lord, 1833, Phil. Mag. **16**, 50.
Rayleigh, J. W. S. Lord, 1887, Phil. Mag. **24**, 145.
Reiman, A. H., 1977, Ph.D. thesis, Princeton University (unpublished).
Reiman, A. H., and A. Bers, 1975, in *Proceedings of the Seventh Conference on Numerical Simulation of Plasmas*, Courant, Institute, N.Y.U., June 1975, p. 188.
Reiman, A., A. Bers, and D. Kaup, 1977, Phys. Rev. Lett. **39**, 245, 850.
Richtmyer, R. D., and K. W. Morton, 1969, *Difference Methods for Initial Value Problems*, 2nd ed. (Interscience, New York).
Sagdeev, R. Z., and A. A. Galeev, 1969, in *Nonlinear Plasma Theory*, edited by T. M. O'Neil and D. L. Book (Benjamin, New York).
Schiff, L. I., 1955, *Quantum Mechanics*, 2nd ed. (McGraw-Hill, New York).
Scott, A. C., F. Y. F. Chu, and D. W. McLaughlin, 1973, Proc. IEEE **61**, 1443.
Shiren, N. S., 1965, Proc. IEEE **53**, 1540.
Silin, V. P., 1965, Sov. Phys. JETP **21**, 1127.
Steudel, H., 1977, Ann. Phys. (Leipz.) **34**, 188.
Stix, T. H., 1962, *The Theory of Plasma Waves* (McGraw-Hill, New York).
Suhl, H., 1957a, Phys. Rev. **106**, 384.
Suhl, H., 1957b, J. Appl. Phys. **28**, 1225.
Svaasand, L. O., 1969, Appl. Phys. Lett. **15**, 300.
Tien, P. K., and H. Suhl, 1958, Proc. IRE **46**, 700.
Tsytovich, V. N., 1970, *Nonlinear Effects in Plasma* (Plenum, New York).
Uhlir, A., Jr., 1956, Proc. IRE **44**, 1183.
Vlannes, N., 1977, S. M. thesis, M.I.T. (unpublished).
Watson, D. C., and A. Bers, 1977, Phys. Fluids **20**, 1704.
Weiland, J., and H. Wilhelmsson, 1977, *Coherent Non-Linear Interaction of Waves in Plasmas* (Pergamon, New York).
Yajima, N., M. Ohkawa, and J. Satsuma, 1978, J. Phys. Soc. Jpn. **44**, 1711.
Yariv, A., 1975, *Quantum Electronics* (Wiley, New York).
Zakharov, V. E., 1976, Dokl. Akad. Nauk. SSSR **228**, 1314 [Sov. Phys. Dokl. **21**, 322 (1976)].
Zakharov, V. E., and S. V. Manakov, 1973, Zh. Eksp. Teor. Fiz. Pis'ma Red. **18**, 413 [Sov. Phys.-JETP Lett. **18**, 243 (1973)].
Zakharov, V. E., and S. V. Manakov, 1975, Zh. Eksp. Teor. Fiz. **69**, 1654 [Sov. Phys.-JETP **42**, 842 (1976)].
Zakharov, V. E., and S. V. Manakov, 1976, Funkts. Anal. [referenced in Zakharov and Manakov, Sov. Phys.-JETP **42**, 842 (1976)].
Zakharov, V. E., and A. B. Shabat, 1971, Zh. Eksp. Teor. Fiz. **61**, 118 [Sov. Phys.-JETP **34**, 62 (1972)].
Zakharov, V. E., and A. B. Shabat, 1974, Funkts. Anal. **8**, 43 [Funct. Anal. Appl. **8**, 226 (1974)].